FLUIDS AND POLYMER COMPOSITES COMPRISING DETONATION NANODIAMOND

By

Blake T. Branson

Dissertation

Submitted to the Faculty of the

Graduate School of Vanderbilt University

in partial fulfillment of the requirements

for the degree of

DOCTOR OF PHILOSOPHY

in

INTERDISCIPLINARY MATERIALS SCIENCE

May, 2010

Nashville, Tennessee

Approved:

Professor Charles Lukehart

Professor Jim Davidson

Professor Scott Guelcher

Professor Weng Poo Kang

To my parents, for instilling in me the importance of education

and

to my wife, for instilling in me the importance of graduation.

ACKNOWLEDGEMENTS

First, I would like to thank my co-advisors, Dr. Jimmy L. Davidson and Dr. Charles M. Lukehart. I have been fortunate to receive guidance and support from not one, but two mentors as I pursued my academic endeavors. Truly, none of this work would be possible without their willingness to allow me to pursue my research goals. I would also like to thank my committee members, Dr. Weng Poo Kang, Dr. Alvin Strauss, and, in particular, Dr. Scott Guelcher for his insight into the characterization of polymer nanocomposites.

My work would also not be possible without the efforts of the former program director, Dr. Len Feldman and our current director, Dr. Tim Hanusa. I would also like to thank our program coordinator, Mrs. Sarah Satterwhite, for her tireless work to help the students in day-to-day operation.

Credit for collecting the thermal conductivity data for nanodiamond/ethylene glycol nanofluids must be extended to Mr. Paul Beauchamp, who collaborated with me in the summer of 2009 through the School of Engineering's Summer Undergraduate Research Program.

In the pursuit of interdisciplinary research, I have graciously been granted access to instruments and facilities across campus. I would like to acknowledge my gratitude for access to the VINSE facilities. I am grateful to Dr. Peter Pintauro for access to the Differential Scanning Calorimeter, as well as the assistance of Jason Ballengee. Thanks go also to Dr. Jeffery Nyman and Matt Murray for access to mechanical testing instruments. I would like to acknowledge the assistance of Mr. Elvin Woodruff for

preparing nanocomposite microtomes. I would like to thank Dr. Don Stec for his assistance in acquiring NMR data. I would also like to thank Dr. Wright for access to the UV-VIS spectrometer. I am grateful to Dr. Mohammed Seif of Alabama A&M for granting me access to nanoindentation facilities. I am grateful for the assistance of Mr. Robin Midget in acquiring access to test equipment and for the skilled work of John Fellenstein and Bob Patchin in the Physics machine shop.

Lastly, this work would not be possible without the financial assistance of both the National Science Foundation's IGERT Program (grant 0333392) and U.S. Army contract W911-NF-04-2-0023.

TABLE OF CONTENTS

Page

LIST OF TABLES

Page

LIST OF FIGURES

Page

CHAPTER I

INTRODUCTION

1.1 Nanotechnology

In the modern sense, the field of nanotechnology was born when the future-Nobel laureate Richard Feynman delivered his speech "There is Plenty of Room at the Bottom" on December 29th, 1959.[1] In his address, Dr. Feynman spoke of both the significant technical challenges that must be addressed at the nanoscale, as well as the potential advances such a technology could provide to society. As is the case with many visionary proclamations, decades passed before this field of research began to gain widespread traction.

Presently, the term "nanotechnology" is pervasive even in the greater community outside of research universities and technology incubators. With such widespread usage, nanotechnology means different things to different individuals. For this work, nanotechnology is taken to mean the efforts of science and engineering to manipulate materials systems where at least one phase has dimensions under 100-nm.

Researchers who investigate various nanoscale materials systems are faced with unique challenges. The dominant physical effects at the macro-scale may have little influence over nanomaterials, while seemingly "weak" interactions become critical. For example, an engineer may be concerned with a material's density and completely discard van der Waal's interactions when selecting materials for macroscopic functions, but the opposite holds true for a materials scientist investigating nanoscale materials.

Advances in nanoscale research will likely have profound impact on the fields of medicine, semiconductor technology, and energy efficiency. The scope of this work, however, is concerned with the role nanoscale materials will play in composite systems. For the research scientist who is concerned with composite materials, nanomaterials posses several key attributes that have the potential to make significant impact on the state of the art. The most important attributes of nanoscale materials in composites applications are the following:

Nanomaterials have high specific surface areas

This concept is best explained by considering how volume and surface area scale as a function of size. For example, consider a sphere, whose volume is given by

$$V = \frac{4}{3}\pi \cdot r^3 \tag{1.1}$$

and whose surface area is given by

$$A_s = 4\pi \cdot r^2 \tag{1.2}$$

If you divide equation (1.2) by equation (1.1), you are left with

$$\frac{A_S}{V} = \frac{3}{r} \tag{1.3}$$

As the characteristic dimension of our material, here it is "r", becomes small, the ratio of surface area to volume becomes very large. Very small particles have enormous specific surface areas (surface area per gram). Nanodiamond of average diameter of 5 nm, for instance, has about 350 m^2 of surface area per gram of nanomaterial.[2] A doubles tennis court, by comparison, has about 260 m^2 of surface area.

This large specific surface area is a critical advantage in composites applications. The performance of a polymer composite is enhanced if the stress transfer across the interface from matrix to reinforcement phase can be improved.[3] By increasing the surface area, the available contact between the matrix and reinforcement phase increases. Traditional fillers used in composite materials are on the microscale; nanocomposites fillers are orders of magnitude smaller in size.

Nanomaterials display exceptional material properties

Traditional materials for structural applications include materials such as steel and aluminum having specific modulus values of about 25 GPa g^{-1} cm^3. These materials are slowly being displaced by carbon-fiber based materials as the pursuit of ever lighter structures continues. Carbon fiber is very stiff but still lightweight. With a specific modulus of over 160 GPa g^{-1} cm^3, carbon fiber composites represent a significant advance in the performance of structural materials.[4]

Nanomaterials, however, have shown material properties that eclipse even the most advanced traditional materials. Single-wall carbon nanotubes (SWCNTs), for example, are believed to have a modulus of elasticity in excess of 1 TPa with a density of around 1.3 g cm^{-3}.[5] This represents an improvement of nearly an order of magnitude in specific modulus when compared to micro-scale carbon fibers presently used in commercial composites.

Nanoscale materials allow for multifunctional composites

The nanoscale fillers of composite systems will do more than just enhance one aspect of a system's properties. The concept of multi-functional nanomaterials is emerging as an important research goal.[6] For instance, ceramic nanoparticles may be embedded in a coating primarily to improve wear resistance, but these same particles may have certain luminescent properties that allow for passive wear detection.[7] Or perhaps nanotubes are used as fiber reinforcements for mechanical properties, but this material also provides electromagnetic radiation shielding to electronics contained within the structure.[8] Use of nanofibers for both mechanical enhancement and damage sensing has also been explored.[9] Finally, the unique size scale of nanofillers allows for the development of mechanically reinforced composites that are transparent in the visible range of light. These are just a few examples of the many ways researchers hope to exploit multiple properties of novel nanomaterials for multifunctional composites.

Nanoscale fillers are effective in smaller doses

Traditional, micro-scale composites typically contain 30 to 70 volume percent of the reinforcing phase. Glass-fiber reinforced vinyl ester composites are approximately 50 volume percent fiber; carbon-fiber composites may have fiber content as high as 70 volume percent.[10]

Nanocomposites, however, often contain much smaller additive loadings. This is due in part to the high specific surface area mentioned earlier; a few grams of nanoscale filler will have as much surface area interaction as a kilogram of glass-fibers. Furthermore, at higher concentrations of added filler are added, the distance between

particles of the reinforcing phase decreases. With nanoscale fillers, relatively small concentrations of filler results in very small inter-particle distances. As filler particle size decreases, this trend becomes more pronounced. Figure 1.1, for example, shows how inter-particle spacing rapidly decreases with increased loading of 5-nm nanoparticles. At 12.5 weight percent nanodiamond, the inter-particle distance is actually smaller than the diameter of the nanoparticles themselves.

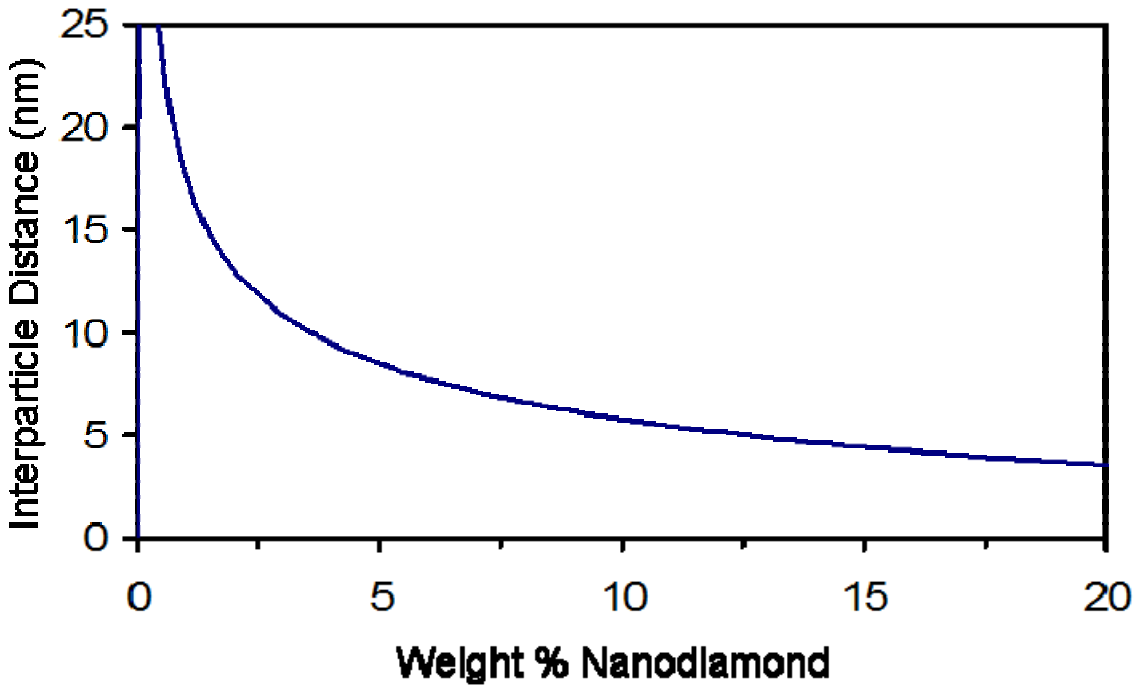

Figure 1.1 Inter-particle spacing of 5-nm nanodiamond particles as a function of weight percent loading at constant volume.

Furthermore, nanoparticles are "super-efficient" reinforcement materials in composites because the particles are small enough to affect the polymer properties at the interface. Polymers behave differently near interfaces and surfaces because polymer chains are constrained differently than are the polymer chais located in the bulk.[3] This

perturbed region extends for several nanometers into the polymer matrix. With nanoscale materials, however, the distance between interfaces may only be a few nanometers. Therefore, even small amounts of nanoscale filler may cause the entire polymer volume to behave as a constrained interfacial material.

1.2 Detonation Nanodiamond

The work reported in this thesis is specifically concerned with nanodiamond-based composite technology. Nanodiamond, generically, refers to any number of synthetically prepared carbon materials; there are even reports of nanoscale diamond found in interstellar dust.[11] In this work, the nanomaterial of interest is detonation nanodiamond, which may also be referred to as Ultra-dispersed diamond (UDD) or nanodiamond (ND). This terminology will be discussed in detail, below.

Detonation nanodiamond was first synthesized in the former Soviet Union in the mid-1960s.[12] The discovery of nanodiamond actually outdates the discovery of other important carbon nanomaterials such as fullerenes[13] and carbon nanotubes,[14] but nanodiamond's discovery was not widely publicized because of the Cold War. In fact, the discovery of detonation nanodiamond was not even well known within the Soviet Union and was "rediscovered" again in the early 1980s.[12]

This material is called detonation nanodiamond because it is synthesized from a detonation reaction that takes place within a closed chamber, such as the chamber shown in Figure 1.2. TNT and RDX are the most common explosives used. Furthermore, there is no additional carbon-containing reagent; the carbon that comprises nanodiamond comes from carbon atoms contained within the explosives. The detonation reaction takes

place in an oxygen-deficient atmosphere; the intense heat and pressure generated by the explosion provide the appropriate conditions to allow liquefied carbon to condense in the diamond phase.[15] The detonation soot is subjected to a number of post-processing steps to purify the reaction product. This processing is described in more detail in Chapter 2.

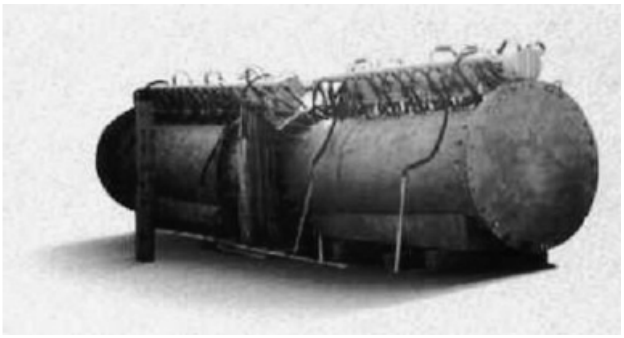

Figure 1.2 Photograph of a detonation chamber used to produce nanodiamond. (Reprinted from reference 16. Copyright 2008 Royal Society of Chemistry)

The detonation reaction is very rapid; the appropriate conditions for diamond formation are very brief. Due to the small diamond growth window, nanodiamond particles are small, between 4-5 nm in diameter, and display a narrow size distribution.[16] The core of nanodiamond is sp^3 bound carbon, but the surface of the nanodiamond particles is reported to have a mixture of sp^2 and sp^3 bound carbon. A high density of oxygen-containing functional groups is present on the surface. A model of nanodiamond's structure is shown in Figure 1.3.

Nanodiamond is an attractive material for applications in composite materials because of diamond's high stiffness, strength, relatively low density and the fact that nanodiamond's surface is well-suited for chemical modification. Development of nanodiamond as an additive to composite materials systems, however, has been hindered by the tendency of the primary nanodiamond particles to form tightly bound aggregates

that cannot be easily separated. This phenomenon of aggregation will be discussed in detail in Chapter 2. Table 1, below, reports key material properties of aggregates of nanodiamond. To date, properties of single nanodiamond particles has not been reported.

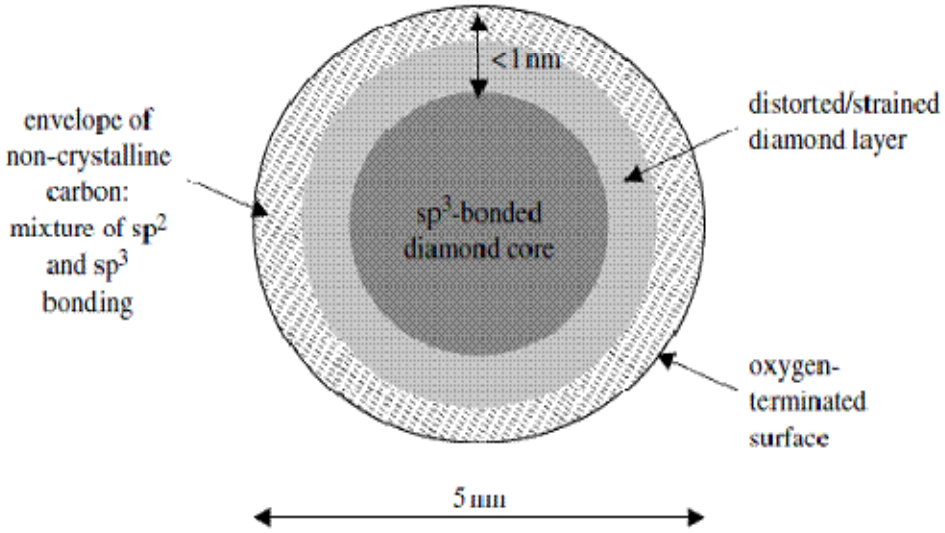

Figure 1.3 Model for the structure of a nanodiamond particle. (Reprinted from reference 17 and Copyright 2007 The Royal Society.)

In this work, the terms "ultra-disperse diamond" (UDD) and "nanodiamond" (ND) are not synonymous. The as-received powder synthesized by a detonation process is UDD; comprises aggregated nanoparticle structures. Nanodiamond, conversely, implies that some de-aggregation processing technique has been applied so that primary diamond particles exist. By definition, ND may only exist within some dispersing media; this media may be a liquid or a solid polymer composite. If the solvent were completely driven off, the ND would re-aggregate into UDD.

There is, understandably, some confusion as to why "ultra-dispersed diamond" is used to confer aggregated nanoparticle structure. This problem is one of historical

context. The UDD moniker was devised long before the ability to de-aggregate UDD was demonstrated.[12] Only very recently has a de-aggregated form of this material existed, and the research community as a whole has yet to settle on a consistent name.

Furthermore, the terms "aggregate" and "agglutinate" have specific meaning in this text. Aggregates of nanodiamond refer to primary particles that have not been subjected to a dispersion technique, and therefore still have covalent bonds binding the particles together. Agglutinates refer to nanodiamond particles that have been subjected to a de-aggregation process but are not fully dispersed in solution, either due to particle agglomeration from solvent drying or to poor solubility in a host fluid.

Table 1.1 Selected properties of detonation nanodiamond. (Reprinted from reference 2. Copyright 2002 Marcel Decker, Inc.)

Structure	Cubic (a=0.3573 ±0.0005 nm)
Density	3.30 g/cm3
Particle size	2-20 nm
Average monocrystal size	4,3 nm
Size of uncrushable aggregates	20-50 nm
Specific surface area	300 - 400 m^2/g
Pore volume in powder	0.3-1 sm^3/g
Density of dislocations	$1,8 . 10^{17}$
Composition (at. %)	C (93.2-100); O (0-6.8)
Initial air oxidation temperature (depends on purity)	$430^{O}C$
Initial vacuum graphitization temperature	$1100\text{-}1200^{O}C$
Resistivity	$7,7 . 10^{9}$ Ωm
Electrophoretic surface charge	-78.44 mV
Refractive index	~2.55 (at λ=580nm)

1.3 Thesis Overview

Previous Lukehart and Davidson group members were successful in incorporating Ultra-disperse Diamond nanoparticles into both liquid and polymer systems.[18, 19] These initial studies were encouraging and validated the potential utility of nanodiamond. In some applications, limitations were encountered due to a high degree of nanodiamond aggregation. This work makes a departure from previous, UDD-based studies because investigations are performed on liquid and solid composites filled with highly dispersed nanodiamond particles.

Chapter II addresses this critical issue of nanodiamond aggregation. First, an overview of the existing theories for the origin of this persistent aggregation is provided. Mechanisms responsible for aggregation include the synthesis process, inter-particle covalent bonding, and coloumbic attraction of nanodiamond facets. Next, successful de-aggregation methods are reviewed. Currently, UDD de-aggregation is achieved by employing mechano-chemical processing steps. Known de-aggregation methods are discussed along with the limitations and challenges associated with these state-of-the-art techniques. Then, experimental evidence is provided that suggests that the Lukehart lab has developed sufficient processing technology to consistently achieve high levels of nanodiamond de-aggregation. Finally, a series of experimental procedures are reported to demonstrate the breadth of systems into which nanodiamond may be successfully dispersed.

Following this progression, Chapter III focuses on nanodiamond-based nanofluids. Specifically, nanodiamond's ability to enhance thermal conductivity of a base fluid is investigated. Two classes of fluids are used; both fluids serve as heat

transfer media in many existing applications. Ethylene glycol is chosen as a representative polar liquid, while mineral oil is the base fluid chosen for the study of non-polar nanofluids. Both processing steps and thermal conductivity experiments are reported. For both systems, nanodiamond displays a pronounced ability to enhance the thermal conductivity of fluids.

In Chapter IV, solid-phase composite systems are investigated. Surface-functionalized nanodiamond is incorporated into the thermoplastic polymers polymethyl methacrylate and polyacrylonitrile. Experiments are reported to investigate the role of particle aggregation and surface functionalization on composite material properties. These composite systems are extensively characterized by both chemical and mechanical means. The degree of particle aggregation is measured by dynamic light scattering. Nanodiamond surface functionalization is characterized by thermal gravimetric analysis, acid-base titration, and by infrared and ^{1}H NMR spectroscopy. Filler dispersion is characterized by electron microscopy of thin-sample sections. Chemical interactions between the nanodiamond surface and the host matrix are examined by IR spectroscopy.
In Chapter IV, mechanical characterization serves as a critical analytical tool. Nanodiamond/polymer composites are first probed with nanoindentation; these tests surprisingly suggest that UDD-filled composites outperform ND composites with good filler dispersion. However, a second series of mechanical tests based on tensile testing of thin films provides an additional perspective on interpreting modulus properties of ND/thermoplastic composites.

To add additional breadth to this investigation, the synthesis and characterization of ND composites with a commercial vinyl ester resin are discussed in Chapter V.

Incorporation of ND into thermosetting resins involves additional complexity in synthesis strategy, because the ND nanoparticles must be both well-dispersed within the resin and also become covalently cross-linked within the polymer phase. As discussed in Chapter IV, a series of chemical and mechanical characterization steps are performed to characterized these ND/thermosetting polymer composites. To our knowledge, this is the first mechanical characterization of well-dispersed nanodiamond composites.

Finally, Chapter VI reviews key conclusions of this work and offers suggestions for future research directions. By developing the processing technology to achieve highly disperse nanodiamond, the potential to exploit both the outstanding properties of diamond and the advantages of nanoscale materials is available for the first time. This work only begins to examine the potential applications of nanodiamond-based composite systems.

1.4 Nomenclature

A final point should be mentioned concerning abbreviations employed herein. Throughout this dissertation, a number of different materials systems and a plethora of processing techniques will be used. Abbreviations for common chemicals may be used. Also, a large portion of the experimental work reported here focuses on functionalizing the nanodiamond surface and dispersing functionalized nanomaterials into liquid media.

The naming system developed here attempts to accurately reflect the state of the surface chemistry. Nanodiamond, abbreviated "ND" can be followed by a " – " or a "•" and a chemical abbreviation. The dash is used where surface functionality is assumed to

be covalently bound to the nanoparticle surface, while the bullet is used to denote non-covalent surface funtionalization.

For example, ND-COOH represents nanodiamond material that has been oxidized to form covalently bound carboxylic acid functional groups. ND-VTMS would denote nanodiamond having vinyltrimethoxysilane sizing covalently bound to the surface sites. Conversely, ND•Oleic acid is a nanodiamond material containing a surfactant layer of oleic acid, but the organic layer is not covalently bound to the nanodiamond surface sites.

CHAPTER II

NANODIAMOND AGGREGATION

2.1 Introduction

The size of detonation nanodiamond is often cited as 4-5 nm in research journals based on observations using electron microscopy and X-ray diffraction.[20] Though this is the size of the primary particles, they are aggregated into larger structures with sizes on the micron scale. There are many examples of carbon nanostructures that aggregate together to reduce the free energy of the system, but nanodiamond forms "primary aggregates" of approximately 100 – 200 nm that cannot be broken down via conventional ultrasonic treatment.[21]

To access the utility of truly nanodiamond material, a method of achieving dispersed, single ND particles from UDD particles is of critical importance. ND is preferable over UDD in a number of applications. A few reasons outlining the need for de-aggregation are discussed below:

1. Increased surface area: Primary particles of nanodiamond have a diameter that is approximately two orders of magnitude smaller than UDD core aggregates. In the dispersed state, there is substantially more surface area available for interaction with a polymer (in the case of composites) or chemical absorption (in the case of drug scaffolding or sensor applications).
2. UDD aggregates are high-defect materials: One of the appeals of nanomaterials as additives for composites is that the reinforcing materials display exceptional

mechanical properties. The superlative strength and moduli reported for materials such as carbon nanotubes and graphene is based on the fact that the structures are composed of many C-C bonds with good order and low defect density. A single crystal of diamond also displays excellent thermal and mechanical properties, but this is severely undermined when grain boundaries exist. The boundaries between particles represent a defective region with poor mechanical properties. Under tension or shear, an aggregate may break apart at a lower stress, thereby weakening the composite structure. Conversely, a dispersed diamond system has only diamond-polymer interfaces, which maximizes the effectiveness of the nanoscale filler.

3. For nanofluid systems, dispersions of additive single crystals are preferable over aggregates for reasons dealing with implementation. Larger particles settle out of solution faster than smaller particles, but sufficiently small particles may remain in suspension indefinitely due to Brownian motion or solvation effects. Furthermore, larger particles may clog small openings in devices like pumps or microchannels. If diamond nanoparticles are to find application in fluid systems, there is a need to achieve good shelf life (low settling rate) and to minimize damage to pumping systems.
4. Transparency of dispersed systems: In applications where transparency would be desirable, additive aggregates must be broken down. Composites filled with particles on the order of the wavelength of light, hundreds of nanometers, are opaque. When composite systems are formed with primary diamond particles, the composite is transparent because the ND particles are much smaller than the

wavelength of visible light. Several of the materials systems discussed in the following chapters meet these criteria.

In this chapter, the underlying cause for the unusually strong aggregation of detonation nanodiamond will be presented. Methods recently developed to de-aggregate UDD will be described, and the mechanism of de-aggregation explained. Finally, a series of examples of de-aggregated nanodiamond/liquid dispersions will be prepared to demonstrate the range of available nanodiamond composite materials systems now available.

2.2 Cause of Nanodiamond Aggregation

For the vast majority of the past four decades that nanodiamond has garnered research interest, it has been studied in the aggregated state. The primary, sub-5 nm detonation nanodiamond particles are not found in the de-aggregated state (ND) but form as aggregated particles (UDD) approximately 40 nm in diameter.[15]

To understand the causes of nanodiamond aggregation, it is first necessary to review the synthesis process. Detonation nanodiamond, as its name implies, uses explosives to create an environment of intense heat and pressure.[2] The carbon within the explosives is liquefied, and condenses in the diamond phase as it cools. Figure 2.1, below, is a phase diagram that illustrates the how rapid cooling (path ii) increases the yield of diamond material.

Even with significant effort to rapidly cool the detonation material, the yield of diamond is not quantitative. The detonation product material, referred to as diamond blende, is usually no more than 75 percent diamond.[15] A series of purification steps, typically involving acid and air oxidation, are employed to purify diamond blende to greater than 90 percent diamond. The multiple processing steps are shown in Figure 2.2.

During synthesis and purification processing, a number of reactions can occur that may lead to aggregation of diamond particles. As the reaction product cools and the pressure drops, carbon solidifies as graphite. A graphitic shell encases multiple primary particles, forming an aggregate as shown in Figure 2.3. The subsequent acid treatments will remove non-diamond material present at the surfaces of the aggregates, but diffusion limitations prevent total removal of this graphitic binding material.[22]

Diamond particle aggregation could also develop through inter-particle covalent bonding. Functional groups such as alcohols and carboxylic acids are present in high numbers on the surfaces of UDD detonation product.[23] These functional groups can interact and form covalent bridges between particles.[24] Examples of such bridging structures is shown in Figure 2.4.

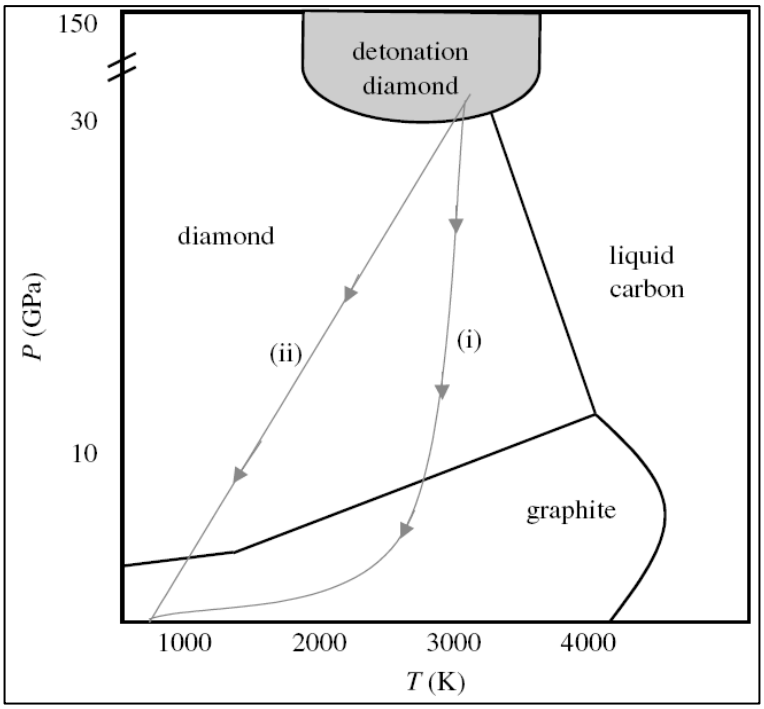

Figure 2.1 Phase diagram of carbon. More rapid cooling (ii) allows for more of the carbon to form in the diamond phase. (Reprinted from ref 17. Copyright 2007 The Royal Society.)

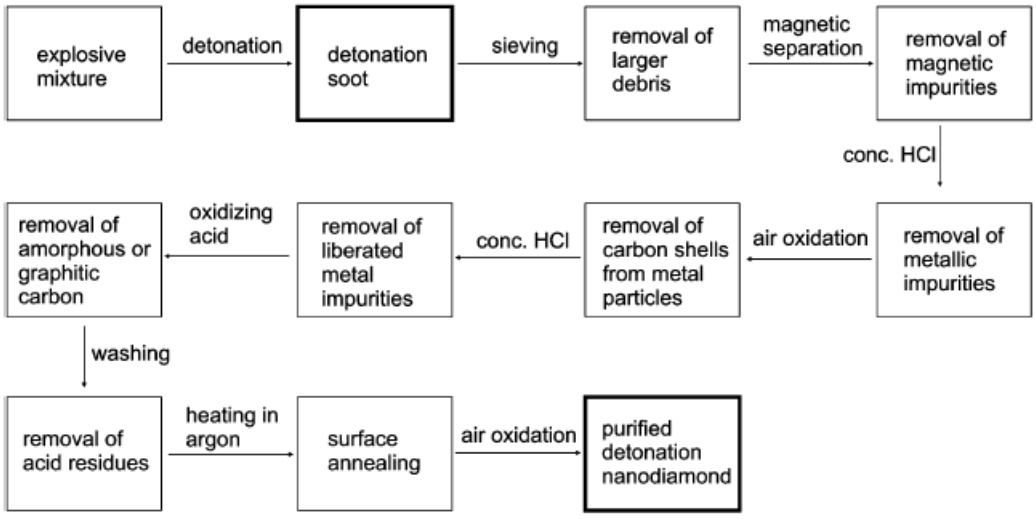

Figure 2.2 Typical processing steps to yield high-purity detonation nanodiamond. (Reprinted rom reference 16. Copyright 2008 Royal Society of Chemistry.)

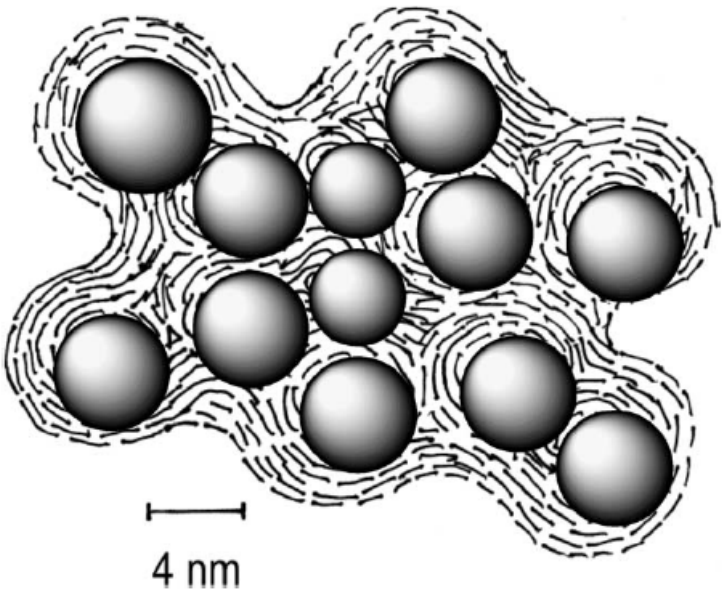

Figure 2.3 The graphitic/soot structure that aids in diamond aggregation. (From ref 22. Copyright 2005 Elsevier Ltd.)

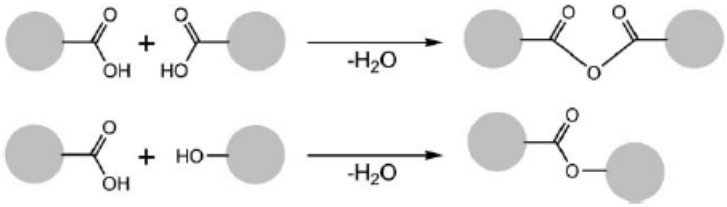

Figure 2.4 Examples of reactions that lead to inter-particle covalent bonding. (Reprinted from ref 24. Copyright 2005 Elsevier Ltd.)

Very recently, Banard, *et. al.*, have proposed that the unusually strong aggregation of primary nanodiamond particles can be attributed to electrostatic forces.[25, 26] Banard employs computational methods to determine the electrostatic potential of the faces of a primary nanodiamond particle. Through the results of this study, the (100) facets are assigned a high positive electrostatic potential and the (111) facets are assigned a negative electrostatic potential, having a strength determined by the degree of

graphitization (see Figure 2.5).[25] When many of these particle are brought together in an anhydrous environment, as expected during the particle synthesis, coulombic attraction between facets on multiple particles will cause the nanodiamond to aggregate, as shown in Figure 2.6.

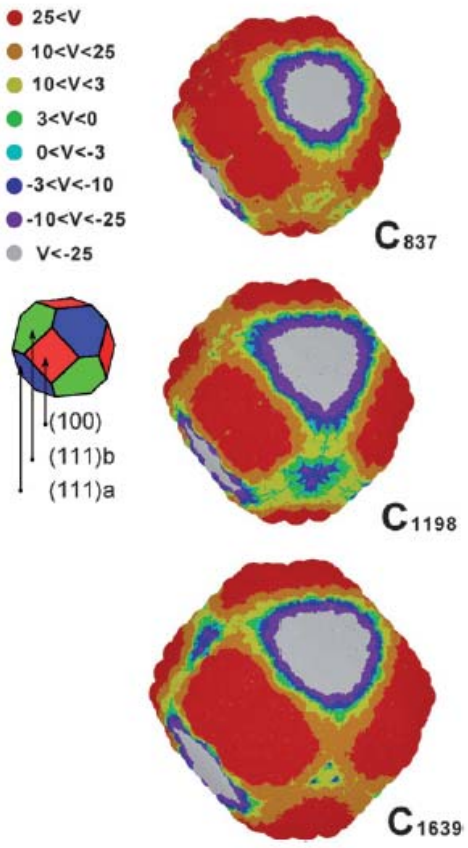

Figure 2.5 Computational simulation of nanodiamond surface showing strong and diverse electrostatic potentials on the facets. (Reprinted from reference 26. Copyright 2008 Royal Society of Chemistry.)

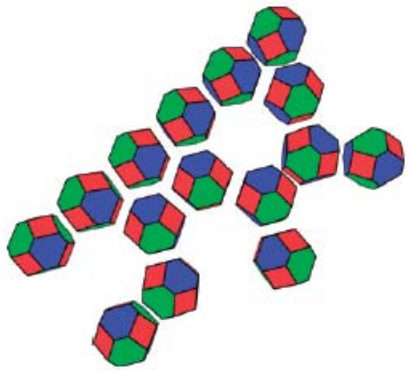

Figure 2.6 Facets of opposing electrostatic potential interact to form nanodiamond aggregates. (Reprinted from reference 26. Copyright 2008 Royal Society of Chemistry.)

Osawa *e.t al.* have raised concerns about the limitations of current theories for nanodiamond aggregation.[27] In the case of electrostatic potentials, the attractive forces are only sufficient if inter-particle distances are very small; the particles must be very well matched in facet size to produce aggregates as tightly bound as experimentally observed. Furthermore, coordinated orientation of many hundreds of primary particles would take a significant amount of time to occur.[27] A second possible explanation, that a graphitic shell binds the primary particles into UDD also presents challenges. For an encompassing graphitic shell, the non-diamond "impurities" may be oxidized away by a number of techniques, yet tightly bound aggregates remain. A third possible mechanism, inter-particle covalent bridging, is hindered by the fact that many bonds must exist simultaneously to achieve sufficient binding energy. If only a few covalent bonds are present between two particles, the C-C or C-O bonds could be broken during ultrasonic processing, which is not observed.

2.3 Methods of De-aggregation

To date, there is only one established method of de-aggregating nanodiamond particles to produce solutions of monodisperse, primary nanodiamonds.[28] This process is an adaptation of stirred-media milling. The grinding media consists of micron-sized ceramic spheres that, when agitated, break down a dispersion of UDD into single nanodiamond particles.

The use of ceramic grinding media is common in industrial scale processes. In the specific case of nanodiamond, introduced by Osawa *et al* in 2005, the ceramic media is yttrium-stabilized zirconia spheres under 100 microns in diameter.[22, 29]

The process described by Osawa is as follows: A zirconia mixing chamber is loaded to about 80 volume percent with zirconia grinding media and a dispersion of aggregated nanodiamond (UDD) with a polar organic solvent. The slurry and grinding media are agitated by spinning a paddle at high speeds through the mixture for a period of time. A solution of de-aggregated nanodiamond is removed from the milling chamber.

A second method, known as Bead Assisted Sonic Deaggregation (BASD) was developed shortly after the stirred-media milling method was published.[30] This method of particle aggregation employs the same ceramic media, but the system is energized by an ultrasonic horn immersed in the target slurry. Figure 2.7, below, illustrates the two methods of de-aggregation.

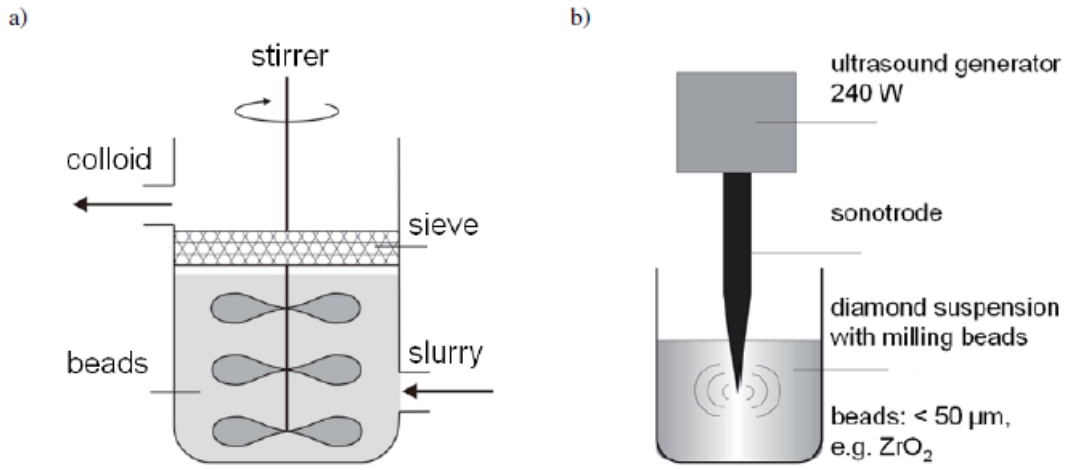

Figure 2.7 Two methods of nanodiamond deaggregation. Stirred-media milling (a) and Bead Assisted Sonic De-aggregation (b). (Reprinted from reference [31] . Copyright 2007 Wiley-VCH.)

2.4 Mechanism of De-aggregation

In both stirred-media milling and Bead Assisted Sonic De-aggregation, the principle that converts UDD into ND is the same; micron-sized balls of high density are caused to collide with each other in a solution of diamond aggregates and organic solvent. As the beads collide, kinetic energy is transferred to the diamond aggregates. These collisions are shown in Figure 2.8. The interfacial region between the diamond aggregates is weaker than the diamond cores and will break apart as a result of kinetic energy transfer.

The de-aggregation process is successful in spite of the large size difference between the particles. It is interesting that spheres with a 50 µm diameter are successful at interacting with 5 nm diamond particles, four orders of magnitude smaller. The grinding media is very smooth and could have a surface roughness that approaches the size scale of primary diamond particles. Conversely, the ceramic beads may be crushing only the larger aggregates, which are often hundreds of nanometers in diameter. As these

aggregates break down, they may act as a grinding media on other aggregates. The attrition of particle size will continue until the particles reach the size of the primary diamond particles. Because the interfacial region between ND particles is weaker than the well-ordered diamond cores, the aggregates will break apart before the diamond cores are crushed.

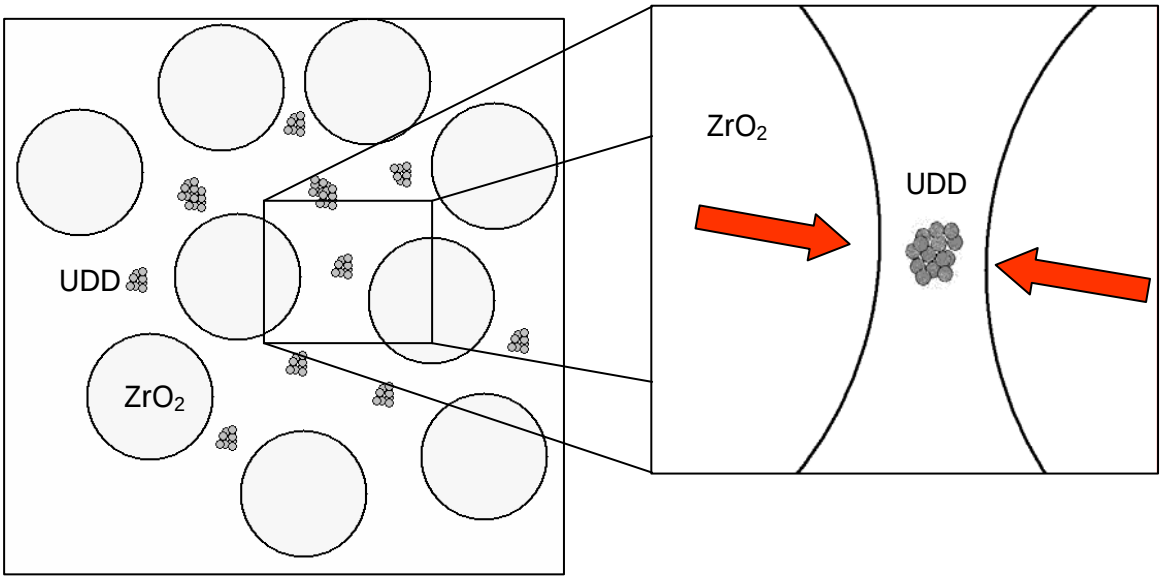

Figure 2.8 A conceptual depiction of the bead-assisted de-aggregation processes. A slurry of zirconia spheres and UDD:DMSO solution is agitated. The UDD is occasionally caught between colliding media, thereby broken apart (ND).

2.5 Drawbacks or Limitations of De-aggregation Processing

Developing a method to de-aggregate UDD into ND is critical to progress the developing technology of nanodiamond composites. These two methods of de-aggregation, however, possess certain limitations that must be mentioned. Like all attrition processes, some contamination from the grinding media is inevitable. The stabilized zirconia particles are chooses because of zirconia's slow wear rate. Earlier

attempts using silica media showed levels of contamination of about 4.9 mass percent.

Furthermore, the BASD method is suitable only for small sample volumes. The de-aggregation process requires that the grinding media posses significant kinetic energy; Osawa's de-aggregation device agitates the zirconia grinding media at 10 cm/s to achieve dispersion.[29] The high-power sonic horn is capable of accelerating the media to these speeds only in small volumes.

The most significant limitation, which is likely independent of de-aggregation method, is the low concentration ceiling and specific solvent requirements. The nanodiamond particles must be carried in a polar solvent, with water and DMSO being the best known solvents. This limitation is attributed to the electrostatic potential discussed above and DMSO's role as a strong hydrogen-bond acceptor.[27, 30] Furthermore, common solvent-exchange techniques, dialysis for example, are not useful, because the nanodiamond will flocculate and fall out of solution with less-polar solvents. When planning subsequent reactions or processing steps, care must be taken to assure good chemical compatablity with the dispersing solvent.

The concentration of UDD in DMSO is limited in practice to well under 10 weight percent. Above this concentration, the de-aggregated nanodiamond forms a gel state and the viscosity increases substantially. Even with a significantly higher density, the zirconia media is slow to settle out of the solution when such a high viscosity is present in the resulting ND:DMSO solution. Furthermore, driving off the solvent entirely results in a re-agglomeration of nanodiamond, and sonication is insufficient to re-disperse the nanodiamond particles, even when using DMSO.

There is a final limitation of this approach to de-aggregation that must be considered; there is a possibility that, during processing, some portion of the diamond conerts to graphite. Such high-energy processing may provide sufficient energy to transform surface carbon atoms from a diamond structure to a graphitic structure. The grinding media has a high density and is agitated to relatively high speeds; there is a good deal of kinetic energy that must be dissipated in grinding media collisions. Breaking the inter-particle bonds of UDD aggregates absorbs some of this energy, but a significant portion is transformed into heat. Macroscopically, the de-aggregation chamber often experiences a rise in temperature in excess of 40°C; typically some form of cooling is employed. Locally, the temperature rise may be much more significant, placing the carbon atoms in a high-temperature, low-pressure environment. The local temperature rise can predicted using Equation 2.1:[29]

$$\Delta T = \left(\frac{\rho_{Zr} v_{Zr}^2}{2C_{Zr}\rho_D}\right)\left(\frac{R}{r}\right)^3 \tag{2.1}$$

where ρ_{Zr}, v_{Zr}, C_{Zr}, and R are the density, velocity, heat capacity, and radius of the grinding media, respectively. r and ρ_D are the size and density of the diamond particles, respectively. The required velocities are on the order of 0.1 to 10 cm/s, which is likely achieved in the de-aggregation processes described earlier.[29] Diamond converts to graphite at around 1000°C, a temperature that may be attained locally for brief periods during de-aggregation processing.

2.6 Experimental Evidence of Nanodiamond De-aggregation

After the successful de-aggregation of UDD was reported using stirred-media milling and Bead Assisted Sonic Deaggregation, it was hypothesized that the de-aggregation could be achieved using other methods to impart energy to the grinding media. A purpose-built de-aggregation device was designed and constructed specifically for the purpose of de-aggregating detonation nanodiamond. By employing novel means of achieving grinding media agitation, a de-aggregation process was developed that is efficient in terms of processing time and specific capacity (grams of UDD processed per gram of grinding media). The device constructed for UDD de-aggregation can process 10 mL of a 5 wt percent UDD:DMSO slurry into a ND:DMSO solution in approximately 20 minutes. Macroscopically, the UDD:DMSO slurry begins the process light gray and in a matter of minutes is transformed to a dark gray then black solution (Figure 2.11).

De-aggregation of UDD is determined by employing dynamic light scattering (DLS) to measure particle size distribution. Briefly, DLS is based on the principle that particles much smaller than the wavelength of light can scatter incident light, as is the case of Rayleigh scattering. These particles, in solution, are constantly moving due to Brownian motion. This movement can be correlated to the light scattering, and Brownian motion affects smaller particles more than larger particles. Combining these facts, particle size distributions can be measured from the light scattering profile. For this work, particle size distribution was determined using a Malvern ZetaSizer Nano ZS with a 633 nm laser. Figure 2.9, below, provides confirmation that the de-aggregation process is successful.

Macroscopically, several marked differences exist between UDD and ND. The most distinguishing characteristic that differentiates UDD from ND is the differences in optical properties. Figure 2.10, below, is a photograph of solutions of both UDD and ND dispersed in DMSO. The cuvette containing de-aggregated nanoparticles is transparent and displays a reddish-brown coloration. The transition from opaque to transparent indicates that the diamond particle size is smaller than the wavelength of light.

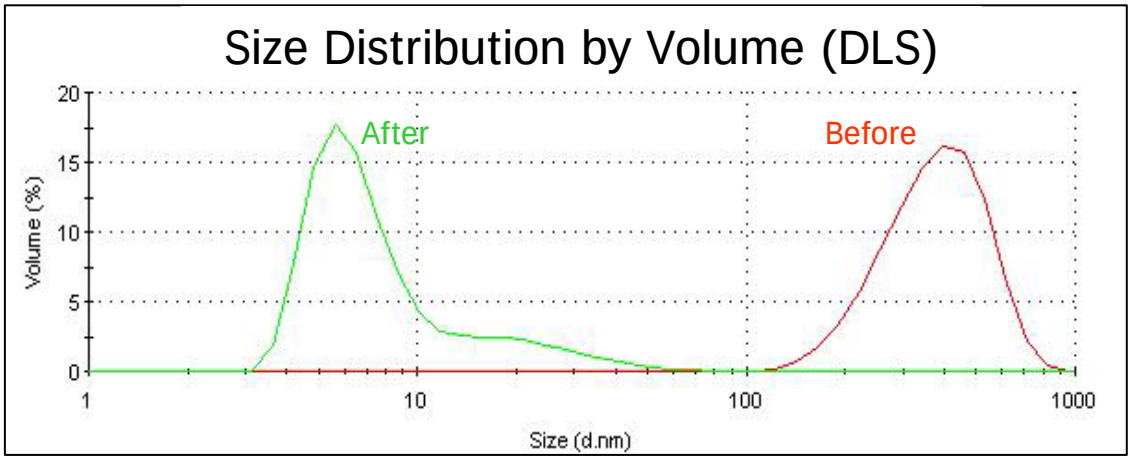

Figure 2.9 Particle size distributions for UDD and ND in DMSO as measured by DLS. The dispersed, ND sample (green line, left) is after 25 minutes of de-aggregation treatment.

The apparent "color" of solutions of nanodiamond in DMSO is strongly dependent on concentration and path length. The solution becomes black at concentration above about 3.0 weight %, but thin films or thin layers of solution are transparent. In Figure 2.11, the high concentration solutions have appear black. This darkening color effect is attributed to Rayleigh scattering,[30] but may also be a molar absorptivity effect due to the presence of graphitic content on ND surfaces. The requirement that $d << \lambda$, where d is the particle diameter and λ us the wavelength of light,

is certainly met in the case of solutions of dispersed nanodiamond, where the majority of particles are under 10 nm in diameter.

Figure 2.10 Solutions of UDD (left) and ND (right) in DMSO. The concentration of each sample is approximately 0.25 weight %.

The reason for the presence reddish-brown coloration, however, is still under debate. Natural diamonds have a brown coloration as a result of defects within the crystal structure. Nitrogen doping of CVD diamond also can result in a brownish color.[32] Both of these conditions, disordered core crystal structure and high levels of nitrogen impurities are expected to be prevalent in detonation nanodiamond and therefore must be considered as possible color centers.

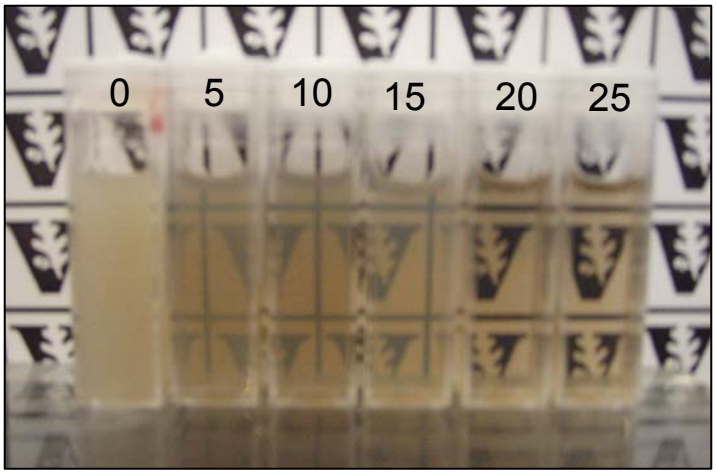

(a)

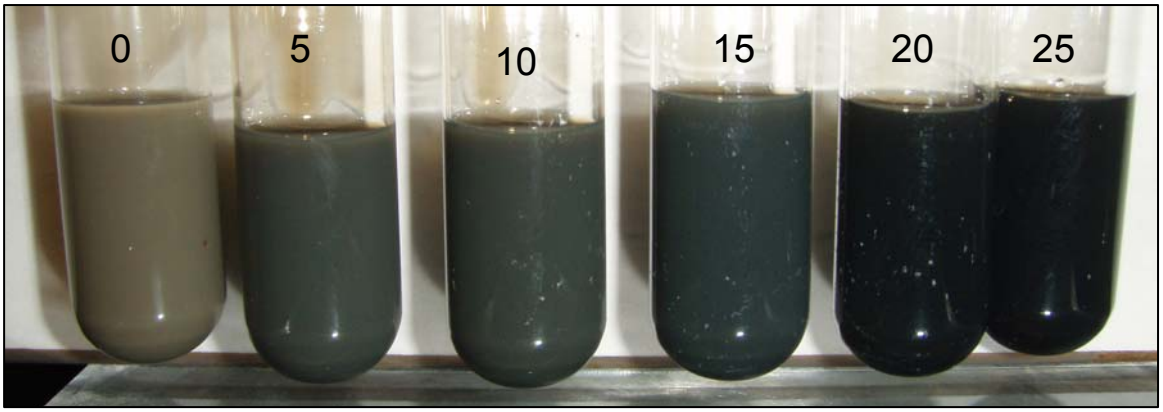

(b)

Figure 2.11 Low concentrations of nanodiamond in DMSO as a function of de-aggregation time (number above each solution corresponds to length of de-aggregation treatment). At 0.1 wt% concentration (a), the change in transparency is apparent; at 4.0 wt% concentration (b), the dark color becomes apparent.

An explanation of the color would not be complete, however, without considering aromatic carbon structures. Solutions containing oxidized sheets of graphene have the same characteristic, reddish-brown coloration.[33] Banard's computational studies of single-nanodiamond particles have suggested that the carbon atoms at the (111) facets of single nanodiamond particles relax into graphitic, sp^2-bound structures.[26] The UDD

powders are subjected to aggressive oxidation steps in order to remove non-diamond carbon[15], so it is reasonable to assume that a significant portion of the nanodiamond surface consists of an oxidized graphitic material. Interestingly, researchers studying graphene oxide solutions can affect a color change from reddish-brown to black by reducing the graphene oxide back to graphene.[33] Unfortunately, the only reports of a dispersion of nanodiamond with reduced surfaces does not make mention of a noticeable shift in color upon surface reduction.[16]

2.7 Examples of Nanodiamond De-aggregation

Detonation nanodiamond can be deaggregated and dispersed into a variety of liquids. In general, 5 mL of UDD and solvent is placed in a 10 mL vessel along with approximately 5 mL of ZrO_2 ceramic grinding media (Figure 2.12). The sample vessel is sealed with a rubber septum and subjected to a proprietary agitation process for varying lengths of time. The sample vessel is then removed from the agitation device and placed aside for 10 minutes to allow the dense ceramic media to settle to the bottom of the sample vessel. The supernatant, which comprises ND and a carrier solvent, is recovered and fresh UDD/solvent is added to the sample vessel. The following are examples of successful de-aggregation dispersions.

2.8.1 ND:DMSO

In a 50-mL round-bottom flask, 1.0 grams of UDD, as received, and 19 grams of dimethyl sulfoxide (DMSO) is added. The solution is shaken by hand vigorously for one

minute, then sonicated in a Branson 2510 bath sonicator for 30 minutes at room temperature. In 5 mL increments, the UDD:DMSO slurry is subjected to de-aggregation processing for 25 minutes. The recovered ND:DMSO solution, now black, is placed in a 15 ml centrifuge tube and again sonicated for 30 minutes.

Figure 2.12 A 10-mL de-aggregation vessel charged with approximately 5 mL of ZrO2 grinding media and sealed with a rubber septum and copper wire.

2.8.2 ND:DER 736

Dispersions of ND can also be achieved in low viscosity epoxy resins. In this case, the Dow Epoxy Resin 736 (DER 736) will be used as an example.

In a 50-mL round-bottom flask, is added 0.50 grams of UDD, as received, and 19.50 grams of DER 736. The solution is shaken vigorously for one minute, then sonicated in a Branson 2510 bath sonicator for 30 minutes. 5 ml of the gray solution is added to the sample vessel and mounted in the de-aggregation machine. The solution, now dark brown to black, is removed after 25 minutes of processing and placed in a 15 ml centrifuge tube. The solution is again sonicated for 30 minutes, yielding a dark brown, but transparent solution.

A photograph of such a solution, diluted to 0.50 weight percent, is shown in Figure 2.13.

Figure 2.13 A 0.50 weight percent ND solution dispersed in DER 736 epoxy resin. The Vanderbilt logo is visible through the 1-cm thick cuvette.

2.8.3 ND:Glycidol

Nanodiamond can also be dispersed in reactive monomer, such as glycidol. This system is useful for further chemical processing and surface derivitization. Characterization of this material combination is discussed in Chapter 3.

2 grams of UDD, as received, are loaded into a quartz boat and placed in a tube furnace and heated under air for 2 hours at 415°C for 2 hours. 0.90 grams of the oxidized UDD (UDD-COOH) and 29.1 grams of glycidol are placed in a 50 ml round-bottom flask. The solution is shaken vigorously for one minute, then sonicated in a Branson 2510 bath sonicator for 30 minutes. 5 ml of the gray solution is added to the sample vessel and mounted in the de-aggregation machine. The solution, now dark brown to black, is removed after 45 minutes of processing and placed in a 15 ml centrifuge tube. The solution is again sonicated for 30 minutes, yielding a dark, but transparent solution.

2.8.4 Nanodiamond dispersed in non-polar liquids

Thus far, the examples have involved dispersing nanodiamond into polar liquids. Presented here is a synthesis method employed to disperse nanodiamond in non-polar liquids. A detailed discussion of this material system is found in Chapter 3.

In a 100-mL round-bottom flask, 2.0 grams if UDD-COOH, 48 ml of octane, and 1.0 ml of oleic acid are combined. The flask is placed in an ultrasonic bath for 40 minutes. The solution is subjected to the de-aggregation process for 40 minutes, then removed to a second 100 ml flask, where it is sonicated for an additional 60 minutes, yielding a transparent, dark colored solution.

2.8.5 ND:Styrene

As in the example above, the addition of a surface agent can improve the dispersion of nanodiamond in liquids that would otherwise be considered poor carriers for dispersed nanodiamond. In this case, a silane coupling agent, vinyltrimethoxysilane (VTMS), is used to facilitate dispersion in a reactive monomer, styrene. Detailed characterization of this materials system is provided in Chapter 5.

In a 200-mL round-bottom flask, 2.50 grams of UDD-COOH and 95 grams of styrene are combined and sonicated for 10 minutes. 2.0 mL of VTMS is added and sonication continues for 30 minutes. In 5-mL batches, the solution is de-aggregated for 55 minutes per batch. The solution is placed in a second 200 ml flask and sonicated for 45 more minutes.

2.8.6 ND:DMF

This example is similar to example 2.8.5 in its use of a silane coupling agent, but here the carrier solvent is dimethylformamide (DMF). Discussion and characterization of this system is found in Chapter 5.

In a 100-mL round bottom flask, 1.21 grams UDD-COOH and 42 ml DMF are combined and sonicated 30 minutes. 0.60 ml VTMS is added and sonication continues for 30 minutes. The solution is subjected to de-aggregation for 60 minutes per 5-mL batch. The now dark ND-VTMS:DMF solution is placed in a second 100 ml flask and sonicated for 45 minutes.

CHAPTER III

NANODIAMOND NANOFLUIDS FOR ENHANCED THERMAL CONDUCTIVITY

3.1 Introduction

Heat-transfer fluids such as water, mineral oil, and ethylene glycol serve important functions in many thermal transport applications but suffer from low thermal conductivity. The efficiency of fluid thermal systems could be enhanced substantially if the thermal conductivity of the working fluid could be increased. Incorporating small solid materials, which have substantially higher thermal conductivity than the fluid, into liquids was shown by Maxwell to improve the thermal conductivity of the host liquid.[34] Adding micron-sized particles to a fluid, however, presents several drawbacks including the need for increased pumping power, clogging narrow channels, erosion of the pipe walls, and rapid settling of the particles.

Recently, interest has emerged in using liquid systems with dispersions of nanometer-sized solid materials. This combination of materials was termed "nanofluids" by Choi in 1995.[35] Reports of experimental data have shown great potential; adding less than one volume percent of nanoparticles has led to double-digit percentage enhancements if thermal conductivity.[36] Conversely, other researchers have reported no anomalous enhancement effect.[37] As an emerging field of study, both the magnitude of these enhancements in the thermal conductivity and the mechanisms responsible continue

to be a topic of debate. Factors among consideration include Brownian motion, radiative heat transfer, interfacial layering, and particle aggregation.[38, 39]

Similar to nanocomposites, investigating nanofluids requires researchers to overcome challenges specific to nanometer-scale materials. The nanomaterial must be well dispersed and stable in the base fluid. In addition to specialized processing techniques, often surface functionalization or the use of surfactants is required to achieve a high-quality colloidal dispersion.

A variety of low-aspect ratio nanomaterials have been studied; metals such as copper[40], silver[41], and gold[39], as well as oxides such as copper oxide[42], alumina[43], and titania[41]. Diamond has several material properties that are attractive for application in nanofluids: very high thermal conductivity, high hardness, relatively low density, and very low electrical conductivity. UDD, produced by the detonation of explosives in an oxygen-deficient chamber,[15] is a readily available source of diamond nanomaterials.

Studies of UDD dispersions in ethylene glycol and various oils have been recently reported.[18, 44-46] These reports, however, state that aggregates of nanodiamond were used as the solid phase. This chapter focuses on the fabrication and thermal characterization of two novel nanofluids comprising of highly-dispersed nanodiamond particles in either ethylene glycol or mineral oil base fluid.

3.2 Experimental

UDD was obtained from Alit Corp (Kiev, Ukraine) and heated for two hours in a 415°C tube furnace under flowing air to increase the carboxylic acid functionality.[47] Glycidol, dimethyl sulfoxide (DMSO), oleic acid, stearic acid, lauric acid, and octane

were purchased from Sigma Aldrich (St. Louis, MO) and used as received. Ethylene glycol, and light mineral oil were purchased from Fisher Scientific (Pittsburg, PA) and used as received.

UDD was dispersed in the chosen solvent by ultrasonic bath using an Branson 3510 benchtop sonicator. Particle size analysis was performed using a Malvern Instruments Zetasizer. Surface functionalization of the nanodiamond was determined by thermogravimetric analysis using a TA Instruments 2950 Thermogravimetric Analyzer with a heating rate of 10°C min^{-1} and by Fourier Transform Infrared Spectroscopy on a Thermo Mattson Satellite FTIR. Nuclear Magnetic Resonance spectroscopy was performed with a Bruker NMR spectrometer operating at 400 MHz. Samples were dispersed in deuterated benzene. Thermal conductivity measurements were performed with a Decagon Devices KD2 Pro, which was calibrated against a sample of glycerol with known thermal conductivity. The single hot-wire probe was immersed in 150 mL of sample with at least 2.5 cm of separation between the probe and sample container. For each concentration and temperature data point, at least ten measurements were recorded with an hour between each test to ensure the sample was at thermal equilibrium.

It is important to mention that the control specimens received the same processing treatment as the nanofluid samples; the carrier solvent was added to the base fluid then evaporated out at reduced pressure in a rotary evaporator with a water bath set at 80°C. This step was included in order to remove any affect that residual solvent could have on both viscosity and thermal conductivity.

Preparation of ND:Ethylene Glycol Nanofluids

A 200 mL flask was charged with 2.0 grams of oxidized UDD and 48.0 grams of DMSO. The gray solution was placed in an ultrasonic bath for 30 minutes, then subjected to a de-aggregation treatment until the UDD aggregates had been broken down to primary ND particles.[22, 29] The ND:DMSO solution was placed in a 200 mL flask with 50 mL glycidol and magnetic stir bar, then sealed with a rubber septum. The flask was placed in a 50°C oil bath and the solution was stirred vigorously under N_2 for 24 hours. The solution was removed from the bath, allowed to cool to room temperature, then placed in a dialysis bag immersed in de-ionized water. The water wash was changed every 12 hours for four days to remove unbound glycidol monomer and solvent.

The ND-glycidol:H_20 dispersion was combined with an appropriate amount of ethylene glycol and placed in an ultrasonic bath for 20 minutes. The solution was then placed in a rotary evaporator under reduced pressure and elevated temperature until it was observed that liquid no longer formed on the condenser unit of the evaporator apparatus.

Preparation of ND:Mineral Oil Nanofluids

A 200 mL round bottom flask was charged with 2.0 grams of UDD, 2.0 grams oleic acid, and 63 grams of octane. The light-gray solution was placed in an ultrasonic bath for one hour. The solution was then subjected to a de-aggregation treatment. This solution of de-aggregated nanodiamond, now black but transparent, was combined with an appropriate amount of mineral oil and sonicated for an additional hour. The solution

was placed in a rotary evaporator under reduced pressure and elevated temperature until liquid was no longer observed condensing within the unit's collector.

3.3 Results and Discussion

Particle size distributions are shown (Figure 3.1) for solutions of UDD in DMSO, ND in DMSO. The as-received UDD has a particle size range from tens of nanometers to two microns. The de-aggregated nanodiamond has a particle size peak under 8 nm, which correlates well with the size of the primary particles[2] and shows a dramatic reduction in size from as-received UDD. A second particle size analysis of the ND-glycidol:ethylene glycol dispersion performed after functionalization and dialysis washin is shown in Figure 3.2a. These surface-functionalized nanodiamond particles have slightly larger particle size.

The size of the nanodiamond aggregates must be reduced in order to achieve a stable dispersion. Comparing the particle size distribution before and after the de-aggregation process (Figure 3.1a and 3.1b), it appears that the aggregates are effectively broken down to the primary particle size. After surface functionalization with the glycidol monomer, the particle size increases by about 3 nm (Figure 3.2a). Because dynamic light scattering measures the hydrodynamic radius of particles, this slight increase in particle size likely the results from surface functionalization by glycidol oligomers.

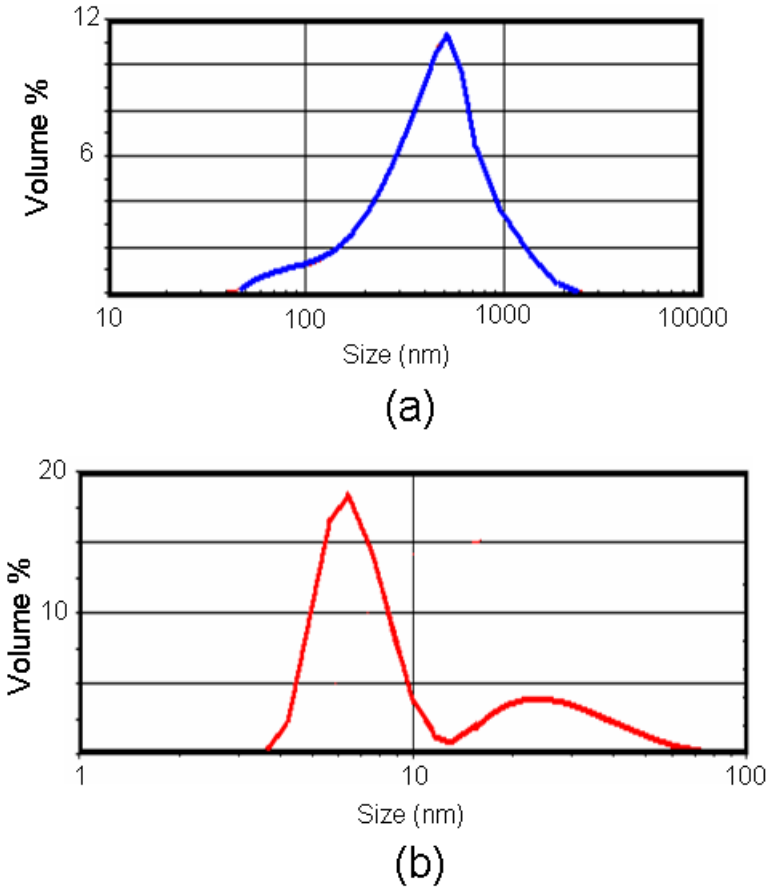

Figure 3.1 Particle size distributions for (a) UDD-COOH and (b) de-aggregated ND:DMSO prior to surface functionalization.

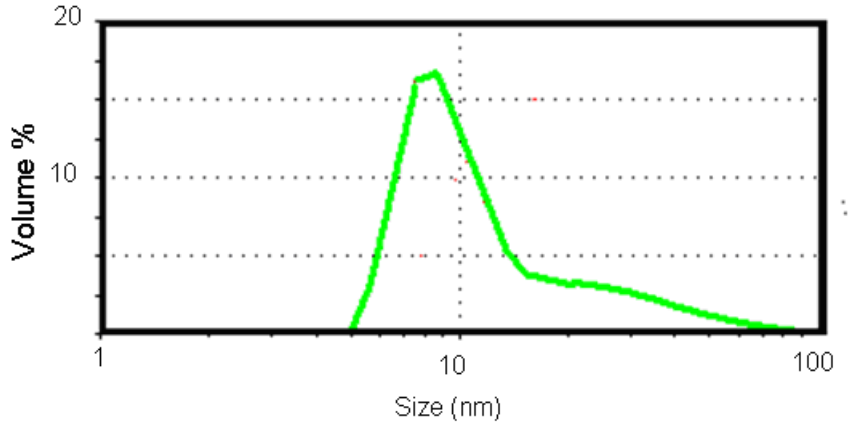

Figure 3.2 DLS particle size distribution of ND-glycidol:H_2O after the surface-functionalization and dialysis steps.

Prolonged particle-dispersion stability, often a challenge in nanodiamond nanofluids[46], requires the use of appropriate surface functional groups for the target fluid. In addition to counteracting particle agglomeration, effective surface functionality is important to achieve good interaction between the nanoparticle surface and the dispersing medium. In the case of nanodiamond, which has a high surface energy and poor dispersion characteristics, some form of surface functionalization is needed to achieve the desired dispersion properties.

For the ethylene glycol nanofluids, covalent surface functionalization with glycidol was employed. The carboxylic acid functional sites present on the nanodiamond surface can serve as ring opening initiators for the glycidol monomer oligomerization.[48] Nanodiamond has been reported to form stable suspensions in polar solvents, but changes in concentration can lead to flocculation.[30] By functionalizing ND nanoparticles with an oligomer or polymer chain, a physical barrier prevents re-agglomeration and improves dispersibility by increasing the presence of hydrophilic hydroxyl groups (Figure 3.3).

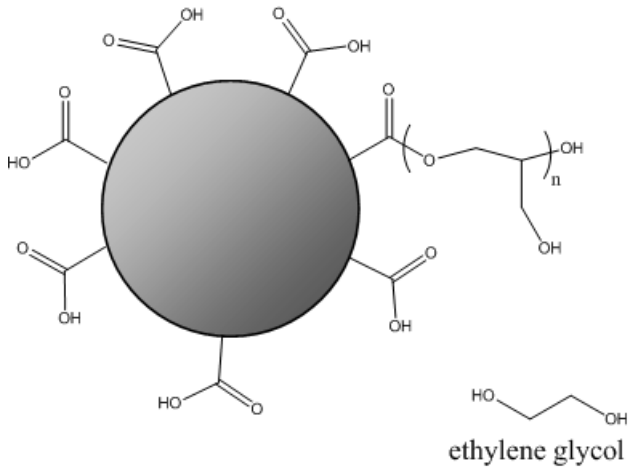

Figure 3.3 Anticipated structure of ND-glycidol:ethylene glycol dispersions.

Thermogravimetric analysis confirms the presence of nanoparticle surface functionalization (Figure 3.4). The ND-glycidol nanoparticles show a mass loss starting at about 300°C, much higher than the boiling point of glycidol. There is no apparent change in mass between the evaporation of the solvent at 100°C and the thermal degradation of the surface groups at about 320°C.

Thermogravimetric analysis confirms a high degree of covalent surface functionalization for the nanodiamond-glycidol material. There is a significant mass loss between 300°C and 400°C, whereas glycidol monomer has a boiling point of only 167°C. It is unlikely that unbound oligomers remain in the dispersion after extensive dialysis washes; these facts suggest that glycidol oligomers are covalently bound to the nanodiamond particles. Furthermore, the amount of mass driven off is substantial; each gram of nanodiamond has more than 3 grams of surface-bound oligomers. Each glycidol chain, however, is likely only a few monomer units in length. Nanodiamond has a specific surface area in excess of 300 $m^2/gram^2$ and acid-base tritration expereiments suggest that the –COOH functional group has a density of 0.0048 mol/g; there are likely hundreds of glycidol chains per nanodiamond particle. If it is assumed that every carboxylic acid functional group serves as an attachment point for an oligomer, then each glycidol chain would have about 8-9 mer units.

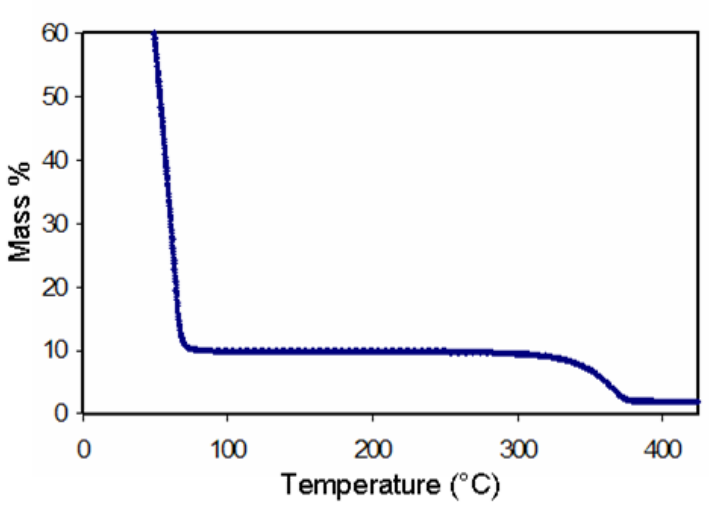

Figure 3.4 Thermogravimetric analysis of ND-glycidol:H_2O nanofluid.

Dynamic light scattering analysis of the mineral oil dispersions could not be obtained because the viscosity of the mineral oil was unknown and not readily measurable. Dynamic light scattering was performed on ND treated with oleic acid surfactant in toluene as a substitute materials dispersion system. A DLS particle size distribution shows a single profile peak at about 18 nm (Figure 3.2b); the increased diameter is consistent with dispersed ND particles having hydrocarbon chains extending from the surface. The solution, however, has a dark brown-black coloration characteristic of de-aggregated nanodiamond solutions (Figure 3.3).[29] Furthermore, the solution appears red at small path length indicative of Rayleigh scattering and serves to confirm that the particle size is much smaller than the wavelength of visible light.

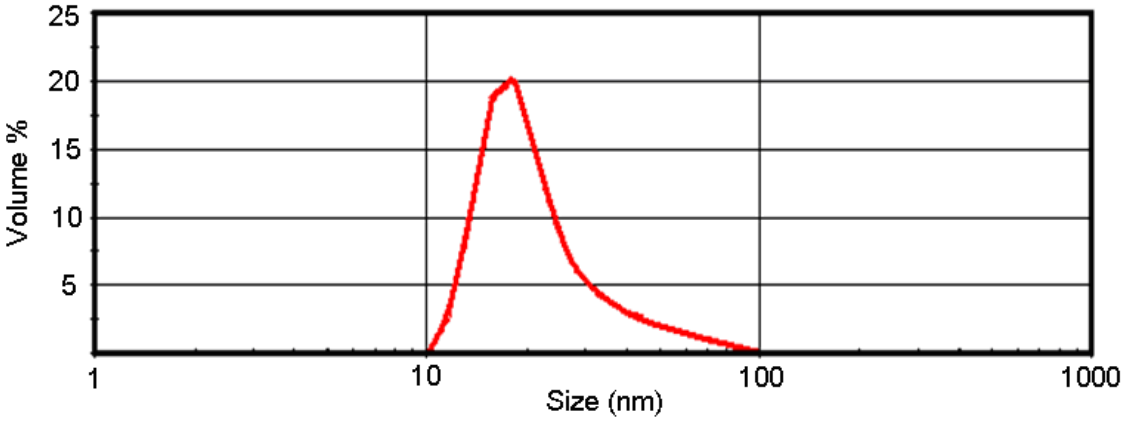

Figure 3.5 DLS particle size distribution for ND•oleic acid:toluene.

Figure 3.6 Photograph of 5 weight percent ND•Oleic Acid:mineral oil disperion. The transparent section on the left has a 1-mm thickness.

Chemical modification is even more critical for achieving stable nanodiamond dispersions in non-polar liquids. Detonation nanodiamond has a poor stability in mineral oil due to the high concentration of oxygen-containing surface groups such as hydroxyls, carboxylic acids, ketones, and ethers.[16] Surface modification to introduce alkyl chains on

the surface of aggregated diamond has been shown to improve nanodiamond stability in non-polar solvents.[49]

Thermogravimetric analysis was used to characterize the quantitiy of organic matter associated with the ND•Oleic acid nanomaterial. Thermograms reveal the mass loss event begins at 150°C and continues until about 490°C. The mass loss represents a functionalization of 60 weight percent. It is important to note that the boiling point for oleic acid is 360°C; mass loss from 150°C to 360°C may be associated with unbound hydrocarbon chains. Approximately half of the mass loss occurs above 360°C, suggesting that the oleic acid surfactant is interacting with the nanodiamond surface.

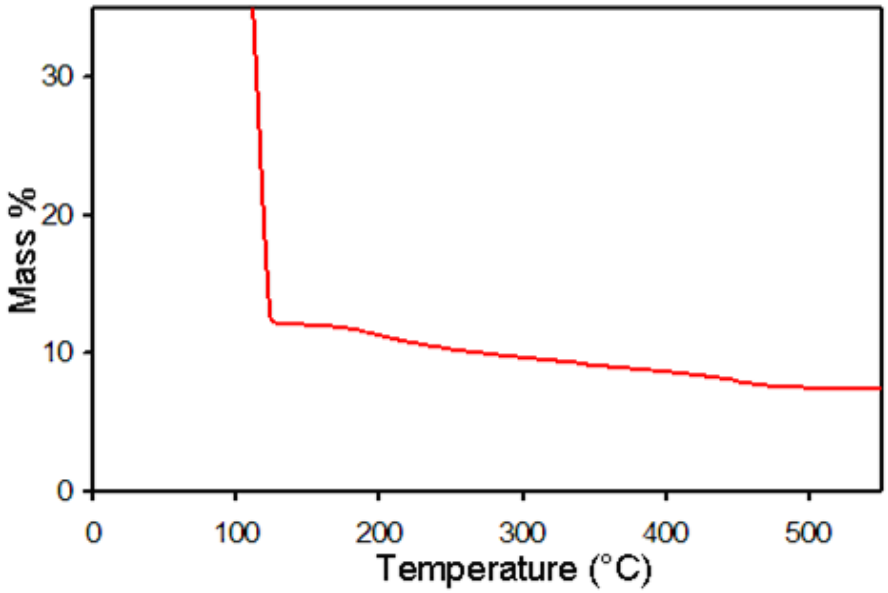

Figure 3.7 Thermogram of ND•Oleic acid:octane nanofluid.

In this study, amphiphilic surfactants were chosen because the surface modification could be performed in parallel with the de-aggregation process. A series of experiments were performed with both cationic and anionic surfactants; octadecylamine (ODA), stearic acid, oleic acid, and lauric acid were selected as surface-modifying agents (Figure 3.5). Though these surfactants will not form covalent bonds, the polar heads of

the surfactants are expected to interact strongly, through hydrogen-bonding, with the carboxylic functional groups present on the nanodiamond surfaces [50]. Of the surfactants studies, only oleic acid surfactants could achieve stable nanodiamond-oil dispersions.

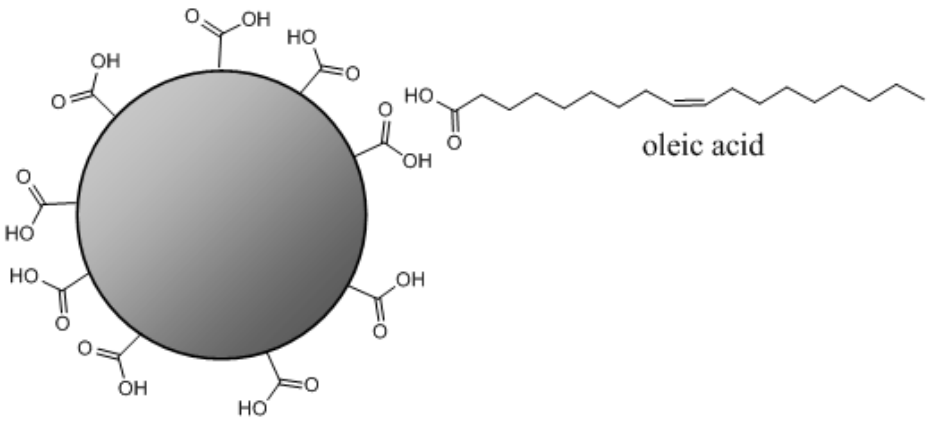

Figure 3.8 Anticipated structure of ND•Oleic acid nanoparticles.

It is not currently understood why ND•Oleic acid nanomaterial displays good dispersion in non-polar media but ODA, stearic acid, and lauric acid were unsuccessful. Stearic acid, lauric acid, and oleic acid each have the same basic structure, a carboxylic acid functional group with a hydrocarbon tail. Hydrogen-bonding between –COOH functional groups present on the ND-COOH surface and the polar functional groups of the surfactant molecules is expected in all three cases. If the dispersibilty was strongly dependent on the molecular weight of the surfactants, then stearic acid would be expected to perform similar to oleic acid. If, on the other hand, dispersibilty depended strongly on the distance the non-polar tail extends into the solvent, then lauric acid would be expected to perform as well as oleic acid because oleic acid has a "kinked" structure due

to the unsaturated C=C bond. The C=C double bond present in the oleic acid, which is the only distinguishing characteristic for each of the two comparisons above, may play a role in achieving good nanoparticle dispersibilty.

For ODA, the dispersibilty issue may be due to less effective hydrogen-bonding between –COOH functional groups on the nanodiamond and the amine polar group of the surfactant. Polar head groups of the surfactant, ODA, are expected to undergo hydrogen-bonding with carboxylic acid sites present on nanodiamond surfaces but dimer structures found in the ND•Oleic acid nanomaterial will not form. This dimer structure may impart necessary additional stability between surfactant and ND-COOH nanoparticle.

Surfactant concentration also influences the stability of the nanofluid dispersion.[50] From base-uptake experiments, the concentration of –COOH groups in ND-COOH was estimated at 4.8×10^{-3} mol/g.[51] If each carboxylic acid present on the nanodiamond surface forms a dimer with an oleic acid molecule, the maximum surfactant loading would be 1.35 grams of surfactant per gram of UDD. Excess surfactant, however, could lead to a bi-layer of surfactant (Figure 3.7) which would counteract particle solubility. To avoid this possibility, only enough surfactant was used to hydrogen-bond with 70 percent of the carboxylic acid functional sites on ND-COOH surfaces. Even at this reduced concentration, there are hundreds molecules of oleic acid present for each primary particle of nanodiamond.

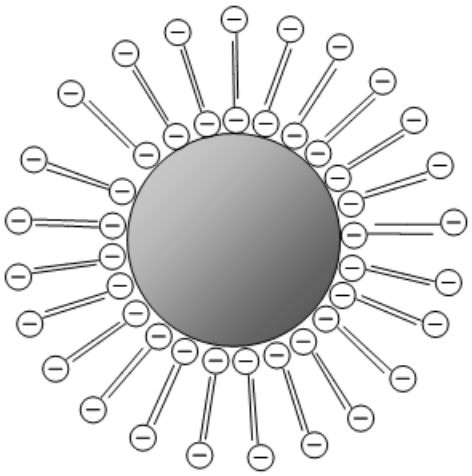

Figure 3.9 Excess surfactant can form a bi-layer structure, which will be detrimental to the solubility of nanodiamond in non-polar liquids.

The presence of oleic acid in the surface functionalization of ND•Oleic acid:octane is further characterized by FT-IR (Figure 3.8). All three spectra show a broad absorption at about 3400 cm^{-1}, attributed to the –OH groups, some of which may likely be absorbed water.[52] The oxidized diamond powder displays an absorption peak at 1770 cm^{-1}, which corresponds to C=O vibrations, indicating the presence of carboxylic acid functional groups.[23, 47] The peak at 1640 cm^{-1} could indicate the presence of C=C bonds, possibly graphitic surfaces of ND-COOH, or –OH groups.[47] Oleic acid displays the expected absorbance at 2930 and 2860 cm^{-1} due to the CH_2 groups.[53] Again, the peak around 1740 cm^{-1} occurs because of the presence of carboxylic acid head groups. Oleic acid is an unsaturated fatty acid, so the presence of a C=C bond vibration is expected; the peak at 1660 cm^{-1} may indicate this. Furthermore, the CH vibrations for alkenes is expected at 3020 cm^{-1}. There is a small peak at this location due to the weak absorptivity and low molar concentration of such bonds in oleic acid.

The nanodiamond particles that have been treated with oleic acid retain many of the IR peaks assigned to the hydrocarbon tail of the surfactant molecules. The peaks at

3020, 2930, and 2860 cm^{-1} are clearly present. The peak at 1710 cm^{-1}, corresponding to the carboxylic acid functional groups of the surfactant, is completely absent. Instead a peak at 1560 cm^{-1} is present; this peak is likely assigned to stretching of the COO- groups. The disappearance of the carboxyl bond vibration strongly suggests that there is no free surfactant and that the head group is chemisorbed to the nanodiamond surface.[19, 53] Finally, the peak at 3020 cm^{-1} remains after the dispersion process. If this peak indicates the presence of alkene functional groups, then its survival through the de-aggregation process would suggest that the oleic acid has not been reduced.

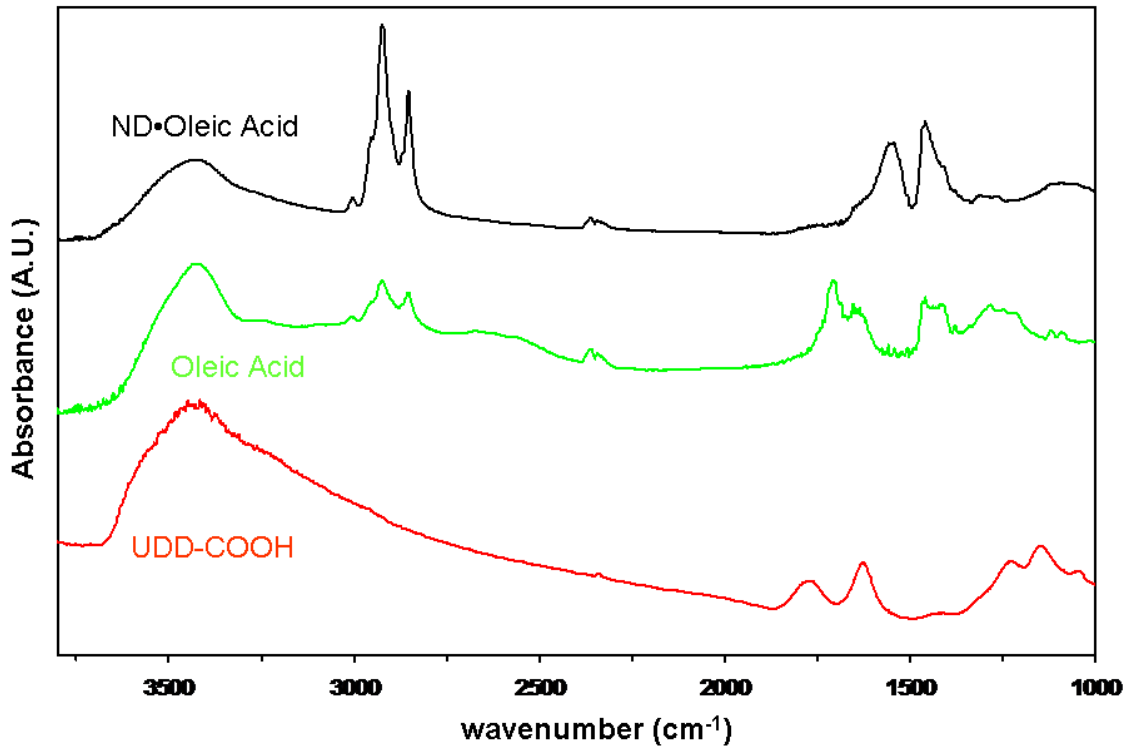

Figure 3.10 FT-IR spectra for oxidized ultradisperse diamond, oleic acid surfactant, and surface treated nanodiamond.

In addition to FT-IR, proton NMR spectroscopy was has been used to characterize the surface functionalization products. Figure 3.9 shows the ^{1}H-NMR spectra for free

oleic acid in deuterated benzene and ND•Oleic Acid dispersed in deuterated benzene. The resonance observed at 1.03 ppm corresponds to the methyl end of the oleic acid molecule. The resonances at 1.46 ppm and 2.31 ppm correspond to -CH_2- groups along the surfactant backbone. The resonance peak at 5.69 ppm is assigned to the vinylic hydrogen atoms. The presence of this peak in the de-aggregated ND sample suggests that the vinyl group survives the de-aggregation process. In addition, the enhanced width of the NMR resonances associated with surface-associated oleic acid molecules is consistent with reduced T_1 relaxation rates expected for chemisorbed molecules.

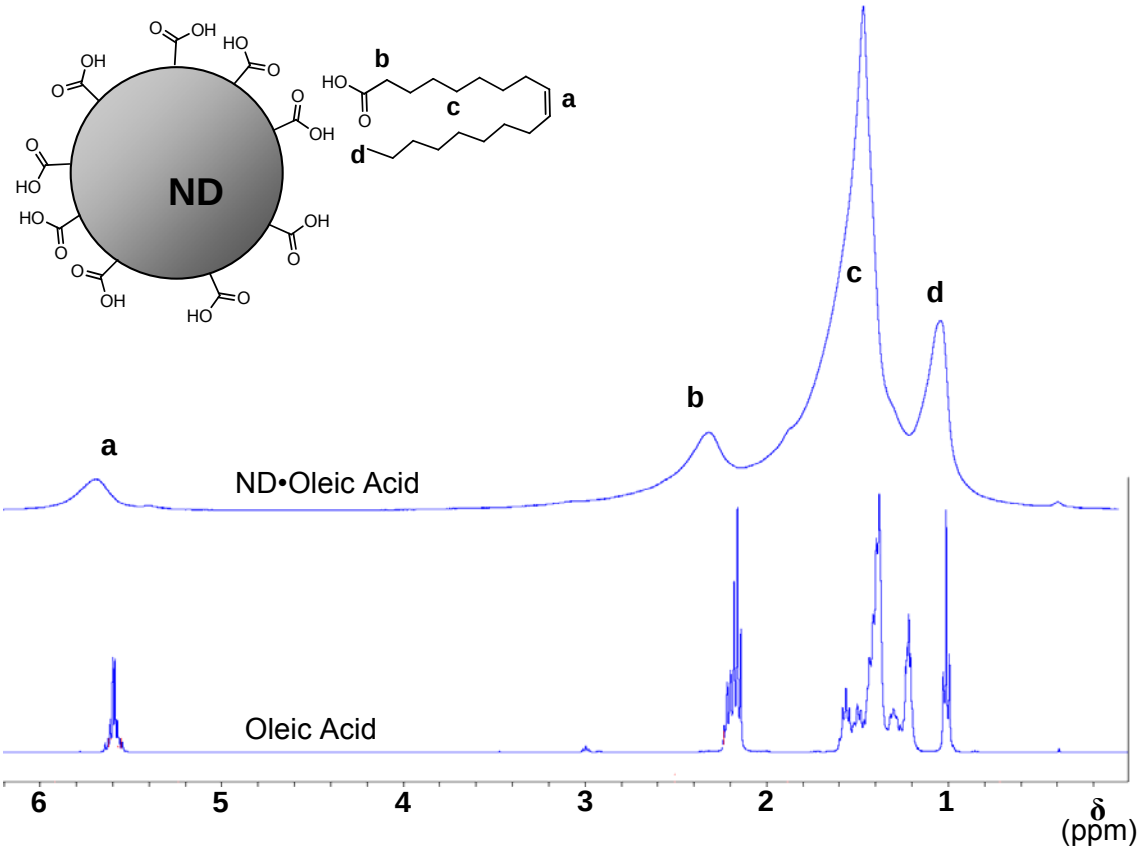

Figure 3.11 NMR spectra for ND with oleic acid surfactant and free oleic acid in deuterated benzene.

The thermal conductivity enhancement of the nanofluids is shown as a function of nanoparticle loading (Figure 3.12). Incorporating nanodiamond into a base fluid improves the thermal conductivity of both the polar and non-polar liquid systems. In the ethylene glycol nanofluids, addition of 0.88 volume percent nanodiamond results in a 12 percent enhancement in thermal conductivity. For the mineral oil, a maximum thermal conductivity enhancement of 11 percent was achieved at a nanodiamond concentration of 1.9 volume percent. The thermal conductivity of the oil-based nanofluids is also plotted as a function of temperature (Figure 3.13) and appear to be temperature-independent.

As expected, incorporating nanodiamond into liquids improves thermal conductivity. In Figure 3.10, the thermal conductivity enhancement is plotted alongside the predicted value using Maxwell's effective medium theory [34], given by:

$$\frac{k_{nf}}{k_f} = \frac{k_p + 2k_f - 2\varphi\left(k_f - k_p\right)}{k_p + 2k_f + \varphi\left(k_f - k_p\right)} \tag{3.1}$$

where k_{nf}, k_f, k_p refer to the thermal conductivities of the nanofluid, the unfilled fluid, and the nanoparticle, respectively, and the volume fraction is given by φ. The thermal conductivity of diamond is several orders of magnitude greater than the fluids studied.[54] In cases where $k_p >> k_f$, such as this, Eq. 1 can be reduced to:

$$\frac{k_{nf}}{k_f} = 1 + 3\varphi \tag{3.2}$$

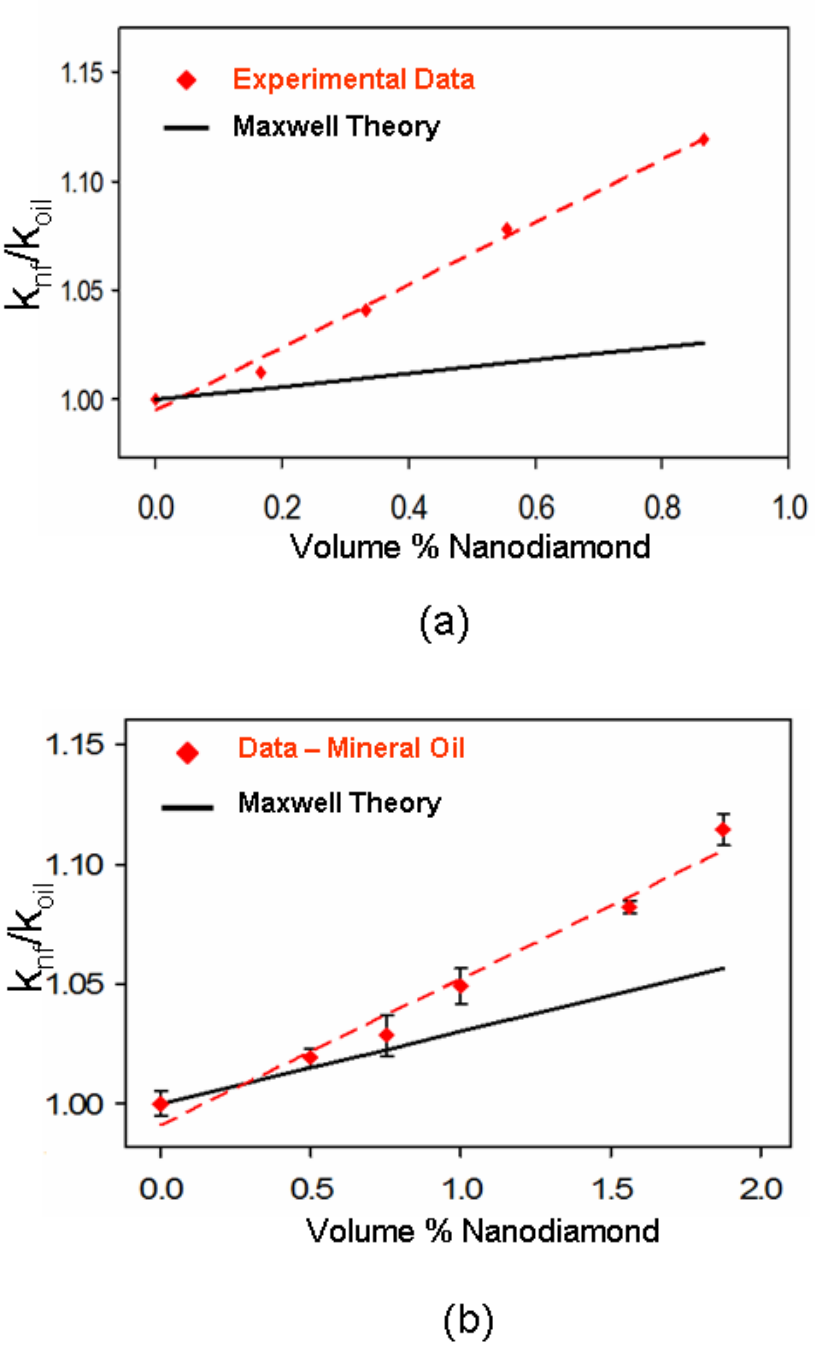

Figure 3.12 Thermal conductivity enhancement as a function of nanodiamond loading for (a) ND-glycidol:ethylene glycol nanofluids and (b) ND•Oleic acid:mineral oil nanofluids.

The experimental data, however, diverge from the theoretical prediction, following:

$$\frac{k_{nf}}{k_f} \approx 1 + 14\varphi \tag{3.3}$$

for the ethylene glycol nanofluids and

$$\frac{k_{nf}}{k_f} \approx 1 + 6\varphi \tag{3.4}$$

for the mineral oil system.

Though this represents a substantial deviation from Maxwell's theory, the data for the nanodiamond-ethylene glycol system shows good correlation to recently reported thermal conductivity data for aggregated nanodiamond.[44] Previous studies of aggregated nanodiamond in non-polar fluids have shown qualitative enhancement of thermal conductivity, but have not provided quantitative values.[18, 46] The nanodiamond-mineral oil system shows a similar enhancement effect to a copper-filled nanofluid.[40]

The enhancement in thermal conductivity is more pronounced in the ethylene glycol nanofluids than in the oil nanofluids by more than a factor of two. Both nanofluid systems use the same nanodiamond material, but the nanodiamond in the ethylene glycol solutions has covalent surface functionalization, whereas the nanodiamond in the mineral oil solutions employs non-covalent surfactants for dispersion. This difference in enhancement efficiency is likely attributable to thermal boundary resistance. It is likely that the surface organic molecules that help disperse the nanoparticles also have good thermal coupling with the host fluid; the thermal resistance occurs at the

organic/nanoparticle interface. The thermal resistance at the interface between the nanoparticle and the fluid can be reduced by improving the coupling between the two phases.[55] Surface agents that are covalently bound to the nanodiamond will have a stronger coupling than surfactant molecules that rely on an ionic or van der Waals interaction. The glycidol-functionalized nanodiamond, with covalent surface functionalization, are therefore more effective additives than the non-covalently functionalized nanodiamond•oleic acid system.

The role of Brownian motion in the enhancement effects of nanofluids remains under debate.[56] An examination of the thermal conductivity enhancement as a function of temperature (Figure 3.11) for the oil-based nanofluids shows that the enhancement is essentially temperature independent. This is of interest because Brownian motion displays a strong temperature dependence if the fluid's viscosity changes with temperature[57], which is certainly the case for oils. If the Brownian diffusion coefficient increases with increasing temperature, we would expect to see increasing enhancement of the nanoparticles at higher temperatures. With no apparent temperature dependence, Brownian motion seems to hold minimal responsibility for the measured thermal conductivity enhancement.

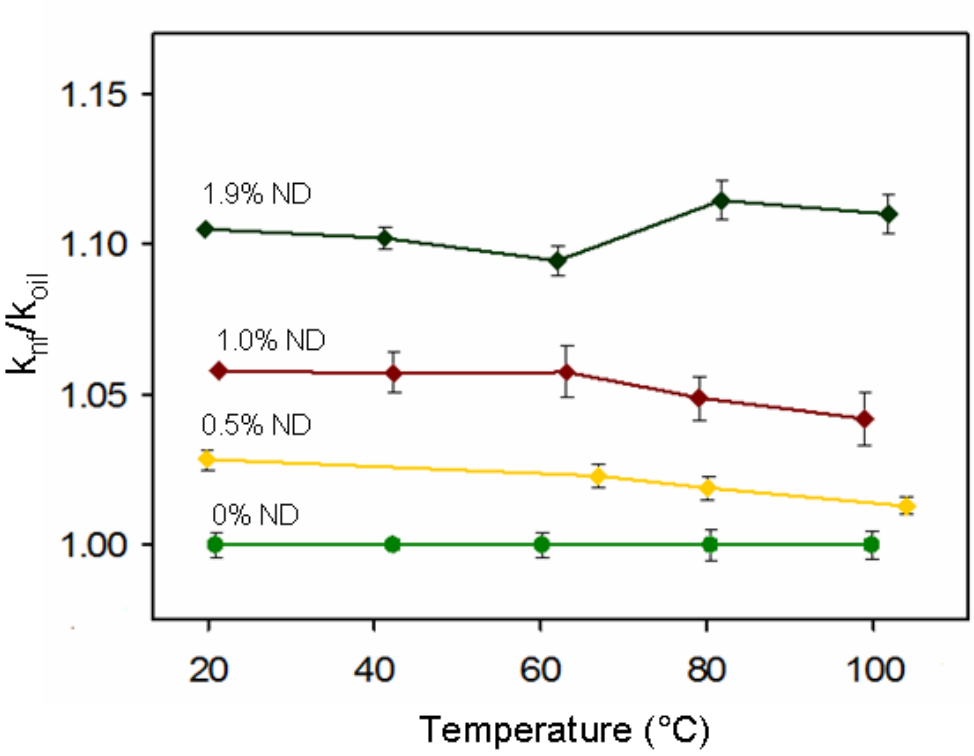

Figure 3.13 Temperature dependence of the thermal conductivity enhancement. Several nanodiamond concentrations are shown for the ND:mineral oil nanofluid system.

3.4 Conclusions

Nanofluids containing diamond nanoparticles have been fabricated and studied. High quality dispersions have been achieved through the use of novel de-aggregation techniques and surface functionalization. The nanodiamond additives enhance the thermal conductivity of both ethylene glycol and mineral oils. The nanoparticles outperform the expected enhancement effect calculated using Maxwell's effective medium approximation. Furthermore, similar concentrations of nanodiamond achieve better enhancement in ethylene glycol than in mineral oil. This discrepancy is attributed to thermal boundary effects that arise when using covalent versus non-covalent surface functionalization methods.

CHAPTER IV

NANODIAMOND NANOCOMPOSITES WITH THERMOPLASTIC MATRICES

4.1 Introduction

Though detonation nanodiamond was first synthesized decades before the discovery of fullerenes or carbon nanotubes, diamond nanomaterial has been the subject of far fewer investigations for use in composite materials.[2, 12] Detonation nanodiamond has a small primary particle size of 4-5 nm, extremely high modulus, and a high specific surface area amenable to chemical functionalization.[2, 17, 47] These characteristics make ND an ideal nanoscale filler for advanced composite materials.

A limited number of diamond-polymer nanocomposites have been reported. Nanodiamond was initially incorporated into rubbers and lubricants for increased wear resistance and functionality[15]. Recently, renewed interest in ND composites has emerged. Nanodiamond has been incorporated into polydimethylsiloxane[58], electrospinning was used to fabricate polyacrylonitrile composites[59], and solution-cast UDD-polyvinylalcohol composites have been reported[60]. It is important to note that state-of-the-art diamond nanocomposites utilize only aggregated diamond nanofillers.

Further development of nanodiamond composites, however, has been hindered by the inability to break down the core aggregates into the primary nanodiamond particles. When synthesized, detonation nanodiamond forms tightly packed aggregates, known as Ultra-Dispersed Diamond (UDD), that do not break apart using conventional dispersion

techniques.[22] Recently, methods to de-aggregate the nanodiamond using stirred-media milling[21, 28-30] and Bead Assisted Sonic De-aggregation[31] have been reported. The ability to produce solutions of dispersed nanodiamond is necessary to form composites with a high-degree of particle dispersion. Fabrication of dispersed nanodiamond composites has been reported, but not characterized.[61]

To fabricate high-quality nanodiamond composites, not only must the aggregates be broken apart, but good chemical compatibility between nanoparticle and matrix is also necessary. Several surface modification approaches have been developed to aide in this effort. Gas phase methods have been used to purify the nanodiamond and increase the concentration of oxygen-containing functional groups.[47, 62] Li *et al* polymerized brush structures from the nanodiamond surface.[19] Krueger *et al* have used reducing methods and silane-coupling agents to functionalize nanodiamond.[24, 52]

In this chapter, de-aggregated nanodiamond composites are fabricated using solution casting techniques and thermoplastic matrix materials. Solution casting is an attractive processing method because the process is scalable and applicable to many useful engineering thermoplastics, but poor particle dispersion has hindered its development for nanodiamond applications.[59] Here, both aggregated and de-aggregated nanodiamond composites are fabricated and characterized to demonstrate the influence of particle dispersion on the properties of nanodiamond composites.

First, a composite system using poly(methyl methacrylate) (PMMA) is studied. This material system demonstrates the feasibility of using solution casting techniques to fabricate well-dispersed nanodiamond composites. Furthermore, the films are

characterized by nanoindentation techniques, a form of materials characterization that is gaining increased attention for nanocomposite materials.

In a second, comprehensive study, the nanodiamond surface functionality is manipulated to investigate the interaction at the nanoparticle-polymer interface and to demonstrate the influence of this interfacial interaction on the composite's bulk mechanical properties. Though interfacial properties have been shown to significantly influence the bulk properties of a nanocomposite system[63], the nanodiamond-polymer interface has received little investigation. Polyacrylonitrile (PAN) is specifically selected as the matrix material due to its strong interaction with carboxylic acid functional groups.[64, 65] A thorough understanding of the nanodiamond-polymer interface must be developed in order to optimize the mechanical enhancement provided by the nanodiamond phase.

The mechanical properties of the ND-PAN composites are investigated with both nanoindentation and tensile testing. Nanoindentation has been employed recently to characterize nanodiamond composites[59, 60], but bulk characterization of nanodiamond composites has not been reported to date. Furthermore, tensile testing is an attractive characterization technique because this allows additional parameters, such as ductility and strength, to be measured for the first time on highly dispersed nanodiamond composite materials.

4.2 Experimental

4.2.1 Materials

Detonation nanodiamond powder (UDD) was obtained from ALIT Corporation (Ukraine). The aggregated diamond powder was treated by air oxidation in a tube furnace (4h at 420°C); additional thermal treatment under nitrogen (4h at 600°C) produced decarboxylated diamond aggregates. PMMA with a molecular weight of 120,000 was purchased from Sigma Aldrich and used as received. Polyacrylonitrile (PAN) with a molecular weight of 150,000 was purchased from Scientific Polymer Products and used as received. Dimethyl sulfoxide (DMSO) was purchased from Sigma-Aldrich and used as received.

4.2.2 Fabrication of Composites

The fabrication of both nanocomposite systems follows the same basic approach: de-aggregation of UDD, co-dissolution of polymer in ND:DMSO solution, casting of the composite solution, consolidation of the composites.

Ultra-dispersed diamond powder was dispersed in DMSO with bath sonication. De-aggregation of nanodiamond has been described above using a novel method and in the literature.[22, 28-31] To produce composite films the polymer was dissolved in DMSO, then an appropriate amount of nanodiamond-DMSO solution was added to the polymer solution. The samples were placed on a laboratory rotisserie for 6 hours, then cast onto glass plates and placed in a vacuum oven to drive off the solvent (8h at 90°C). In the case of the PAN-based composites and additional thermal treatment was performed by

placing films between glass slides and placing in a tube furnace under nitrogen at 240°C for up to 48 h.

Composite films were prepared for nanoindentation by mounting approx. 5 mm by 5 mm segments of the cast films onto glass microscope slides with epoxy. Nanoindentation films were approximately 100 microns thick to avoid substrate effects. Tensile specimens were prepared by cutting the dog-bone samples with a die-cutter built in accordance to ASTM D1708 specifications. Ultrathin sections of 60 nm were prepared with a Leica Ultracut UCT 54 microtome.

4.2.3 Characterization

TEM sections were examined with a Phillips CM10 TEM operating at 80 kV. IR spectra were obtained with a ThermoMattson Satellite FTIR. Particle size distribution was determined by Dynamic Light Scattering with a Malvern Instruments ZetaSizer. Differential Scanning Calorimetry (DSC) was performed with a TA Instruments Q200 at a heating rate of 10°C min^{-1}. Thermogravimetric analysis was conducted on a TA Instruments TGA 2950, heating under nitrogen at 10°C min^{-1}.

Nanoindentation was performed on an MTS G200 Nanoindenter with a Berkovich indenter. Maximum load was 5 mN and the dwell time was 10 seconds. The instrument was calibrated with a fused silica sample prior to sample measurements. Tensile tests were performed in accordance to ASTM D1708 and D698 standards on an Instron Load Frame; the strain rate was 1mm min^{-1} for all tests.

4.3 Results and Discussion

As-received detonation nanodiamond powder was subjected to tube furnace oxidation to increase the density of carboxylic acid functionality on the nanoparticle surface.[47] Subsequent thermal treatment of two hours at 650°C in an inert atmosphere decarboxylates the nanodiamond powder. Base uptake experiments indicate that the density of –COOH sites is about twenty times higher for the oxidized powders.[66] The base uptake experiments are conducted with a known mass of diamond sample, allowing for the "density" of surface-bound –COOH groups to be calculated per gram of nanodiamond. The results of these base uptake experiments are shown in Table 4.1, below.

Table 4.1 Carboxylic Acid Functionality of UDD-based Materials for Various Thermal Treatments

Sample	**[-COOH] (M/g)**
UDD (as received)	2.1E-04
ND-COOH	8.5E-03
ND-H	2.1E-04
UDD-COOH	4.8E-03

In addition to base uptake experiments, the IR spectra of the various nanodiamond samples confirm that a change in the surface functionality takes place. In the FT-IR spectra in Figure 1, below, the C=O signal at around 1750 cm^{-1} for the oxidized nanodiamond (UDD-COOH) is significantly less intense in the as received or

decarboxylated nanodiamond samples than in the oxidized diamond samples.[23] The nanodiamond samples with high concentration of carboxylic acid sites are designated ND-COOH, while the powders with low concentration of carboxylic acid functionality are designated ND-H.

Controlling surface chemistry is only one facet of this study; the role of particle aggregation is examined by exerting control over particle size. Though primary particles of detonation nanodiamond are typically under 5 nm in diameter, the synthesized powders are comprised of tightly bound aggregates that are tens to hundreds of nanometers in size.[22] Recently, several mechano-chemical processing techniques have been developed to break these aggregates into dispersions of sub-10 nm diamond particles.[21, 28, 31, 67] After employing a de-aggregation step, solutions of dispersed nanodiamond were obtained; particle size is measured by Dynamic Light Scattering (Figure 2a). The transparent solutions have a brownish-red coloration (Figure 2b), which darkens with increasing concentration.

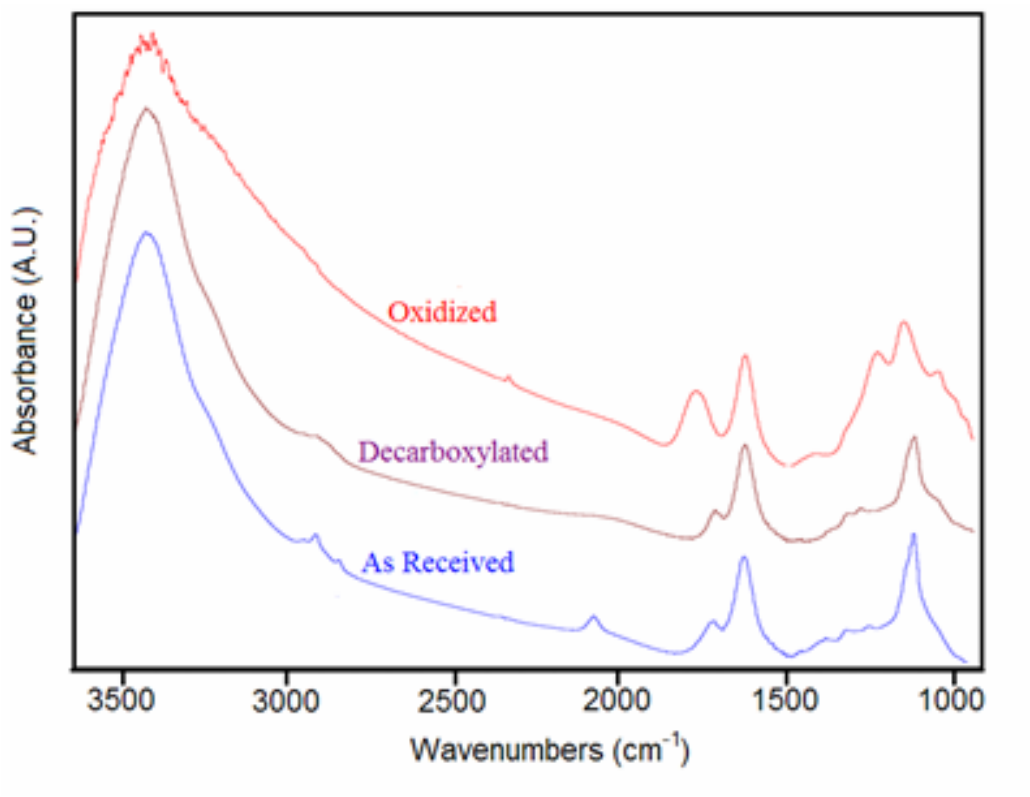

Figure 4.1 FT-IR spectra for as-received UDD, oxidized UDD (UDD-COOH), and decarboxylated UDD.

Good dispersion in a solvent, however, is only the first step in fabricating nanocomposites with good particle dispersion; even distribution must carry over to the final composite. Dispersed nanodiamond composites were fabricated by co-dissolving the matrix polymer, PMMA or PAN, then solution casting thick films onto glass plates. For the PAN composites study, control nanocomposite films were also prepared with oxidized, but aggregated diamond powders (UDD-COOH) for comparison. Also, nanodiamond that had been subjected to the second, decarboxylating treatment, were used to create composites with lower interfacial interaction capacity. TEM images (Figure 4.3) illustrate the marked difference in nanoparticle dispersion between the aggregated and dispersed composites. Note also that the dispersed nanodiamond

composites are transparent, while the composites filled with aggregated nanodiamond are opaque (not shown).

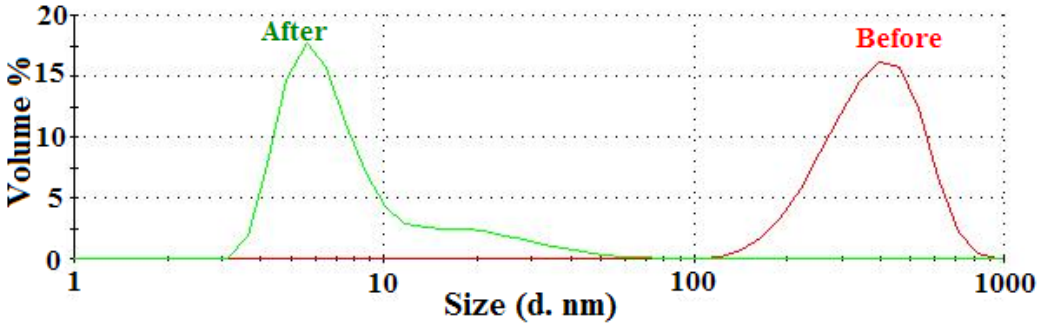

(a)

(b)

Figure 4.2 (a) DLS measurements showing reduction in particle size before and after the de-aggregation process and (b) photographs of aggregated and de-aggregated solutions.

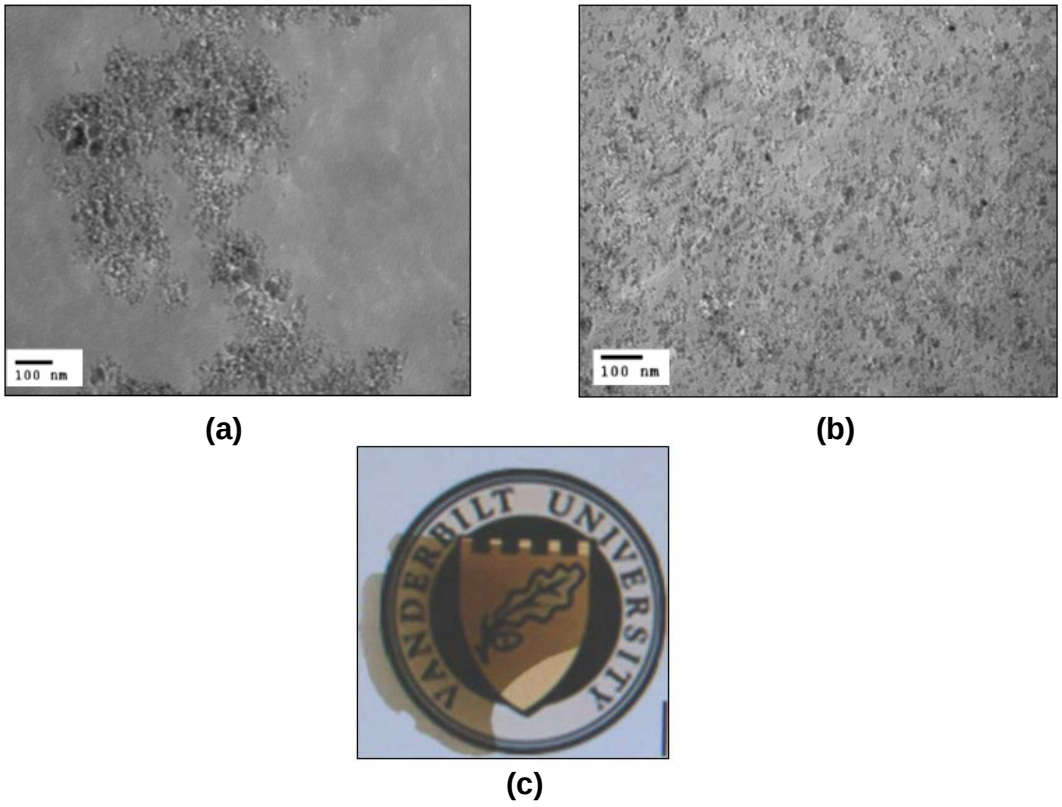

Figure 4.3 TEM images of 60-nm slices of nanocomposites with (a) UDD filler, (b) ND filler; (c) optical photograph of 100-µm thick film of ND:PMMA showing the transparency of the composite.

The PAN composite films were characterized by Energy Dispsersive X-ray Spectroscopy (EDS). This technique can detect the presence of the various elements present in the composite sample. Table 4.2, below, reports the results of the EDS experiments on three composite films; unfilled PAN, and PAN filled with 10 weight percent ND-COOH and 20 weight percent ND-COOH. In the unfilled PAN composite, the presence of carbon, nitrogen, and oxygen is expected. Sulfur is present because DMSO was the solvent used in the fabrication of the composite films. DMSO has a boiling point of 189°C and a vapor pressure of 0.42 mm Hg at 20°C; this solvent is difficult to evaporate entirely. As the nanodiamond loading increases, the elemental

concentration of carbon increases with a subsequent decrease in the relative concentration of nitrogen. The concentration of oxygen also increases with increased nanodiamond content; this oxygen is likely present due to the –COOH surface groups on the oxidized nanodiamond.

Table 4.2 Elemental Analysis of ND-COOH:PAN Composite Films

	Elemental Analysis (atomic %)				
Sample Name	**C**	**N**	**O**	**S**	**Zr**
0 ND:PAN	**71.00**	**21.32**	**6.39**	**1.29**	**0.00**
10% ND:PAN	**74.86**	**15.63**	**8.65**	**0.80**	**0.06**
20:ND:PAN	**75.24**	**12.78**	**11.39**	**0.50**	**0.09**

Zirconium is found in the composite samples as a contaminant resulting from the breakdown of the zirconia grinding media. Previous studies of de-aggregated nanodiamond have also reported a presence of zirconia contamination.[30] The abundance of zirconia is tied directly to the nanodiamond loading; increasing the concentration of nanodiamond results in an increase in zirconium content. Currently, no special precautions are taken to reduce the presence of zirconia. In fact, it is likely that a significant portion of the zirconia contamination could be removed by a centrifugation step. The ceramic media has a density of 5.68 g/cm^3, which is significantly higher than the dispersing solvent or the nanodiamond particles.

Interestingly, the PAN nanocomposite films filled with seven volume percent ND-COOH are significantly more difficult to re-dissolve than unfilled PAN films. Unfilled PAN films re-dissolve in DMSO within a few hours, while the ND-COOH filled

composites appear unaffected after several weeks of submersion in solvent. A photograph of two films, unfilled PAN and PAN filled with seven volume percent ND-COOH, is shown in Figure 4.4. This is suggestive of a strong interaction between the nanodiamond filler and the matrix; most likely between the –COOH groups present on the nanoparticle surface and the nitrile groups of the PAN. The carboxylic acid sites present on the nanoparticle surface, through an ionic reaction, may covalently bond with the nitrile side chains of the polymer matrix.[65]

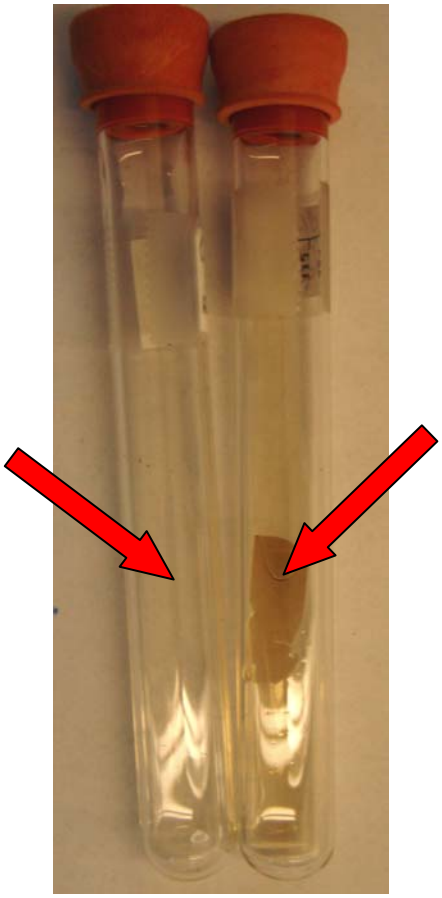

Figure 4.4 Photograph of PAN films after immersion in DMSO. The unfilled PAN film (left) completely dissolves within an hour, but the seven volume percent ND-COOH:PAN composite remains intact for weeks (right).

This strong interaction between the oxidized nanodiamond surfaces and the polymer sidechains is further illustrated in the FTIR spectra of the PAN nanocomposites (Figure 4.5). A comparison of the spectra shows a stronger absorbance at 1650 cm^{-1}, the peak indicating C=N bonding, in the ND-COOH samples than in the UDD-COOH or unfilled polymer films. It is possible that the mild heating conditions during the film casting step (90°C for 8 hours in vacuum) is sufficient to initiate a covalent reaction between the carboxyl groups present on the oxidized nanodiamond and the nitrile side groups. The C=N bonds found in the neat PAN are formed via a radical reaction mechanism.[64, 65] The dispersed and oxidized nanocomposite (ND-COOH:PAN) sample has a higher concentration of the C=N bonds than the aggregated and oxidized composite (UDD-COOH:PAN) because the de-aggregated nanoparticles have more available surface area to interact with the polymer, resulting in more reactions occurring at the particle-polymer interface per unit volume.

The thermal behavior of the composite films was further characterized with DSC and TGA (Figure 4.7). The unfilled polymer and UDD-COOH:PAN composites show a single exothermic peak because cyclization occurs simultaneously with dehydrogenation and oxidation. In the well dispersed composite sample, two distinct peaks emerge as cyclization initiation occurs at a lower temperature than the other thermo-oxidative reactions because the presence of the carboxylate groups facilitates the reaction.[65] The exothermic peak is approximately 20°C higher in the aggregated diamond composite than the unfilled PAN, and 40°C higher in the well-dispersed diamond nanocomposite. Previous work reveals that inclusion of nanoparticles in PAN lowers the onset temperature of cyclization reactions relative to the unfilled polymer.[65, 68] TGA also

indicates that nanodiamond serves as a thermally stabilizing phase. The onset of thermal degradation was increased 15°C and 30°C above the unfilled polymer for the aggregated and dispersed nanodiamond composites, respectively. The ND-COOH:PAN sample exhibits a two-fold increase in thermal degradation temperature, as compared to the UDD-COOH:PAN sample, because the increased surface area affords significantly higher degree of constrained polymer volume. This constraint may be steric hindrance at the polymer-nanoparticle interface or an increase in the number of covalent bonds between the PAN matrix and the ND-COOH nanoparticles.

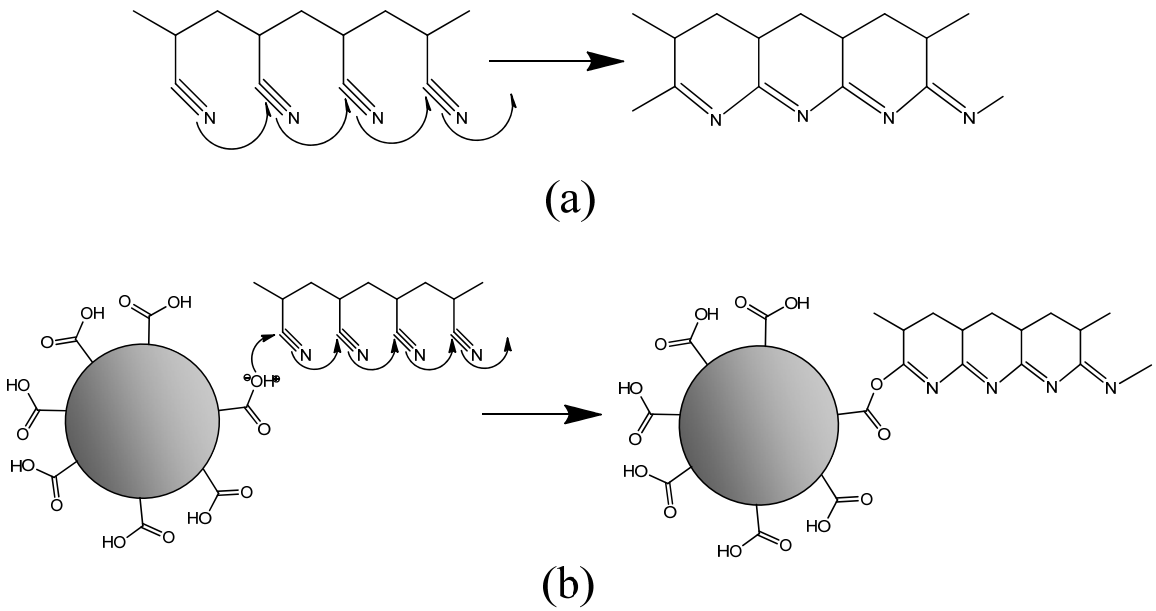

Figure 4.5 Possible cyclization reactions that occur in (a) neat PAN via a radical mechanism or (b) in the presence of ND-COOH via an ionic mechanism. (Adapted from reference [65]. Copyright 2007 Elsevier Ltd.)

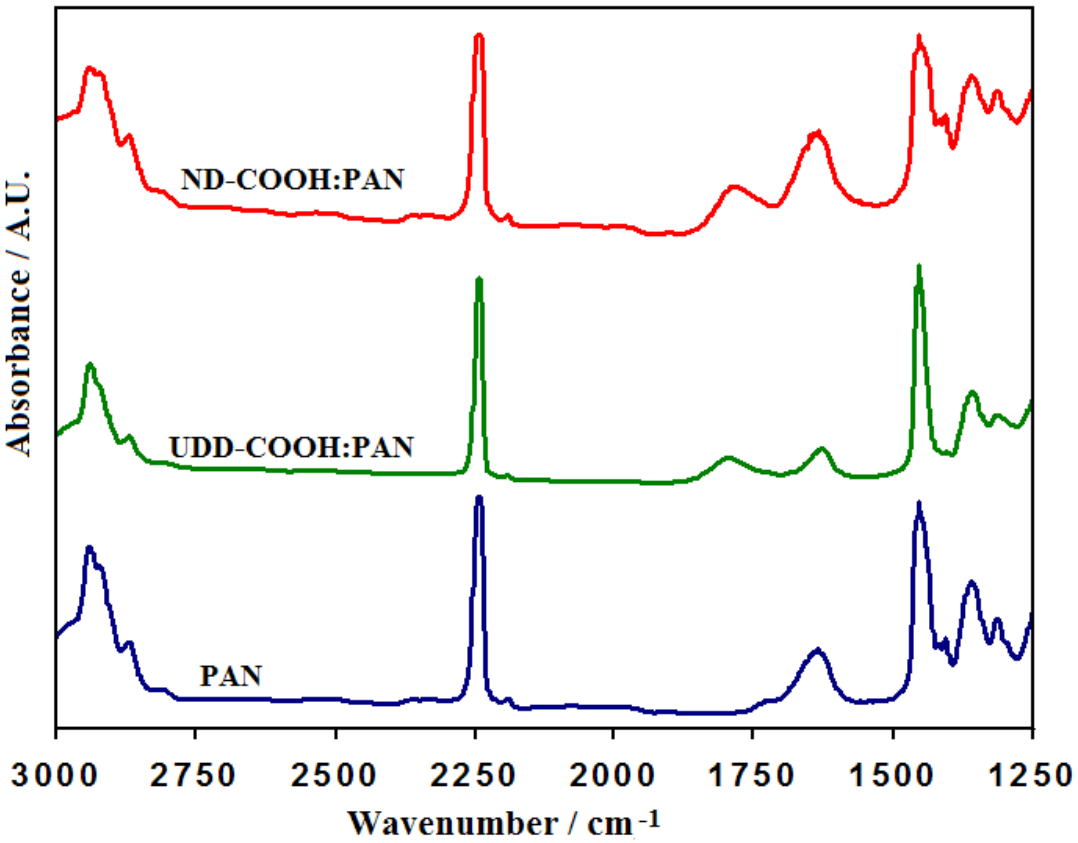

Figure 4.6 FT-IR spectra for ND-COOH:PAN and UDD-COOH:PAN nanocomposites. The peak at 1650 cm^{-1} is assigned to the stretching bands of C=N bonds, from either chain cyclization or nanodiamond-polymer interactions.

To further explore the chemical interaction across the polymer-particle interface, a series of thermal treatments were conducted. Dispersed nanodiamond composites and unfilled polymer samples were placed in a tube furnace under nitrogen and heated at 240°C for up to 48 hours. The composite films were examined via FTIR after 8 and 24 hours of heating; the spectra are shown in Figure 4.8. The peak at 1650 cm^{-1} for C=N bonding, indicating polymer cyclization, becomes increasingly intense in the pure PAN sample, but changes relatively little in the nanodiamond composites. DSC data suggests that the stabilization reactions, where by the nitrile side chains of the PAN form cyclic structures, occur at higher temperatures for the nanodiamond composites It is likely that

the reduced C=N bonding in the ND-COOH and UDD-COOH composites is kinetically limited. Furthermore, the carboxylic acid functional groups could disrupt nitrile oligomerization, limiting the degree of cyclization.[64]

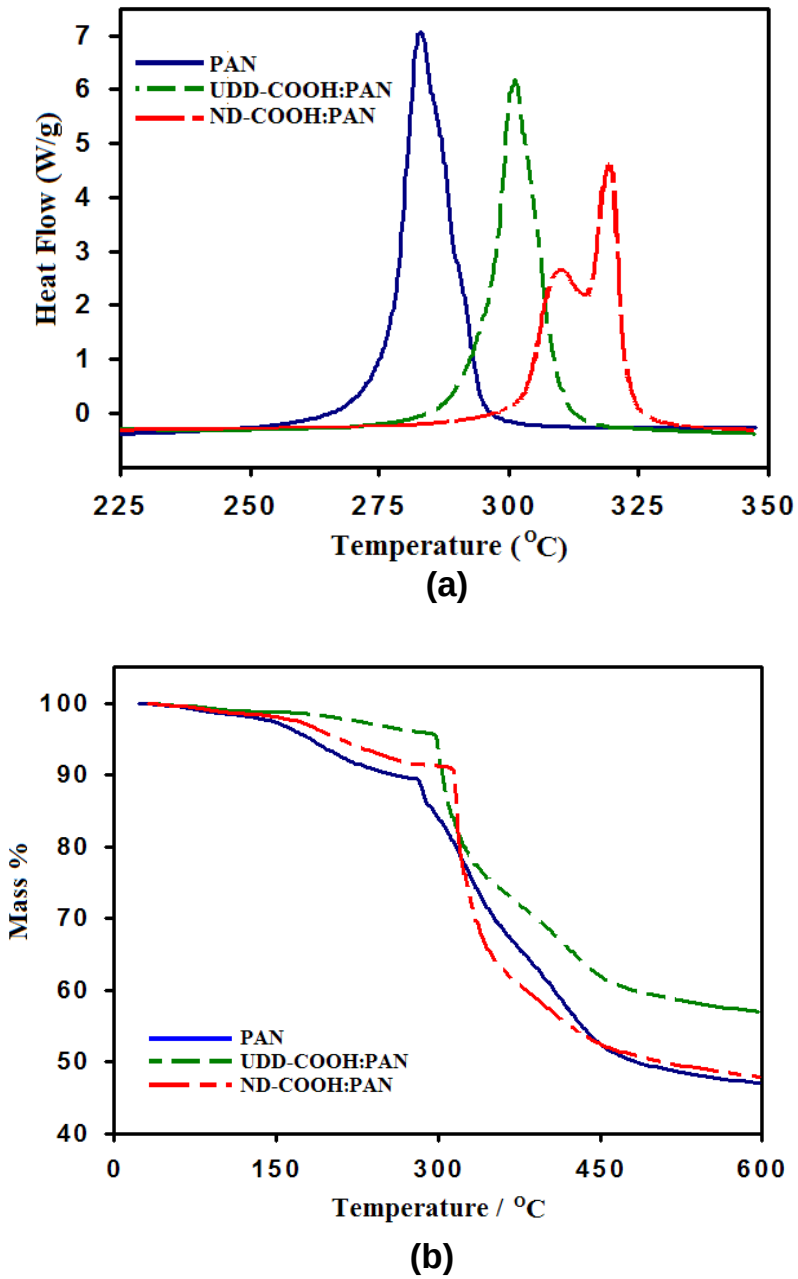

Figure 4.7 Thermal characterization of neat PAN and ND-COOH and UDD-COOH nanocomposites; (a) DSC scans, and (b) TGA thermographs.

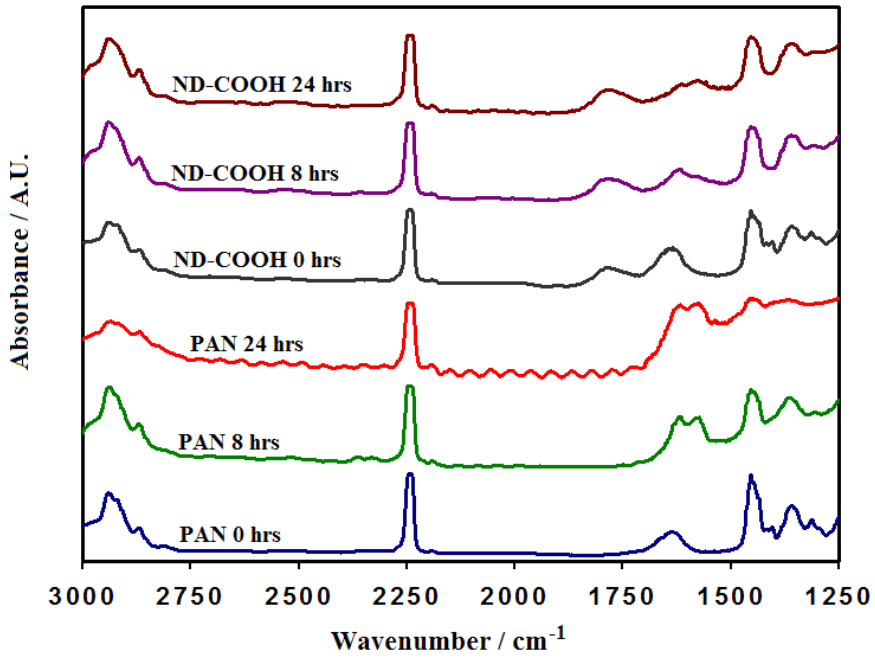

Figure 4.8 FT-IR spectra for PAN and ND-COOH:PAN composites after annealing at 240°C for variable periods.

Recently, nanoindentation has been used to characterize the mechanical properties of nanodiamond-filled polymer composites.[59, 60] Nanoindentation was performed on composite specimens where the nanodiamond concentration, surface functionality, and aggregation were varied independently in order to investigate the role of each variable. For the first time the effect of nanodiamond de-aggregation on composite mechanical properties can be studied. The enhancement in modulus of elasticity, measured by nanoindentation, for ND-COOH:PMMA nanocomposites is shown in Figure 4.8.

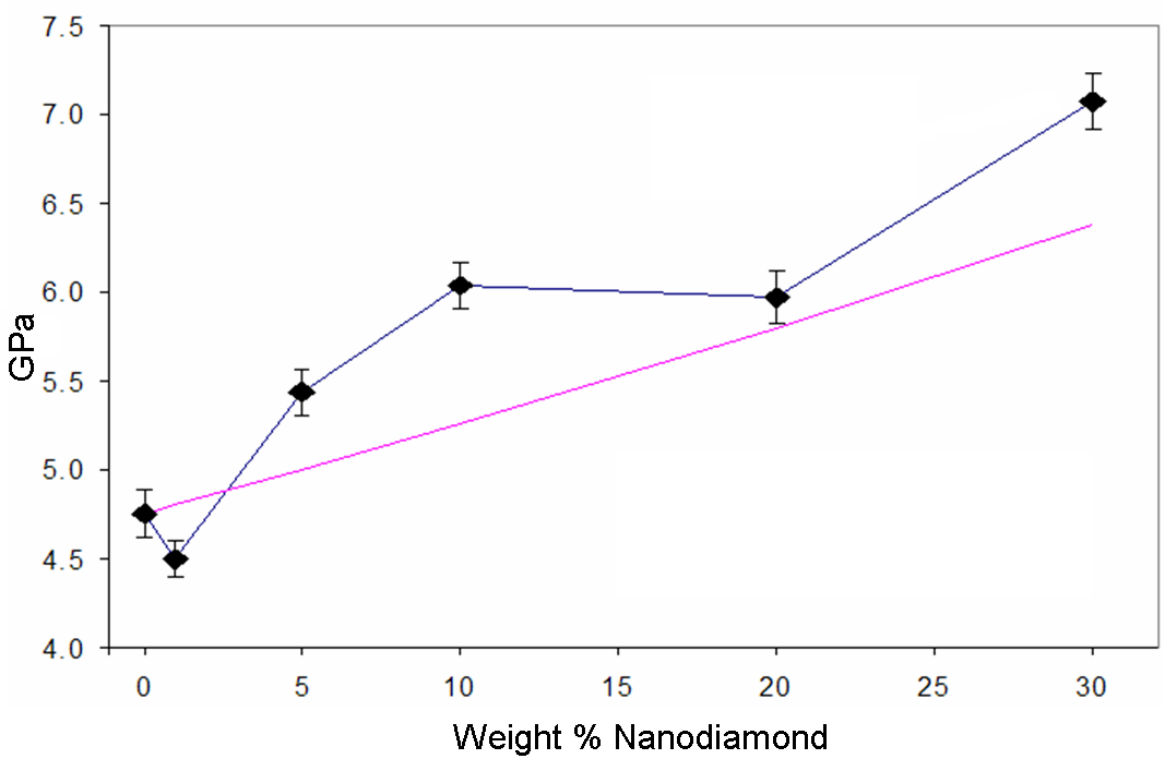

Figure 4.9 Nanoindentation results for dispersed ND-COOH in PMMA. The solid pink line corresponds to the Halpin-Tsai predicted values.

The ND-COOH:PMMA composite samples show a strong correlation between increased elastic modulus and nanodiamond content. At 30 weight percent concentration, which corresponds to 10 volume percent, the composite sample is 50 percent stiffer than the unfilled polymer. The ND-COOH:PMMA composites slightly outperform the theoretical moduli as predicted with the Halpin-Tsai equations.[3] Two data points, 1 wt% and 20 wt%, show less enhancement than expected; TGA analysis (not shown) reveals that these samples had a slightly higher concentration of residual solvent, which likely is responsible for the decrease in mechanical properties.

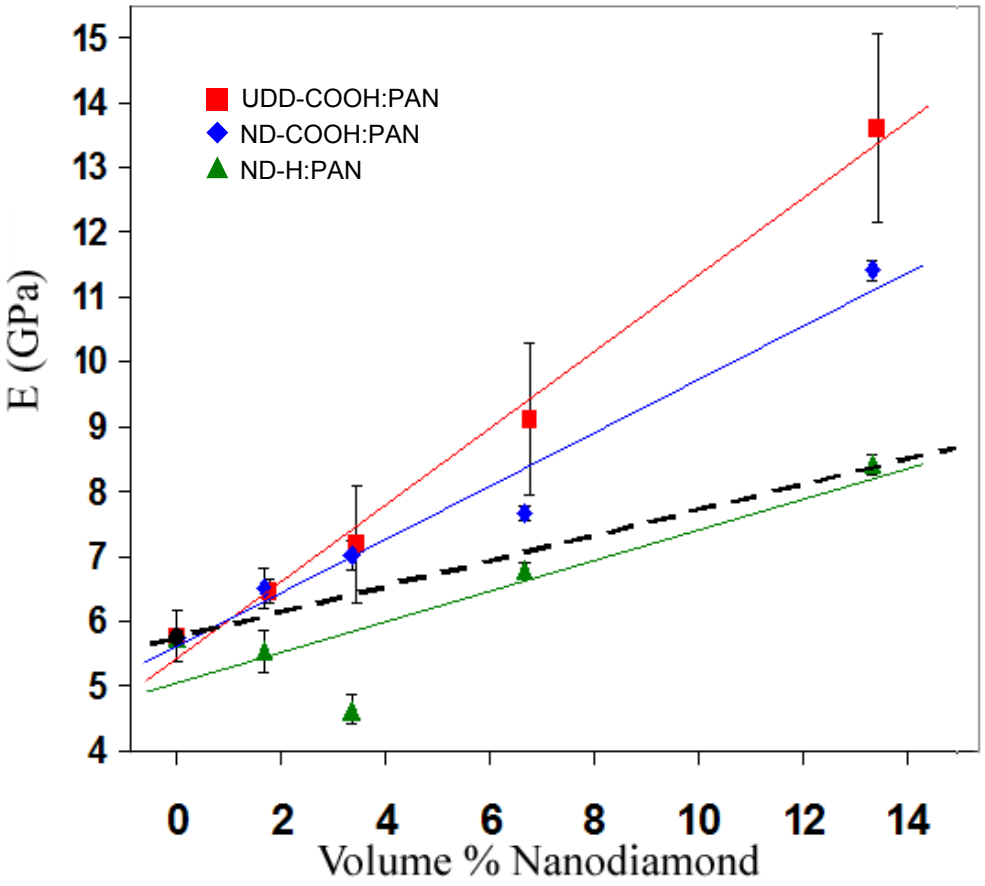

Figure 4.10 Nanoindentation results for PAN nanocomposites. The red square, blue diamonds, and green triangles correspond to UDD-COOH, ND-COOH, and ND-H fillers, respectively. The dashed black line is the Halpin-Tsai prediction.

Nanoindentation was employed to characterize the mechanical properties of nanocomposites comprising a PAN matrix and UDD-COOH, ND-COOH, and ND-H fillers (Figure 4.10). A comparison between the composites loaded with ND-COOH (blue diamonds) and the ND-H (green triangles) illustrates how surface chemistry influences bulk mechanical properties. Both samples have good dispersion, but the oxidized nanodiamond sample has a significantly higher concentration of functional groups that interact favorably with the polymer matrix, and subsequently is more effective at enhancing the composite's elastic modulus.

The dashed line in Figure 4.10 represents the theoretical elastic modulus as predicted with the Halpin-Tsai equations.[3] The model fits well for the decarboxylated nanodiamond samples, but significantly underestimates the enhancement in modulus for both oxidized nanodiamond samples, ND-COOH and UDD-COOH. A recent study of micro- and nanocomposite systems found that the ξ parameter in the Halpin-Tsai equations had to be adjusted to achieve good agreement in the nanocomposite system.[69] The Halpin-Tsai equations were developed to predict the change in elastic modulus for micro-scale composite systems. In micro-scale composites, the interfacial volume is small compared to the volume of the filler. The opposite holds true in nanocomposite systems: the interfacial volume is often on the same order of magnitude as the filler volume. This disparity for nanocomposites could be attributed to the nanoparticle affecting a volume of polymer surrounding the filler, increasing the effective volume fraction of reinforcement.[70] In the case of the decarboxylated nanodiamond, the nanoparticle-polymer interaction is weaker, reducing the influence of the nanofiller on the surrounding polymer. Without a strong influence on the surrounding volume, the case for the ND-H:PAN composites, the theoretical assumptions remain valid and the Halpin-Tsai equation will yield a sufficiently accurate estimate.

A comparison between the two surface oxidized samples, ND-COOH and UDD-COOH, yields an unexpected result; the aggregated nanodiamond composites are more effective at stiffening the composite than well-dispersed nanodiamond with the same surface treatment. This result counters the widely held assumption that good dispersion and reduced particle agglomeration are desired for efficient reinforcement of polymers.[71-74] Aggregated or agglomerated nanoparticles have less available surface area to interact

with the polymer matrix than well-dispersed nanoparticles at the same concentration. Further investigation of the nanoindentation results shows that the aggregated nanodiamond composites have much more scatter in the data than the well-dispersed nanocomposites, indicated by the larger error bars in Figure 4.10. This raises concern that nanoindentation may not accurately characterize elastic modulus in situations where inhomogeneities exist that approach the size scale of the instrument probe, in this case hundreds of nanometers.

Specifically, there exists a strong possibility that nanoindentation is an in-appropriate characterization technique for non-homogenous materials systems. In nanoindentation testing, the stress placed on the test material is calculated from the measured force of the indenter and an assumed area, which corresponds to the known geometry of the indenter tip. If, for instance, an operator had changed indenters without changing the instrument's settings, an erroneous stress value would be reported. In this same manner, if a tip contacts an inhomogeneous region within the composite, the reported stress value may be incorrect.

An example of such a scenario is shown in Figure 4.11. Here, the nanoindenter probes an UDD aggregate. As the probe continues to penetrate the nanocomposite, it now has to push the aggregate through the polymer matrix. The calculated stress assumes that only polymer contacting the probe is responsible for the resistive forces. In this instance, however, the polymer around the aggregate is also contributing to the resistance to penetration.

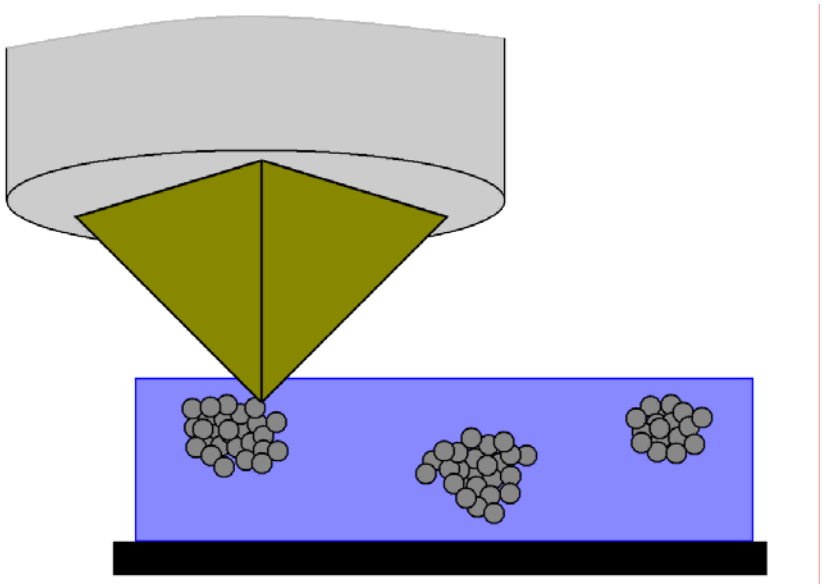

Figure 4.11 Nanoindentation probe contacting an aggregate of UDD.

Conversely, the nanoindenter may probe a region devoid of UDD aggregates (Figure 4.12). Here, the modulus will be very close to the modulus of the matrix material. These data points will show a much lower modulus value. In nanoindentation tests, many local tests are performed on any given sample and the reported modulus is an average of the individual tests. When examining the experimental data shown in Figure 4.10, it is immediately apparent that the standard deviation for the UDD composites is significantly larger than for either of the de-aggregated diamond composites. Furthermore, the standard deviations reported in the UDD composites increase as diamond content increases. De-aggregated diamond composites, however, have very small deviations because the indenter probe "sees" the same material system regardless of the specific spot that is tested (Figure 4.13). The increased scatter in the experimental data strongly suggests that the inhomogeneities in the UDD-COOH:PAN composites invalidate the assumptions required to derive moduli data from nanoindentation tests.

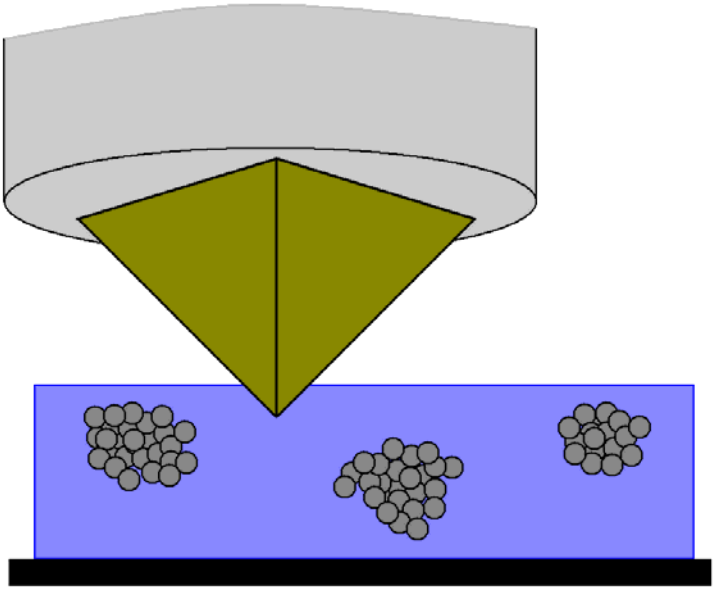

Figure 4.12 The nanoindenter probing a region devoid of diamond aggregates.

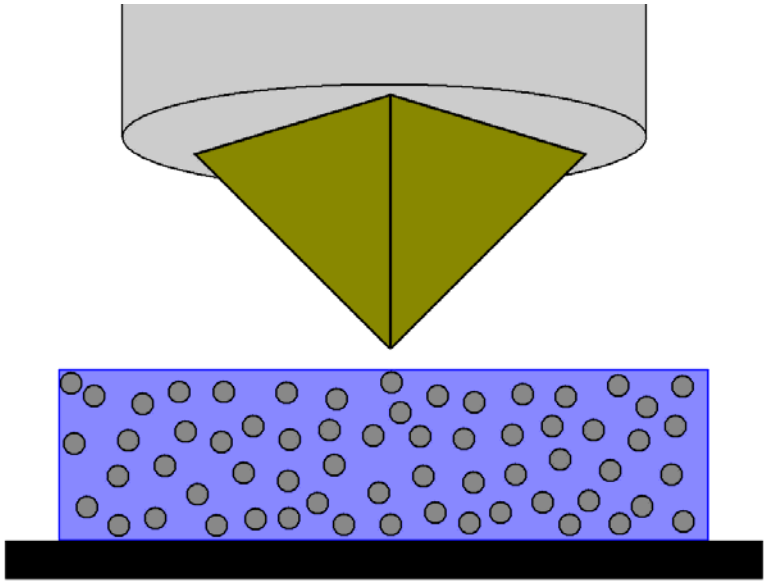

Figure 4.13 Nanoindenter probing ND-COOH:PAN composite material. Mechanical response to indentation probing is location independent.

If nanoindentation may not be confidently employed to characterize the mechanical properties of the nanocomposites, a bulk material test method must be used. Tensile tests were conducted on the ND-COOH:PAN and UDD-COOH:PAN nanocomposites to evaluate the composite materials' mechanical properties. In addition to avoiding the problem of sampling regions of varying particle concentration, tensile testing provides information about the composite's strength and ductility. The results of the tensile testing are shown in Figures 4.14 – 4.16. Tensile testing confirms that nanodiamond is an effective nanoscale filler for polymers; the polymer's elastic modulus was enhanced by nearly 80 percent and the tensile strength was increased by nearly 60 percent at 10 volume percent particle loading.

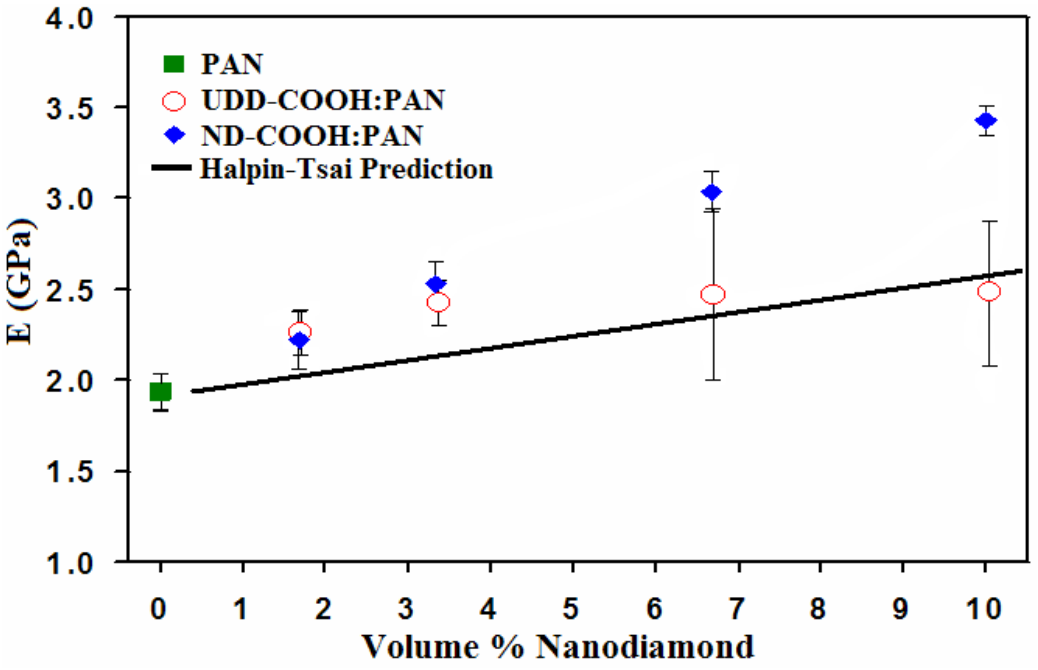

Figure 4.14 Modulus of Elasticity for PAN composites with aggregated (UDD-COOH:PAN) and de-aggregated (ND-COOH:PAN) nanodiamond filler.

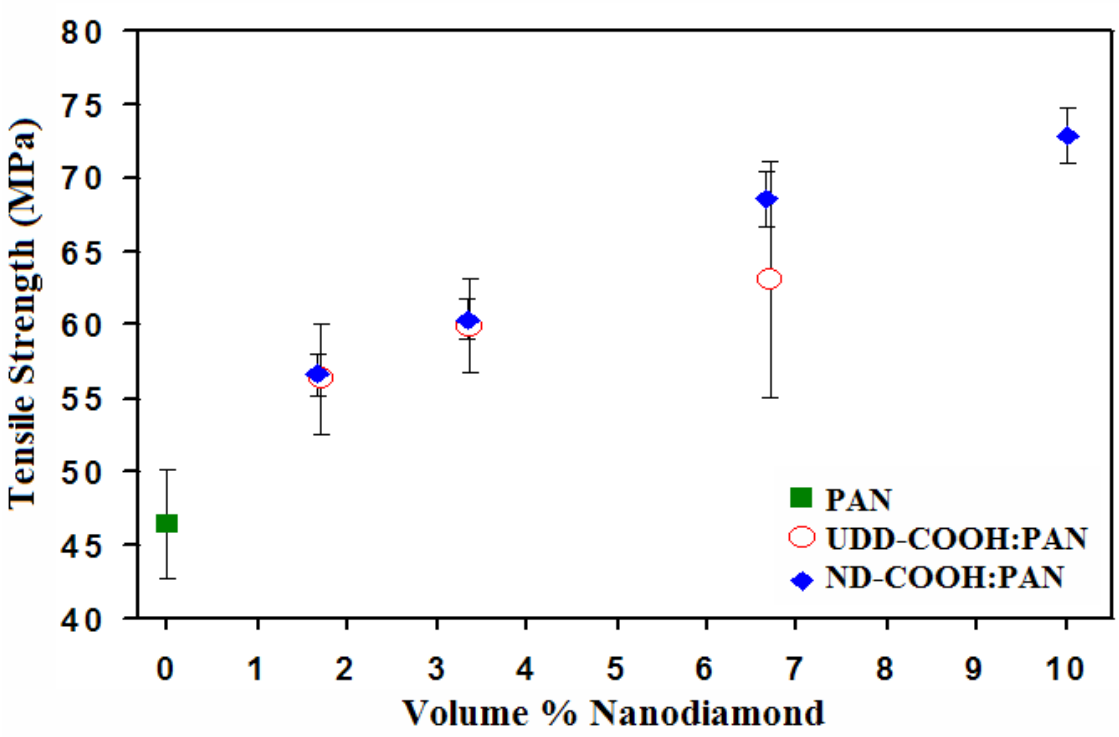

Figure 4.15 Tensile strength results for the ND-COOH:PAN and UDD-COOH:PAN composites as a functional of filler concentration.

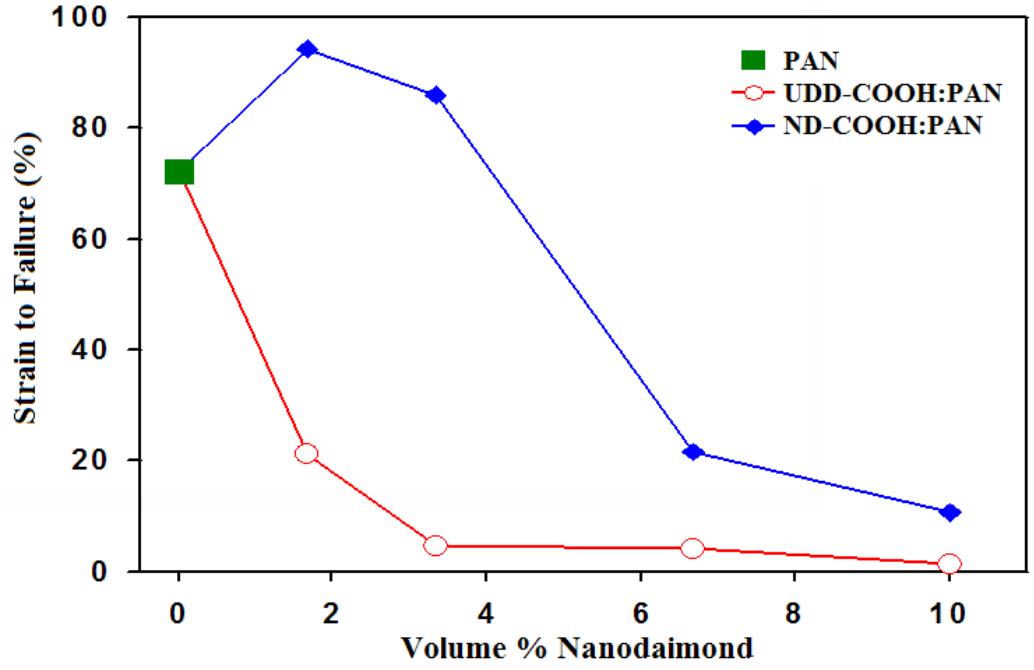

Figure 4.16 Elongation data for the UDD-COOH:PAN and ND-COOH:PAN composites as a function of filler concentration.

It is important to highlight that the de-aggregated nanocomposite ND-COOH:PAN, outperforms the aggregated nanodiamond composites at particle concentrations above about three volume percent. In the case of elastic modulus, no additional improvement is seen in the aggregated nanodiamond sample above three volume percent. For the de-aggregated filler, however, modulus enhancement increases linearly with increased particle concentration, as expected from theory.[3] Tensile strength is strongly dependent upon particle aggregation. In the UDD-COOH:PAN samples, there is only a small improvement in strength between composite samples with seven volume percent nanodiamond over the samples with 3.5 volume percent nanodiamond. At 10 volume percent loading, the aggregated nanocomposite has a lower tensile strength than even the unfilled polymer (not shown). The well-dispersed nanocomposites, however, show only slight deviation from a linear enhancement as particle concentration increases.

The failure mode for the aggregated and dispersed nanodiamond composites is markedly different. The addition of even low concentration of aggregated filler quickly results in composites that fail after very little strain. In the case of the dispersed nanodiamond, the 1.7 and 3.3 volume percent samples are able to sustain more strain than the neat polymer before fracturing. Even at the highest particle loading, the dispersed nanocomposite strained more than 10 percent prior to fracture, which is approximately an order of magnitude more strain than the aggregated nanodiamond composite endured at the same concentration. It is possible that the aggregates, which are highly defective, are acting as crack initiation points. A high defect density results in brittle fracture. Furthermore, amorphous polymeric materials are able to sustain significant deformations without fracturing because the polymer chains can rearrange their conformation prior to

the breaking of covalent bonds.[75] The nanodiamond aggregates are sufficiently large to inhibit the polymer chains from significantly rearranging, thereby limiting the ductility of the composite. The dispersed nanodiamond composites, with smaller diamond phases, allow the polymer chains to change conformation and retain bulk polymer ductility.

At higher diamond concentrations, however, there is decrease in strain to failure for the composites. This decrease in ductility may be indicative of the challenge to achieve good dispersion at higher loadings; aggregation may be occurring. Reduced chain mobility, however, must also be accounted for. At higher diamond concentrations, it is likely that the entire matrix volume is contained within an interfacial region. The polymer that is interacting with the nanodiamond surfaces have a reduced number of available conformations, so the polymer is not able to easily achieve stress relaxation by chain movement.

Additional tensile tests were performed on thermally-treated composites and pure PAN to determine if the increased interfacial bonding improved overall mechanical properties (Figure 4.17). The unfilled PAN samples see a strong increase in tensile modulus and strength after a 12 hour thermal treatment, but additional heating does not yield further improvement in tensile properties. This is unexpected because the FTIR data suggests that additional cylcization occurs with increased heat treatment time. The five volume percent nanodiamond composites follow a general trend of increasing strength and stiffness with the increased duration of heat treatment. DSC data shows that the peak temperature for the stabilization reactions is much higher for the ND:PAN composite samples; at 240°C, the reaction occurs much more slowly in the composite samples than

in the unfilled PAN. Additional annealing time or higher treatment temperatures may yield additional improvements in tensile properties for the composite samples.

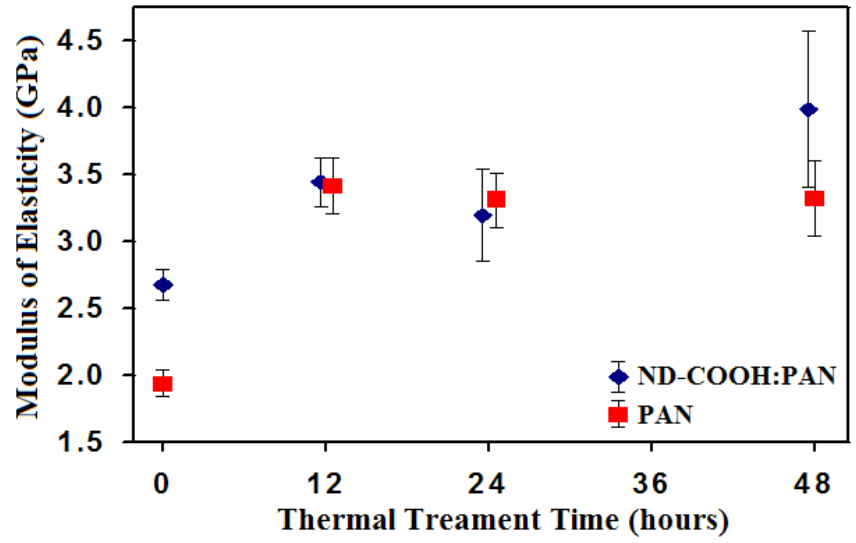

(a)

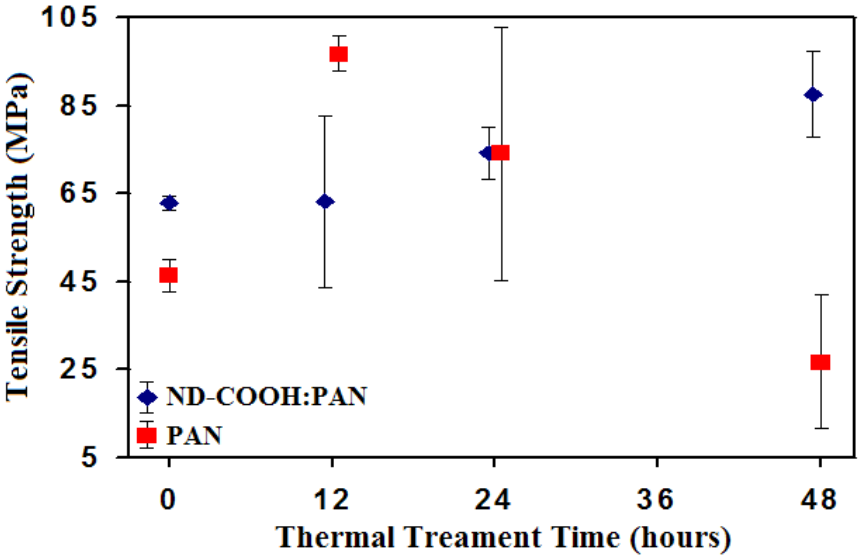

(b)

Figure 4.17 Tensile test data for thermally-treated films. Modulus of elasticity (a) and tensile strength (b) for 5 volume percent ND-COOH:PAN and unfilled PAN films as a function of heating time.

4.4 Conclusions

Aggregated- and dispersed- nanodiamond polymer composite films have been fabricated via solution-casting techniques. The nanodiamond filler was subjected to various thermal treatments to modify the surface chemistry. Spectroscopic data suggests that nanodiamond's surface functional groups covalently bind to the polyacrylonitrile matrix; nanodiamond composites are markedly more resistant to solvents than the unfilled polymer. Nanoindentation test indicate that surface functionality significantly influences the composite's mechanical properties; the modulus of ND-filled composites is improved significantly by increasing the density of carboxylic acid sites on the nanoparticle's surface. Tensile tests reveal that particle dispersion leads to desirable enhancement in mechanical properties over aggregated diamond nanoparticles with comparable surface functionality.

Mechanical characterization indicates that nanodiamond is an effective reinforcement for polymer nanocomposites. At a concentration of 10 volume percent, dispersed nanodiamond enhances the polymer's modulus of elasticity by 80 percent and the tensile strength by nearly 60 percent. At lower concentrations, significant enhancement in mechanical properties is possible without a loss in ductility, but only in the case of well-dispersed nanodiamond composites.

CHAPTER V

NANODIAMOD NANOCOMPOSITES WITH THERMOSETTING MATRICES

5.1 Introduction

The previous chapter explored incorporating nanodiamond as a mechanical reinforcement in thermoplastic matrices. While this is an important materials system, a thorough examination of nanodiamond composites would be incomplete without exploring a composite system that employs a thermosetting polymer as the matrix material. Thermosetting polymers differ from thermoplastics by the ability to cross-link, in which the polymer chains covalently bind together to form essentially a single polymer network with infinite molecular weight.

Thermosetting polymers represent an important class of engineering polymers for use in structural composite applications. Most fiber-reinforced polymer composites rely on a matrix of unsaturated polyester, viny ester, or epoxy resin.[10] Uunsaturated polyester and vinyl ester resins contain C=C bonds that can be opened by a radical catalyst to initiate cross-linking. Epoxy resins, on the other hand, contain three-membered-ring epoxy functional groups that are opened by nucleophilic attack of a curing agent, often a secondary- or tertiary amine, that are incorporated into the resulting polymers as an end group.

Epoxy resins have superior mechanical properties when compared to unsaturated polyesters or vinyl ester resins, but epoxy resins are more costly and many require a

curing step at elevated temperatures. Vinyl ester resins, however, offer good mechanical properties, good chemical resistance, and can be cured at room temperature.[76] For these reasons, vinyl ester resins are often selected as the matrix material of choice for large composite structures such as boat hulls and wind turbine blades.

Vinyl ester resins are typically a blend of vinyl ester monomer and a low viscosity monomer that can covalently crosslink to the matrix. The diluent monomer is most commonly styrene, though divinyl benzene, chlorostyrene, and vinyl toluene are substituted for specific applications.[76] Styrene content in vinyl ester resins typically falls between 30 and 50 weight percent.

Vinyl ester monomers sometimes referred to as "epoxy vinyl ester," but this name may be misleading. There are no epoxy rings present in the resin; this name originates from the synthesis of the vinyl ester molecule. Vinyl ester is synthesized from reacting digylcidyl ether of bisphenol A, the most common epoxy resin material, with methacrylic acid (Figure 5.1). The epoxy rings are catalytically opened and reacted with the methacrylic acid.[76] The product (Figure 5.2) has both ester and vinyl structures, but no epoxy structure.

Vinyl ester resins are considered a good compromise between unsaturated polyesters and epoxy resins. The backbone of the vinyl ester molecule is structurally similar to that of epoxies and provides good mechanical properties. The reactive ends, however, are similar to unsaturated polyesters. The vinyl end groups can react at room temperatures with a radical catalyst, allowing for more convenient cure processing than epoxy resins. Also, the hydroxyl groups along the polymer chain can participate in

hydrogen bonding, both with other vinyl ester chains or with the reinforcement phase of the composite.

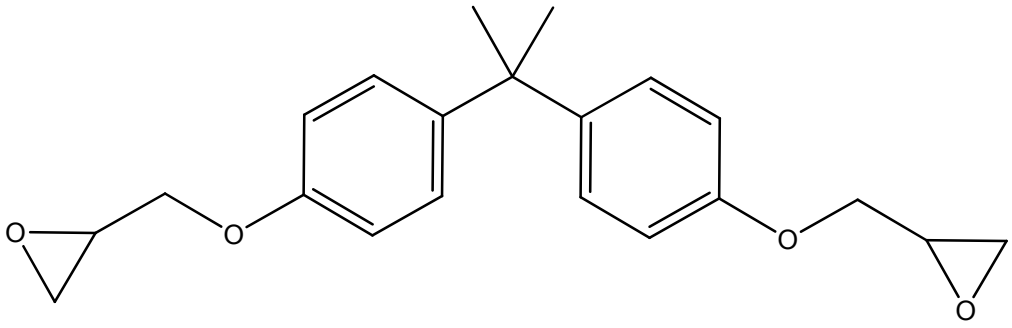

diglycidyl ether of bisphenol A

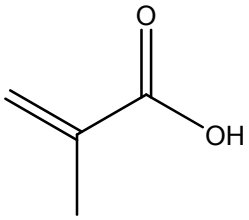

methacrylic acid

Figure 5.1 Diglycidyl ether of bisphenol A (epoxy resin) and methacrylic acid, the precursors to vinyl ester resins.

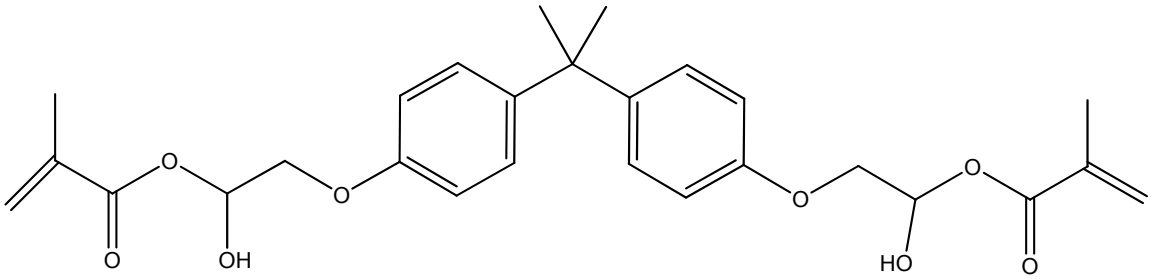

Figure 5.2 Vinyl ester molecule. Note the vinyl groups at the ends of the molecule in place of the epoxy rings.

Many studies of nanomaterials and thermosetting polymers have been reported, though the majority of the research has focused on carbon nanotubes and epoxy resins.

This specific research area has been intensely studied and reviewed.[77, 78] In fact, commercial applications of CNT/epoxy composites have begun to emerge into the marketplace. Epoxy resins have also been used in conjunction with low-aspect ratio fillers such as silica[79] and alumina.[80]

Studies of nanocomposites using polyester or vinyl ester resins are slightly less prevalent. Again, carbon nanotubes have been used as a desired nanoscale reinforcement additive.[81, 82] Polyester resin composites filled with alumina exhibit enhanced toughness.[83] Vinyl ester resins filled with alumina,[84] silicon carbide,[85, 86] copper oxide,[87] and zinc oxide[88] have all shown enhanced mechanical properties.

Nanodiamond, however, has received little study as a filler in thermosetting polymers. UDD has been added to a diglycidyl ether of bishenol A epoxy with loadings up to one weight percent; a 25 percent increase in Young's modulus and a 47 percent increase in strength with the addition of 0.5 weight percent aggregated nanodiamond was reported.[89] Li reported an increase in hardness of surface functionalized UDD composites, also in epoxy resins.[48] No studies of de-aggregated nanodiamond in thermosetting composites have been reported to date.

In this work, a surface functionalization strategy utilizing silane linker molecules is selected. The use of silane linker molecules was first demonstrated on nanodiamond by Krueger *et al*.[24, 31, 52] Silane linkers are an attractive choice because of the wide selection of variants readily available; substituent groups can be selected for the particular application without having to adapt a completely new synthesis strategy. Furthermore, silane linker molecules are already widely accepted in the traditional composites industry. Variants of these functionalizing reagents are used to improve the

interfacial properties between the glass or carbon fibers and the polymer matrix. In the composite's industry, these reagents are referred to as "sizing" agents.[10]

In this chapter the results of a study of dispersed and functionalized nanodiamond incorporated into thermosetting polymers is reported. Particular attention is paid to selecting processing steps that achieve high-quality dispersions without adversely damaging the thermosetting polymer through process steps that require thermal treatments. Nanodiamond composites are fabricated with vinyl ester resin matrices and characterized both chemically and mechanically.

5.2 Experimental

5.2.1 Materials

Nanodiamond was obtained from ALIT Corporation. Acetonitrile (ACN), styrene, vinyltrimethoxysilane (VTMS), 3-(trimethoxysilane) propyl methacrylate (TMSPM), acetone, dimethylformamide (DMF), acrylic acid, and dimethylsulfoxide (DMSO) were obtained from Sigma-Aldrich and used as received. The vinyl ester resin used in this report is Derakane 411-350, manufactured by Ashland Inc. The catalyst used for curing the resin is methyl ethyl ketone peroxide (MEKP), supplied by Aircraft Spruce and accelerated with a cobalt naphthenate solution purchased from Sigma-Aldrich.

5.2.2 Procedure

The as-received UDD powder was subjected to a tube furnace oxidation procedure to increase the concentration of carboxylic acid functional sites.[47]

Approximately 1.5 grams of UDD is placed in a quartz boat. The boat is placed in a 415°C tube furnace with compressed air flowing for 4 hours.

The oxidized powder, UDD-COOH, is then subjected to a simultaneous de-aggregation and surface functionalization treatment. For example, a 2.0% (w:w) solution is prepared by placing 1.00 grams of UDD-COOH in a 100 mL round-bottom flask with 62 mL of acetonitrile. The flask is sealed with a rubber septum and placed in a sonic bath for 30 minutes. Next, 0.50 mL of VTMS is injected into the solution and the flask is placed in the sonicator for an additional 30 minutes.

The light gray solution is then subjected to the novel de-aggregation process described above for approximately 45 minutes or until the solution becomes dark but transparent in thin sections. The solution of de-aggregated and surface functionalized nanodiamond, referred to as ND-VTMS:ACN, is decanted and placed in a second 100 mL round-bottom flask. The NT-VTMS:ACN solution is then placed in a sonic bath for a final, 30 minute ultrasonic treatment.

To prepare the nanodiamond:vinyl ester composites, the functionalized nanodiamond must be transferred to the resin and the acetonitrile removed. To minimize the solvent content, the ND-VTMS:ACN solution is concentrated by rotary evaporation. Additionally, all samples were prepared with the same total acetonitrile content to eliminate the possibility that the higher diamond content composites also had a higher concentration of residual solvent. For this reason, additional ACN was added to all samples except the 2.4 volume percent specimen. The ND-VTMS:VE composite resins may now be prepared.

As an example, the 1.2 volume percent composite specimens are prepared as follows: In a 15 mL test tube, 5.0 grams of Derakane 411-350 vinyl ester resin, 2.90 grams of ND-VTMS:ACN solution, and 3.29 grams of acetonitrile were combined. The mixture was sealed by placing a sheet of aluminum foil over the tube end, then a rubber septum was inserted and sealed with copper wire. The aluminum foil sheet assures that the styrene present in the vinyl ester resin does not absorb into the rubber septum. The tube is shaken vigorously be hand for two minutes then placed in a sonic bath for 15 minutes. The solution appears dark, but transparent, with no sign of turbidity or particle settling.

The solution is then case onto a 5" x 5" glass plate and placed in a vacuum oven at 70° for 2.75 hours. The plate is removed from the oven and the thin films are quickly scraped with a straight-edge razor to collect the functionalized nanodiamond dispersed in vinyl-ester monomer. This step is performed while the plates are still warm, so that the films may be collected while the vinyl ester monomer is still above its glass-transition temperature. If the films are allowed to cool, they become hard and brittle and are significantly more difficult to collect and manipulate in the cooled state.

The collected material is placed in a new 15 mL test tube and styrene monomer is added to bring the resin back to the original 45 weight percent styrene content. The tube is again sealed with foil and a septum, then placed in a sonic bath for 20 minutes to aid in dispersion.

Finally, 3-point bending bars are fabricated for mechanical characterization. The bars are 1.0 mm x 10.0 mm x 50 mm. First, molds are fabricated by gluing together glass microscope slides in the appropriate dimensions. The mold surfaces are treated with a

Teflon® solution to act as a mold-release agent, then plugged on one end with an injection of silicone sealant. For reference, a diagram of the mold is provided (Figure 5.3).

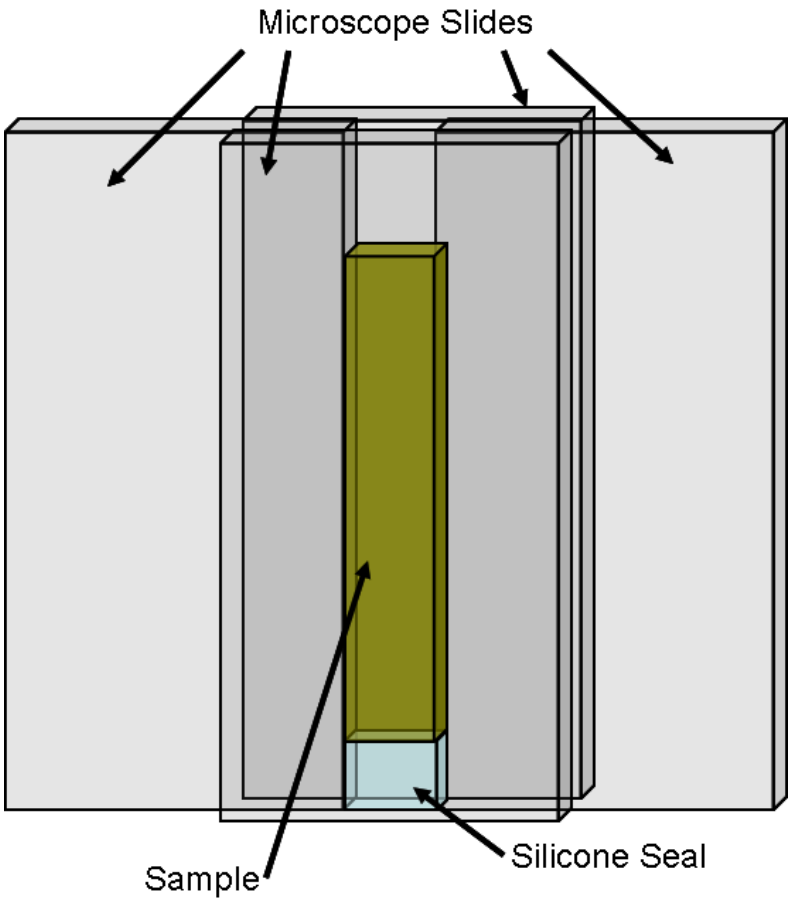

Figure 5.3 Design of sample mold for 3-point-bending tests. The mold is formed by gluing microscope slides together with cyanoacrylate glue and sealing the bottom with silicone grease.

Again, the 1.2 volume percent sample will serve as a typical sample procedure. In a 6 mL disposable syringe is placed 3.0 grams ND-VTMS:VE resin with 0.01 grams Cobalt Naphthenate solution, and 0.06 grams MEKP catalyst. The curing agents are mixed with the ND-VTMS:VE resin solution by stirring the syringe contents for 2

minutes with a glass rod, then the syringe is placed in a vacuum oven for 5 minutes to degas. The degassed solution is injected into the mold from the bottom to avoid trapping air bubbles. The filled mold is then placed in a 90°C oven at atmospheric pressure for 1 hour to cure. Once removed and cooled, the glass mold is broken to remove the nanodiamond-vinyl ester composite specimens.

5.2.3 Characterization

The concentration of –COOH functional sites was measured via a base-uptake technique.[51] Particle size was determined using Dynamic Light Scattering (DLS) with a Malvern ZetaSizer equipped with a 633 nm laser. The concentration of functionalized ND in acetonitrile is determined by thermogravimetric analysis on a Thermal Instruments TGA 2950 with a heating rate of 10°C min^{-1}. Thermogravimetric analysis was also used to monitor the solvent evaporation process.

X-ray Diffraction was performed on a Scintag X1 powder XRD. Energy Dispersive X-Ray Spectroscopy (EDS) was performed for chemical characterization of the nanodiamond filler using an Oxford Instruments INCA EDS in conjunction with a Hitachi S-4200 Scanning Electron Microscope. Fourier Transform Infrared Spectroscopy (FT-IR) was conducted with a ThermoMattson Satellite FTIR. Nuclear Magnetic Resonance (NMR) was preformed using a Bruker NMR operating at 400 MHz. The composite's mechanical properties were characterized on an Instron Dynamight 8841 benchtop load frame in three point bending mode. The loading rate was 1 mm min^{-1} and the test was conducted in accordance to ASTM D 790 test standards. The glass transition temperature was measured by Differential Scanning Calorimetry (DSC) using a TA

Instruments Q200 with a heating rate of 10°C min^{-1}. Thin films were sectioned using an ultramicrotome and imaged in a Phillips CM10 Tunneling Electron Microscope operating at 80 kV.

5.3 Results and Discussion

Overall, three main functions must be performed for this study: de-aggregation of the UDD powder, modification of the nanodiamond surface, and dispersion of the nanofillers into a resin. The processing steps for each of these steps must be selected such that they do not either degrade a previous step or prevent a subsequent step. These limitations add an extra degree of complexity to the design of a synthesis route. For example, a common and effective method of surface functionalizing nanocarbon material is to use thionyl chloride to convert the carboxylic acid into an acyl chloride.[19] The chlorine atom is a good leaving group, facilitating the covalent attachment of a variety of linker molecules. This synthesis strategy, however, is inappropriate for de-aggregated nanodiamond because thionyl chloride reacts with DMSO, which is the only known solvent for de-aggregating UDD-COOH at practical concentrations.

For the fabrication of ND:thermosetting polymer composites, an alternative synthesis strategy is required. Previously in Chapter 3, ND dispersions in ethylene glycol, water, and even toluene were successfully formed using surfactant-stabilized ND particles. Here, the de-aggregation step and the functionalization step take place simultaneously by de-aggregating the UDD-COOH powder in the presence of a silane linker molecule.

Combining these two processing steps is advantageous for several reasons. First, the fact that both steps take place at once implies compatibility. From a practical standpoint, streamlining the fabrication process improves efficiency in terms of time required to produce the nanocomposite and improves product yield because there are fewer product transfer steps that could result in loss of sample. Finally, achieving ND functionalization without requiring prior de-aggregation of UDD provides significantly more flexibility in selection of carrier solvents. UDD-COOH forms stable dispersions only in a select few solvents and is practical only in DMSO because flocculation occurs in other solvents upon dilution.[30] However, by using an in situ surface treatment, it is possible to achieve good dispersion in other solvents.

It is important to select a silane linker molecule with a reactive tail tailored for the target resin. For example, a silane linker with a hydrocarbon tail, such as n-octadecyltrimethoxysilane, would be appropriate for dispersion in non-polar solvents. Vinyltrimethoxysilane, with the vinyl group available to crosslink to a vinyl ester resin matrix, would be a good choice for VE composites. Furthermore, the concentration of linker molecules is also of critical importance. Ideally, a monolayer of coverage would impart maximum stress transfer from the nanoparticle to the matrix. A formula for determining the appropriate concentration of silane surface treatment has been proposed[85]:

$$\frac{m_f}{m_{ND}} = \frac{M_f A_{ND}}{A_f} \tag{5.1}$$

where m_f is the mass of the silane linker, m_{ND} is the mass of the nanodiamond, M_f is the molar mass of the silane linker, A_{ND} the specific surface area of nanodiamond, and

A_f the molar area coverage of the linker molecule. A_f is independent of the tail group, and set by Hahn *et al* to be 10^5 m^2 mol^{-1}, which equates to about six linker molecules adsorbed per nm^2.[85, 86, 90, 91] This amounts to relatively high concentrations; typically micron-scale composites have a 1-3% mass fraction of silane linkers, but a monolayer dosage of vinyltrimethoxysilane for nanodiamond would have a mass fraction of approximately 60%.

This high concentration, however, would be detrimental if the number of linker molecules were in excess of the surface sights available for binding. The presence of free silane linkers would not only be an inefficient use of reagent but could reduce the cross-linking density of the final composite structure and, thereby, adversely affect mechanical properties. Conveniently, base-uptake experiments have shown that the density of –COOH sites on the diamond nanoparticles is about eight functional groups per nm^2.[51, 66] Therefore, employing the silane loading levels suggested by Hahn *et al* would be sufficiently high to provide a monolayer coverage of coupling agent but the concentration of –COOH sites is in stociometric excess of the silane linker molecules. Excess –COOH functional groups is desired to prevent oligomerization of the silane linker molecules.

With a comfortable understanding of silane dosages, the focus returns to appropriate solvent selection. In this study, the exploration of other solvents was initially demonstrated with dimethylformamide. DMF was selected because it is a polar, aprotic solvent with a lower boiling point than DMSO; DMF boils 36°C lower than DMSO. The functional molecule used here was (3-glycidyloxypropyl)trimethoxysilane (GTMS). This linker molecule has a siloxy ester head group expected to react with the nanodiamond

surface and a reactive tail with an epoxy group that could be used to crosslink into epoxy resins.

The particle size distribution of ND-GTMS:DMF solution after de-aggregation, shown in Figure 5.5, shows encouraging trends. The particle size distribution maximum occurs at seven to eight nanometers in diameter. Dynamic light scattering measures the solvodynamic radius of the particles in solution, so a 2-3 nm increase in diameter correlates very well with a 5 nm ND particle that has been surface functionalized with (3-Glycidyloxypropyl)trimethoxysilane linker molecules.

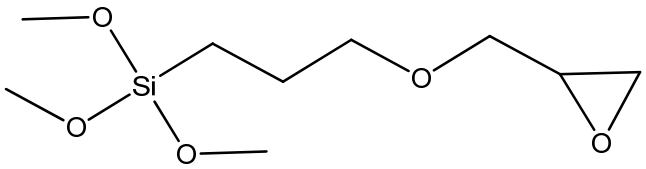

Figure 5.4 Molecular structure of (3-Glycidyloxypropyl)trimethoxysilane linker molecule showing its bi-reactive terminal groups.

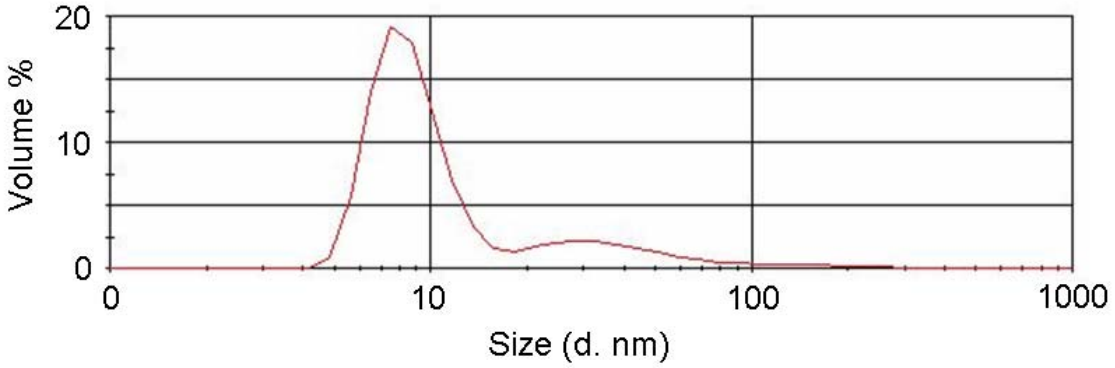

Figure 5.5 DLS particle size distribution of ND functionalized with (3-glycidyloxypropyl)trimethoxysilane. It is important to note here that the solvent is DMF.

Demonstrating the ability to disperse nanodiamond in solvents other than DMSO is a valuable exercise, but DMF still is not an ideal solvent for the subsequent processing steps. After de-aggregating and functionalizing the nanodiamond, it must be incorporated into uncured resin. This process is facilitated most efficiently when using solvents with high vapor pressure and low boiling points.

A series of de-aggregation experiments were conducted using styrene as the dispersing solvent. Styrene is an attractive solvent because not only is the boiling point lower and the vapor pressure higher than DMF, but styrene is already present in large quantities in vinyl ester resins. This precludes the issue of solvent contamination; as long as the concentration of styrene is controlled, it is irrelevant if the styrene originated as diluent in the as received resin or if it is added as the carrier solvent for the ND-VTMS nanoparticles.

Uncured vinyl ester resins containing de-aggregated and surface-functionalized nanodiamond were produced by following the above procedure (Figure 5.6). Macroscopically, the resins showed good dispersion with the characteristic dark, though transparent coloration.[30] Thermogravimetric analysis, however, reveals an undesirable side reaction when producing ND-VTMS:styrene solutions via the de-aggregation process described above. A thermogram of a ND-VTMS:styrene solution is shown in Figure 5.7. There is a 90 percent mass loss between 20°C and 100°C; this is the loss of the free styrene. There remains a mass of about 10 percent present until a second major mass loss that occurs between 375°C and 440°C, amounting to a loss of an additional five mass percent. In this sample, the combined mass of nanodiamond and surface sizing agent, vinyltrimethoxysilane, account for the five mass percent that remains at 450°C. A

mass loss above 100°C of approximately five weight percent would be expected if only the nanodiamond and surface sizing agent were present. This additional mass loss that is present from 100°C to 375°C is likely due to the presence of styrene oligomers that have thermal stabilities 200°C above the boiling point of styrene.

Figure 5.6 Uncured VE resins containing ND-VTMS filler up to 7.5 weight percent. The concentration of nanodiamond, from left to right, is 0.00, 0.10, 0.25, 0.50, 0.75, 1.00, 1.50, 2.00, 3.00, 5.00, and 7.00 wt percent.

Styrene oligomerization is further suggested by the empirical observation that the ND and organic matter that remains after driving off the solvent quickly re-disperses in styrene, but this same material is poorly miscible with vinyl ester molecules. Styrene monomer is expected to be a good solvent for polystyrene oligomers, which would account for the rapid dissolution of the de-aggregation product in pure monomer.[3] In the case of the vinyl ester molecules, however, polymerized styrene is less mobile than the monomer, and therefore a poor dispersing agent.[3]

The question remains as to what mechanism is responsible to account for such unwanted polymerization of styrene during the de-aggregation process. Styrene is known to polymerize under exposure to UV radiation.[92] This mechanism, however, is unlikely to occur because the de-aggregation steps are performed under low-light conditions. Vinyl ester resins are intentionally cured by radical catalysts, typically methyl ethyl ketone peroxide (MEKP).[76] It has been posited that the primary diamond particles may be covalently bound to each other.[24] If so, then de-aggregation of ND could lead to homolytically broken C-C bonds. These dangling bonds are present as unpaired electron radicals that may initiate styrene polymerization.

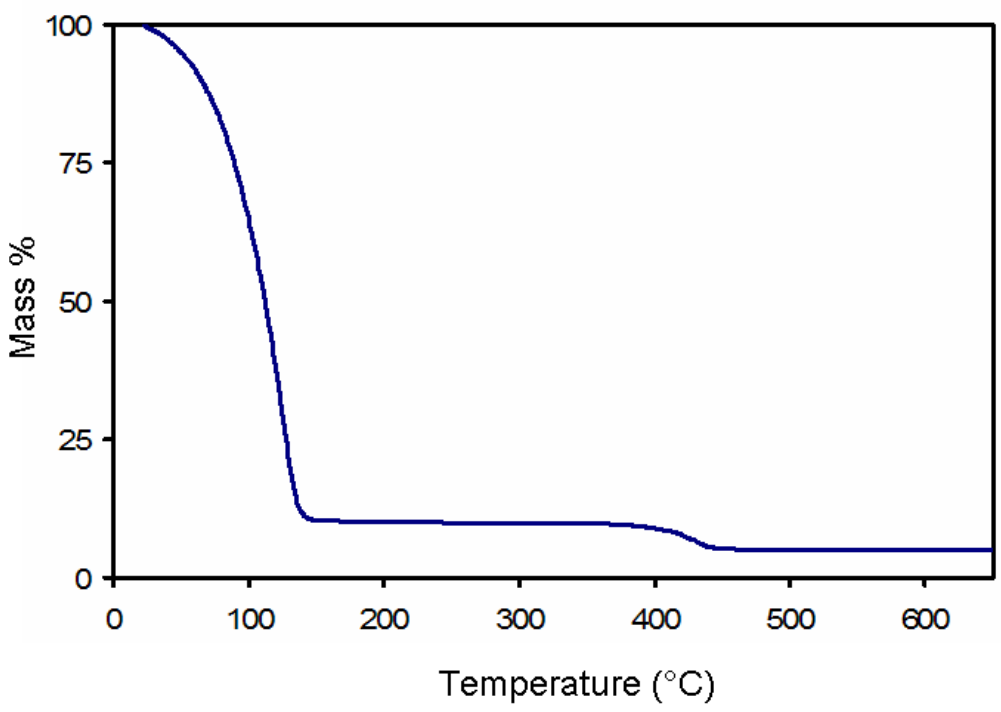

Figure 5.7 Thermogram of a 5.0 wt percent ND-VTMS:styrene solution. The mass present from 200°C to 375°C is approximately 10 wt percent.

To avoid the challenges associated with uncontrolled polymerization, other lower-boiling-point and aprotic solvents were explored as possible replacements for DMSO and DMF. Acetonotrile (ACN) is an attractive choice, because the solvent has a boiling point of 82°C, but a dipole moment of 3.92 debyes. ACN is almost as polar as DMSO (and more polar than DMF) but can be driven off at a significantly lower temperature. Furthermore, a boiling point of 82°C is attractive from a processing perspective, because it is not so low that the frictional heating that occurs during the de-aggregation process causes significant solvent evaporation at inopportune times.

While UDD-COOH does not de-aggregate in ACN alone, adding a surface functional group during the de-aggregation process does form stable ND dispersions in ACN. Here, UDD-COOH was de-aggregated in ACN in the presence of vinyltrimethoxysilane (VTMS) or 3-(trimethoxysilyl)propyl methacrylate (TMSPM). Both silane linkers, shown in Figure 5.8, are bi-reactive. The methoxy groups are expected to bind to the nanodiamond surface, while the vinyl group is available to crosslink into the vinyl ester resin.

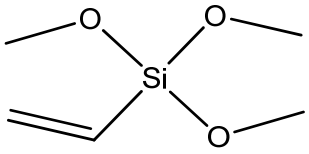

(a)

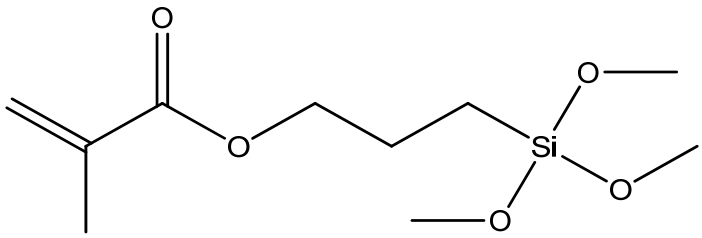

(b)

Figure 5.8 Silane linker molecules. (a) vinyltrimethoxysilane and (b) 3-(trimethoxysilyl)propyl methacrylate.

Use of silane linkers to functionalize nanodiamond during the de-aggregation process was first reported by Krueger *et al* in 2009.[52] This approach is appealing because it allows for ND dispersions in a wider range of solvents. Furthermore,de-aggregation takes place at a relatively low macroscopic temperature, under 80°C. The local temperatures experienced at the nanoparticle surfaces undergoing de-aggregation, however, is likely much higher.[29] Conveniently, the highest temperatures are local to the nanodiamond surface, the same place where chemical reaction is desired. A drawback to this method, however, should be mentioned. The silane linkers may condense on the surface of the ceramic milling media; improving the solubility of the ceramic media may lead to a higher oxide concentration in the de-aggregation supernatant. This may enhance zirconia contamination in the final product.

In Figure 5.9, dynamic light scattering shows that de-aggregation does take place in ACN, though the particle size distribution is larger than in the example of the epoxy-functionalized ND dispersed in DMF. Particle size distribution peak maxima occur at 40 nm for the ND-VTMS sample and at about 70 nm for the ND-TMSPM sample. It is interesting that the VTMS linker molecule produces better dispersions than the TMSPM silane linker. This may be due to the smaller size of the vinyltrimethoxysilane linker molecule. Higher molecular weight molecules diffuse more slowly than low-molecular weight molecules. If the TMSPM linkers cannot quickly penetrate between recently separated primary diamond nanoparticles, then the particles may re-aggregate. During de-aggregation, primary particles may undergo separation and recombination many times before large linker molecules can penetrate the particle-particle gap and prevent re-aggregation. Conversely, smaller linker molecules, like vinyltrimethoxysilane, can more rapidly penetrate between primary particles. With a higher diffusion rate, a smaller linker molecule is statistically more successful at functionalizing and stabilizing the surfaces of primary nanodiamond particles.

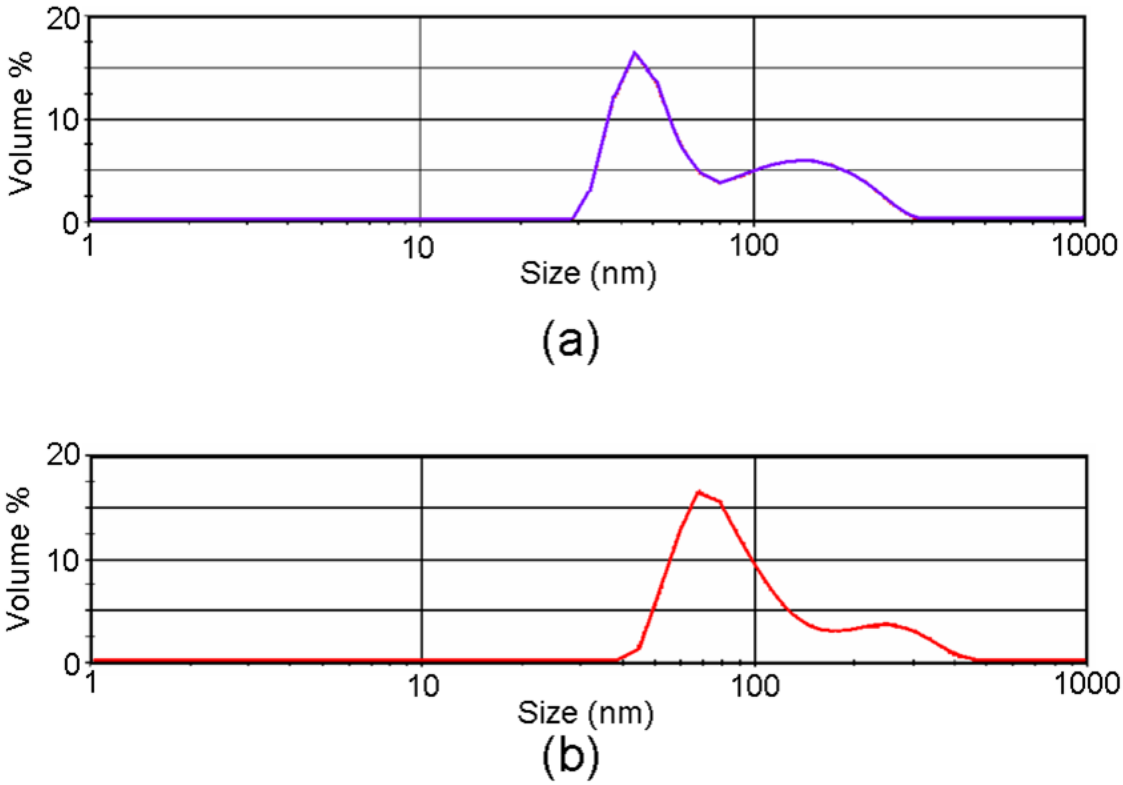

Figure 5.9 DLS particle-size distribution of (a) ND-VTMS nanoparticles and (b) ND-TMSPM nanoparticles in acetonitrile.

A series of dispersion experiments were conducted on a control system that employed UDD-COOH and ACN with acrylic acid as the surface functional agent. The goal of the dispersion study was to form the dimer structure shown in Figure 5.10. Use of non-covalent interaction of surface –COOH groups with –COOH groups of the surface treatment was successfully implemented in the ND•Oleic Acid materials system (Chapter 3) and was expected to form stable ND•Acrylic Acid suspensions in ACN. Surprisingly, a route to stable ND dispersions was not found; the presence of acrylic acid actually caused nanoparticle flocculation. This was unexpected both because acrylic acid has a similar pK_a to oleic acid and ND is more likely to disperse in a polar solvent such as ACN than a non-polar solvent like octane.

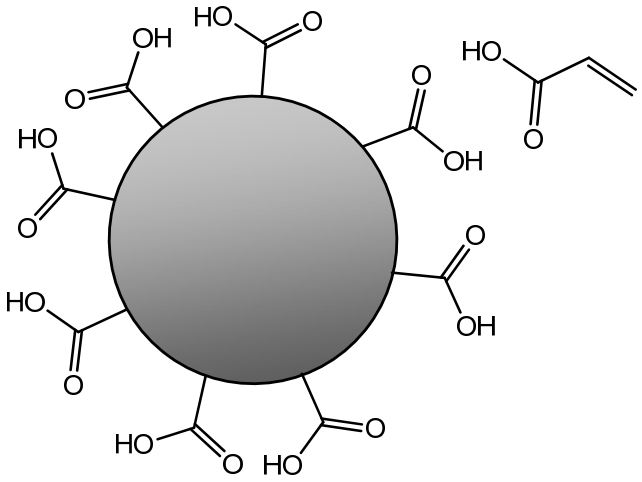

Figure 5.10 Anticipated acrylc acid/ND-COOH dimeric structure.

Surface functionalization with silane linker molecules in the ND-VTMS:ACN solution is implied by the stability of primary nanodiamond particles in ACN solvent, which does not occur without surface modification. Silane surface functionalization, however, was examined via FT-IR spectroscopy to qualitatively asses the bonds present on ND surfaces. The ND-VTMS and ND-TMSPM samples were subjected to a dialysis treatment prior to FT-IR measurement. The extensive washing removes free organic material from the dispersion; material remaining after the dialysis is likely to be only chemisorbed onto the nanodiamond surface. These diamond nanoparticles remained well-dispersed after dialysis.

FT-IR spectra of ND-VTMS and ND-TMSPM samples are shown in Figure 5.11 and Figure 5.12, respectively. The ND-VTMS sample displays a broad absorbance peak at about 3400 cm^{-1}, which is also present in the ND-COOH sample and attributed to O-H stretching bands of the OH functional groups of COOH and adsorbed water.[93, 94] Ideally, the existence of the C=C structure could be determined by the peak at approximately

1640 cm^{-1}, but this peak is likely masked by the peak due to water in the ND-COOH sample.[23] The vinylic =C-H bonds, however, absorb at about 3020 cm^{-1}. Though the peak is small, it is present both in the pure VTMS sample and the ND-VTMS sample. This suggests that the vinyl group survives the de-aggregation and functionalization processes; an important fact if subsequent cross-linking to the vinyl ester resin is desired for the nanocomposite. The peaks at 2850 cm-1 to 2960 cm-1, which are assigned to the C-H stretching bands of alkane C-H groups, are stronger in the linker molecule sample than in the ND-VTMS sample. The reduced intensity may suggest a reduction in the presence of methyl groups; the methyl groups would react with the –OH groups of the ND to form a methanol product which would be removed via dialysis. Finally, the strong peak at 1110 cm^{-1} in the VTMS sample is assigned to the vibration of the C-O-Si groups.[52] In the ND-VTMS samples, the peak broadens and shifts from 1030 cm^{-1} to 950 cm^{-1}. This peak shift correlates very well with published accounts of functionalized, single particle nanodiamond dispersions, which reported a shift from around 1110 cm^{-1} to a broad peak ranging from 1010 cm^{-1} to 940 cm^{-1}.[52]

The spectra for the ND-TMSPM samples show similar peaks for the alkane C-H and O-H stretching vibrations, and the C-O-Si vibrations as are found in the ND-VTMS samples. The peaks at 1720 cm-1 and 1640 cm-1 are assigned to the acrylate ester C=O group bands on the tail of the silane linker molecule.[52]

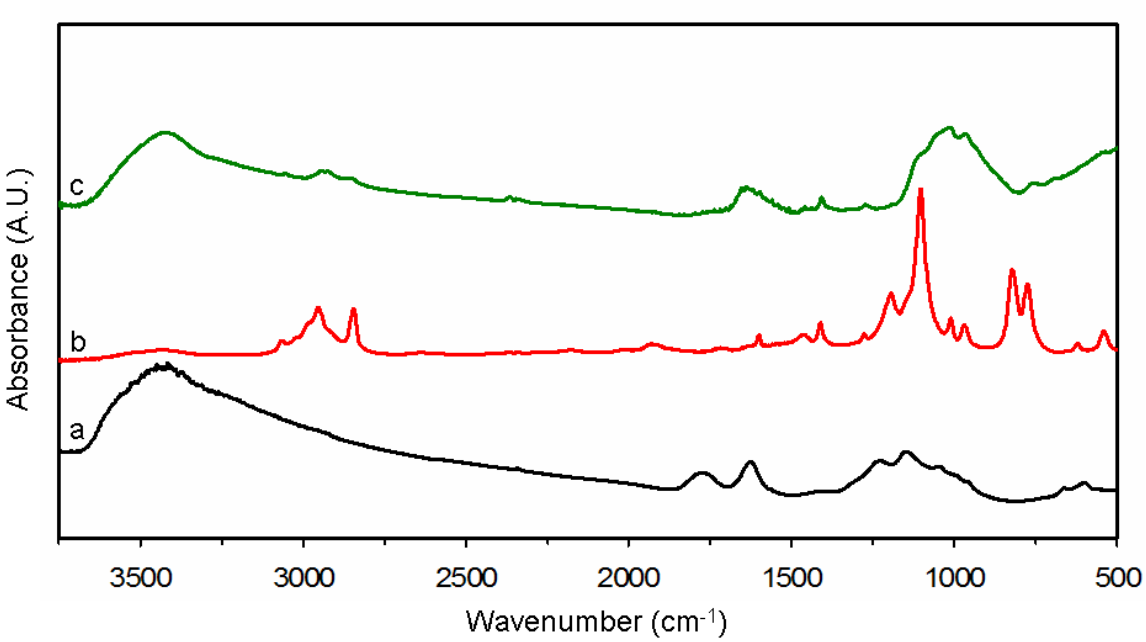

Figure 5.11 FT-IR spectra for (a) ND-COOH, (b) as-received VTMS, and (c) ND-VMTS after dialysis.

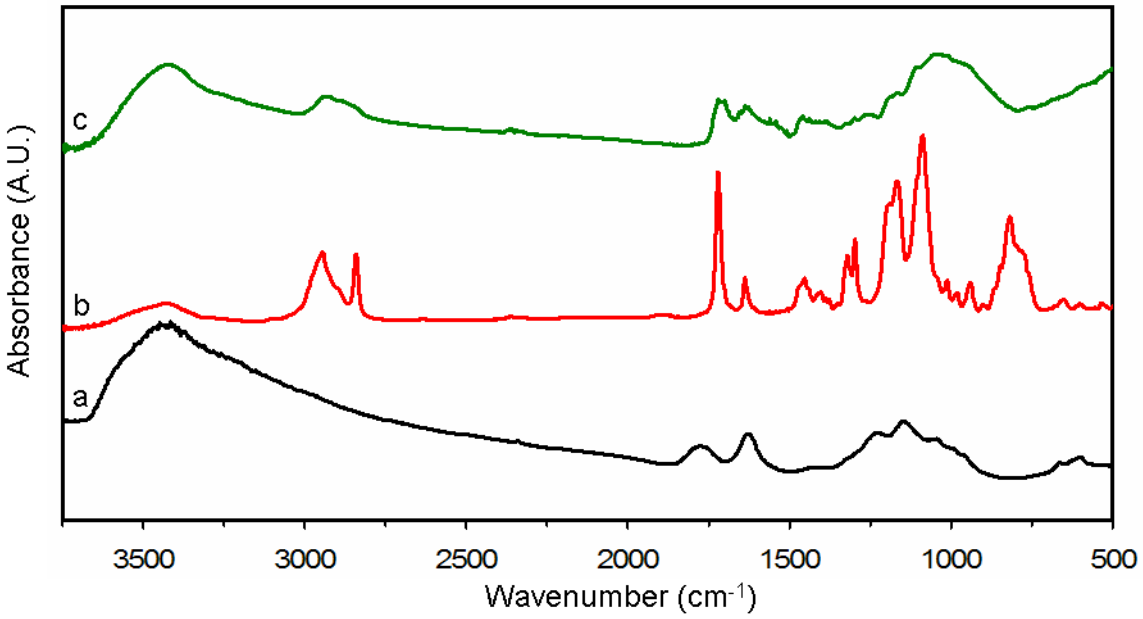

Figure 5.12 FT-IR spectra for (a) ND-COOH, (b) as-received TMSPM, and (c) ND-TMSPM after dialysis.

The surface functionalization was of ND-VTMS sample was analyzed by solution NMR. The strong peak in the ^{1}H NMR spectra for free VTMS in deuterated DMSO at 3.45 ppm is assigned to the three methyl groups present in trimethoxysilane linker molecules that have not undergone hydrolysis. The peaks around 6 ppm are lower in intensity and correlate to the vinylic H atoms. In the ^{1}H NMR spectra for the ND-VTMS sample, the peaks at 4 ppm and 3.2 ppm are assigned to the hydrogen atoms present in the OH and methyl groups of free methanol, respectively. The presence of methanol in the solution suggests that some of the methoxy groups of the VTMS linker have undergone hydrolysis. This evidence alone cannot confirm that the VTMS linker molecules are covalently bound to the nanoparticle surface. Covalent bonding of the silane sizing reagent to the nanodiamond surface sites is strongly suggested by coupling the evidence provided by ^{1}H NMR with the FT-IR spectra showing C-O-Si functionality after dialysis washing to remove free organic material.

The peaks between 2.5 ppm and 3.0 ppm are assigned to methoxy methyls which would be expected if the VTMS linkers are not fully bound to nanodiamond functional sites. There is a broad peak with low intensity from approximately 6.1 ppm to 5.6 ppm, shown in the inset of Figure 5.14 for clarity. This peak suggests the presence of olefinic structures. Previous studies utilizing VTMS linker molecules report a broadening and decrease in intensity of the peaks in the region around 6 ppm that correspond to the vinyl reactive tail of the sizing reagent after the VTMS molecule has covalently bound to a surface.[78, 95]

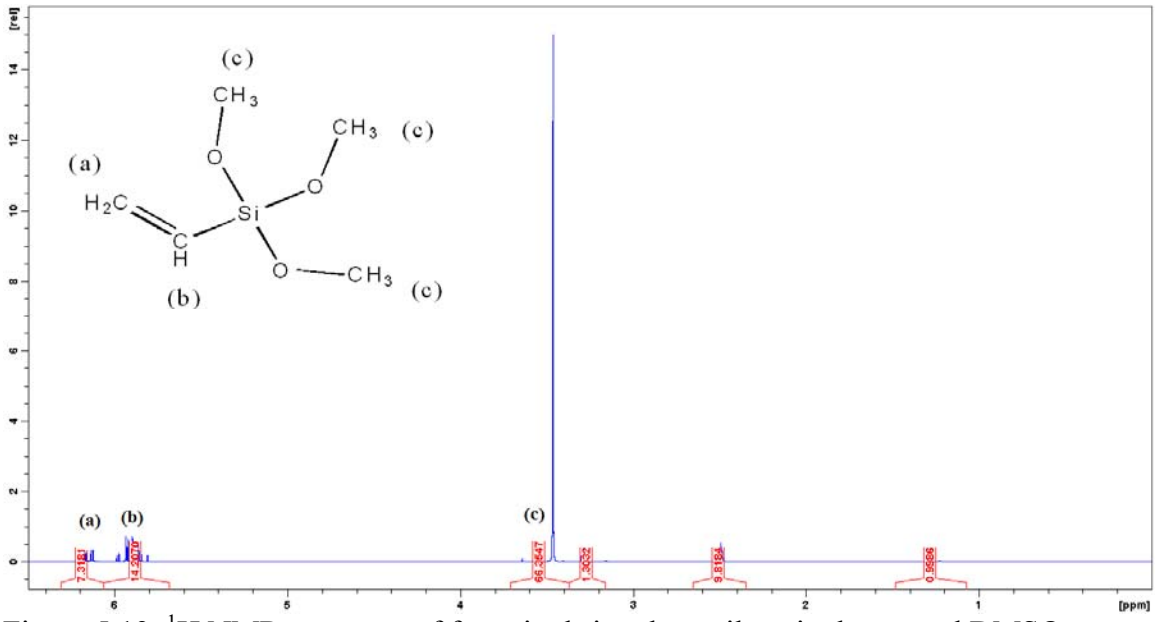

Figure 5.13 ^{1}H NMR spectrum of free vinyltrimethoxysilane in deuterated DMSO.

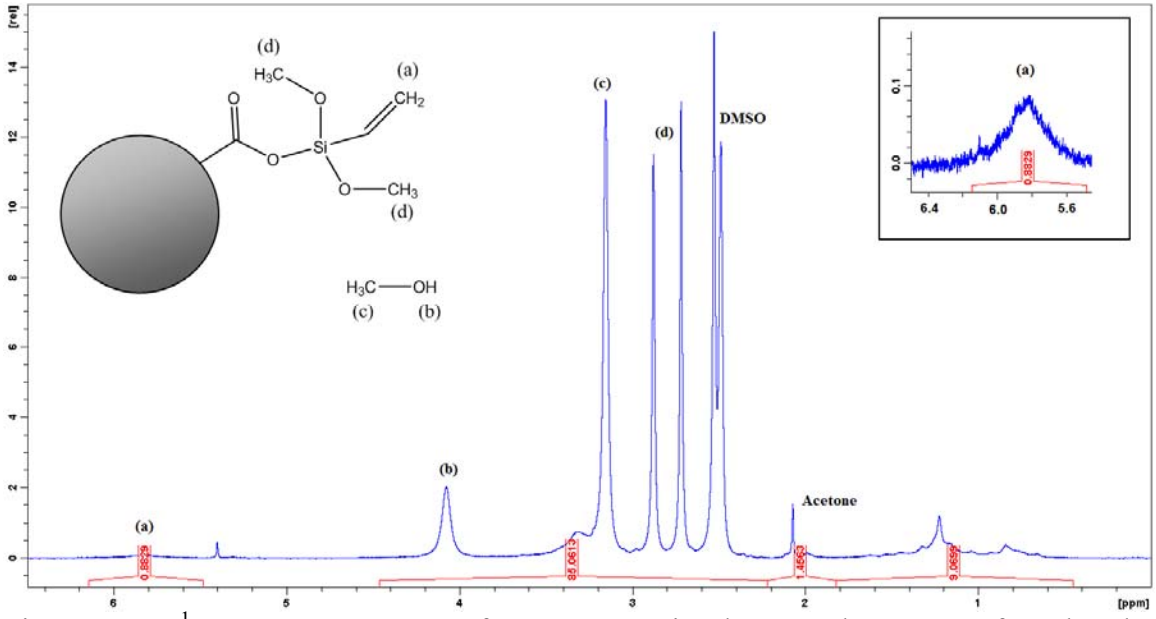

Figure 5.14 ^{1}H NMR spectrum of ND-VTMS in deuterated DMSO after the de-aggregation and functionalization processing.

The quantitative amount of surface functionalization was determined by thermogravimetric analysis. Figure 5.15 shows the thermograms of ND-VTMS and ND-TMSPM samples that were subjected to dialysis to remove any free organic material.

The mass loss for the ND-TMSPM sample, totaling approximately 13 weight percent, occurs between 300°C and 500°C. This mass loss is more pronounced than the mass loss event in the ND-VTMS samples in which about six weight percent is lost between 250°C and 500°C. The difference in mass loss can be explained by the examining the composition of the linker molecules. The trimethoxysilyl heads of the linker molecules likely do not thermally decompose from the nanodiamond surface if the methoxy branches have undergone hydrolysis and condensation reactions. Only vinyl tail groups and unreacted methoxy groups are driven off during the thermal analysis. Therefore, the vinyltrimethoxysilane linker molecule will display a modest mass loss while the propyl methacrylate tail of the ND-TMSPM samples will experience a greater mass loss. If the vinyltrimethoxysilane linker molecules were fully condensed on the nanoparticle surface, the expected mass loss would be approximately four wt percent. The ND-VTMS thermograms show a slightly higher mass loss of six wt percent. The additional mass loss could be attributed to the presence of un-reacted methoxy groups; these functional groups would be present if the siloxane linkers are partially condensed. The expected mass loss for the ND-TMSPM sample would be approximately 25 wt % because of the much larger tail group. The actual mass loss was approximately half of the expected mass loss. This discrepancy would suggest that fewer TMSPM linker molecules achieved covalent binding with nanodiamond surfaces; any un-reacted TMSPM linker molecules are likely removed during the dialysis washing.

The hypothesis that silicon from the sizing molecule remains on the nanoparticle surface following thermal treatment was tested by performing elemental analysis on the functionalized nanodiamond samples with Energy Dispersive X-ray Spectroscopy. Table

5.1, below, shows the relative concentration of elements of interest, including carbon, oxygen, silicon, and zirconium. Silicon is not detected in either the as-received sample or in nanodiamond that has undergone de-aggregation in DMSO. Silicon is present in the ND-VTMS sample both before and after the thermal analysis. The relative concentration of oxygen, silicon, and zirconium increases after the annealing step because the surface organic content, which in the case of ND-VTMS is carbon, is driven off.

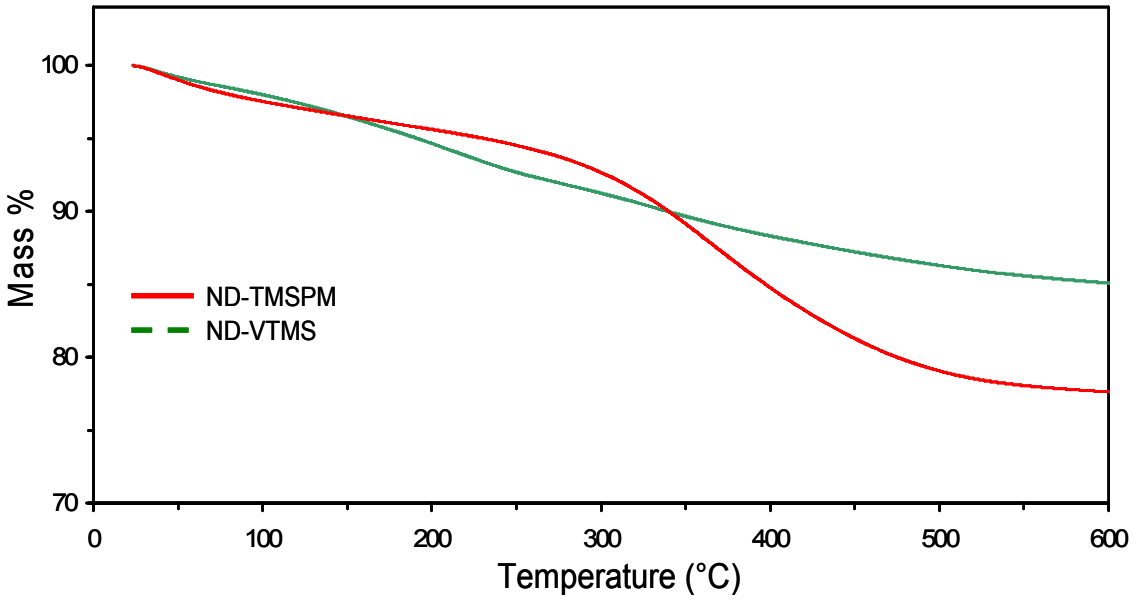

Figure 5.15 Thermogram of ND-VTMS and ND-TMSPM after dialysis and drying.

Table 5.1 Elemental analysis of UDD- and ND-based materials.

	Atomic %			
Sample Name	**C**	**O**	**Si**	**Zr**
UDD-COOH	89.8	10.2	0.0	0.0
ND-COOH	87.2	11.1	0.0	0.9
ND-VTMS	88.3	9.8	0.4	0.8
ND-VTMS (Δ)	70.3	25.3	2.1	2.3

The presence of zirconia is not increased by de-aggregating nanodiamond in the presence of reactive silane linkers. The concentration of zirconia remains almost identical for the nanodiamond de-aggregated in DMSO as for the nanodiamond de-aggregated in ACN with VTMS linker molecules. Again, the dramatic increase in zirconium content in the annealed sample is due to the fact that zirconia survives the thermal processes.

With the nanodiamond material adequately de-aggregrated, surface functionalized, and the functional groups characterized, the task remains to incorporate the nanofiller into a thermosetting polymer matrix. During this processing step, care was taken to minimize the resin exposure to oxygen and UV light. The dried films, which contain only functionalized ND and vinyl ester molecules, not styrene or acetonitrile, show good optical properties indicative of a high-quality dispersion. A photograph of vinyl ester film filled with 1.2 volume percent ND-VTMS is shown in Figure 5.16, below.

ACN was chosen as the carrier solvent because it has a relatively low boiling point and is miscible with both functionalized nanodiamond and vinyl ester resin. Residual solvent can have an adverse effect on the composite material's mechanical properties.[3] An effort must be made to remove as much solvent as possible without over-exposing the thermosetting matrix to conditions which could initiate curing. The carrier solvent was driven off under reduced pressure to minimize the time that the vinyl ester molecules were subjected to elevated temperatures. Residual solvent would be apparent in the thermogravimetric analysis as an inconsistent mass loss below 100°C. Thermograms are shown for each mechanical sample in Figure 5.17. The dried samples

all show a nearly identical mass at 100°C and all but the 0.6 volume percent ND-VTMS sample show identical mass at 250°C. The 0.6 volume percent ND-VTMS sample may have a slightly higher concentration of residual solvent. As expected the samples display different masses above 500°C. The samples with increased diamond content have a correspondingly higher residual mass above 500°C. The as-received vinyl ester resin is shown for comparison; there is a substantial mass loss under 100°C and all of the solvent is driven off by 200°C.

Figure 5.16 An uncured vinyl ester film containing 1.2 volume percent ND-VTMS showing excellent optical transparency.

Though the samples are subjected to a vacuum oven treatment at 70°C for nearly 3 hours, it is unlikely that the vinyl ester molecules have been adversely affected. Without exposure to UV light or radical initiators, the vinyl groups present on the nanodiamond surface and the monomer should remain un-reacted. Qualitatively, this is confirmed by the fact that the ND-VTMS:VE films can be rapidly dispersed into styrene

monomer. If the vinyl groups had begun to react, dissolution in styrene would be markedly slower or not possible at all. Furthermore, the uncured composites did not show any sign of dramatically enhanced viscosity even at the highest loading. In fact, all samples could pass through a 20 gauge needle with little effort.

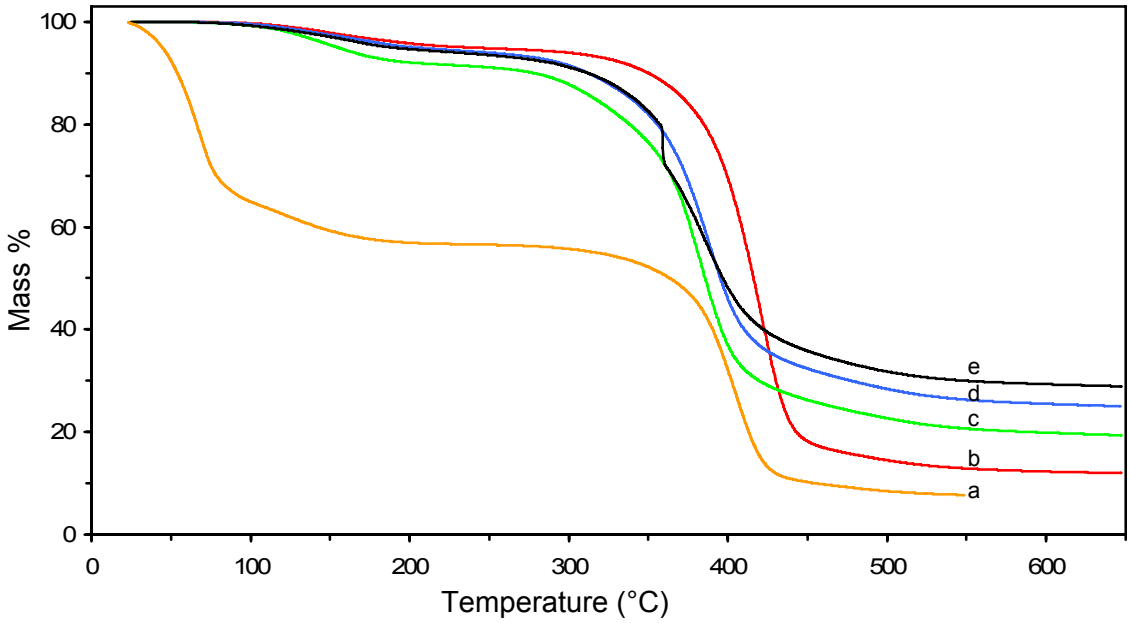

Figure 5.17 Thermograms for (a) as received vinyl ester resin, and after driving off solvent for (b) 0 volume percent ND vinyl ester control, (c) 0.6 volume percent ND-VTMS, (d) 1.2 volume percent ND-VTMS, and (e) 2.4 volume percent ND-VTMS samples.

The final characterization that is performed prior to mechanical tests is to examine the nanofiller dispersion qualitatively by Transmission Electron Microscopy. TEM images of thin sections of 1.2 volume percent ND-VTMS:VE resin samples show both aggregates up to 100 nm in diameter as well as single particles under 10 nm in diameter. A representative image is shown in Figure 5.18. The particle-size distribution appears to be smaller than suggested by Dynamic Light Scattering measurements. In

fact, single particles can be identified readily and extensive examination of the microtomed samples did not reveal any aggregates over 200 nm in diameter and few that exceeded 100 nm in diameter.

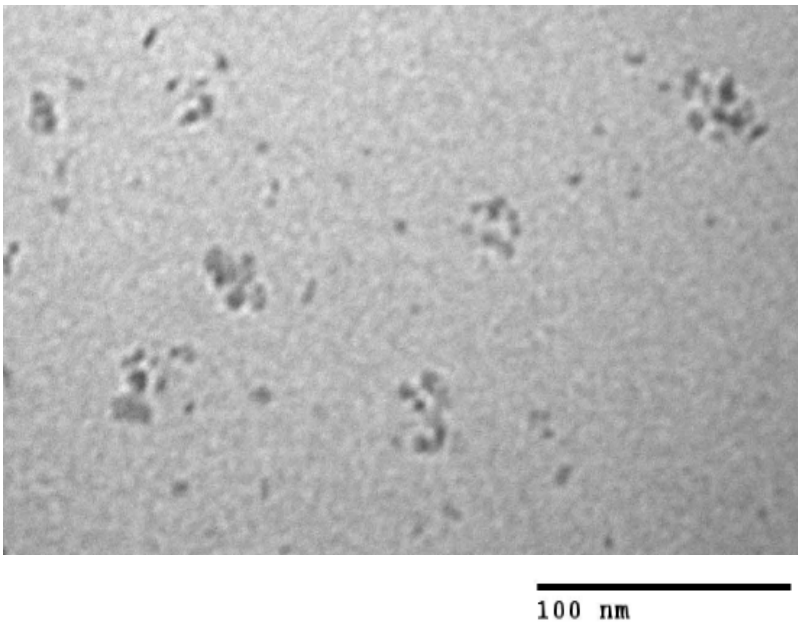

Figure 5.18 TEM image of a 40 nm microtome of the vinyl ester composite filled 1.2 volume percent with ND-VTMS.

Cured composite specimens were subjected to thermal analysis by Differential Scanning Calorimetry (DSC), shown in Figure 5.19. The glass transition temperature, T_g, was determined to be 107°C for the neat resin, 100°C for the 1.2 volume percent ND-VTMS sample, and 103°C for the 2.4 volume percent ND-VTMS sample. The inclusion of nanoparticles into the vinyl ester resin matrix did not significantly affect the glass transition temperature.

Finally, vinyl ester composites were characterized mechanically using three-point bending tests. Nanodiamond functionalized with either vinyltrimethoxysilane or 3-

(trimethoxysilyl) propyl methacrylate were incorporated into the vinyl ester resin matrix at loadings up to 2.4 volume percent. A control sample with no nanodiamond was produced under identical processing parameters. The results of the mechanical tests are shown in the Figures 5.20 through 5.22

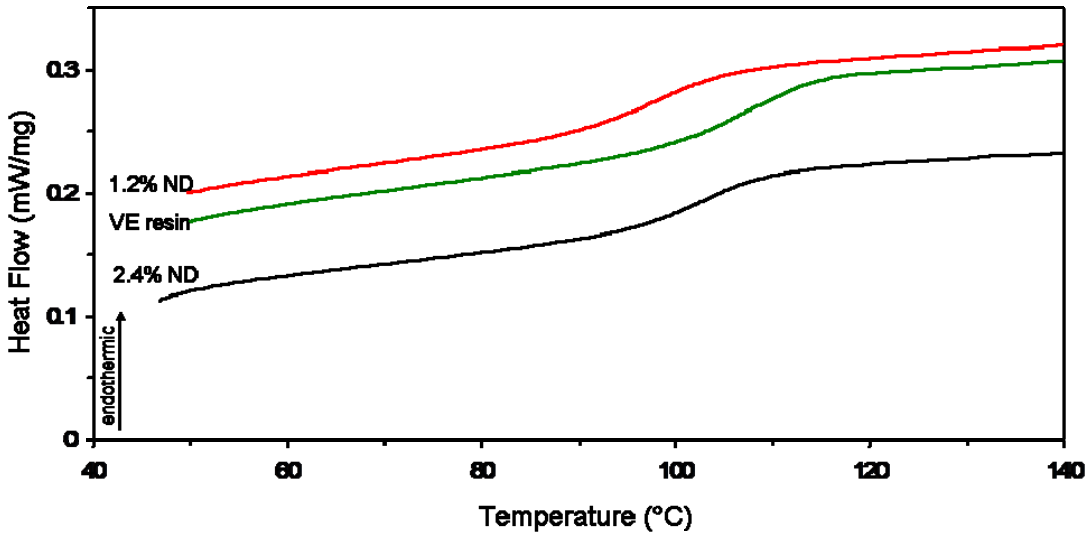

Figure 5.19 DSC scans for neat vinyl ester resin (middle), 1.2 volume percent ND-VTMS (top), and 2.4 volume percent ND-VTMS (bottom).

The surface-functionalized nanodiamond filler displays a significant ability to enhance the flexural modulus of the vinyl ester composites. At 1.2 volume percent loading, the flexural modulus was enhanced 25 percent over the neat resin. At 2.4 volume percent, the nanodiamond additive improves the flexural stiffness by 35 percent. Furthermore, the enhancement trend of the nanodiamond additive outperforms theoretical values as would be predicted by the Halpin-Tsai equations.[96] The enhanced performance of nanodiamond additives relative to theoretical predictions is attributed to

the high specific surface area unique to nanoscale fillers and not adjusted for in traditional composite models.

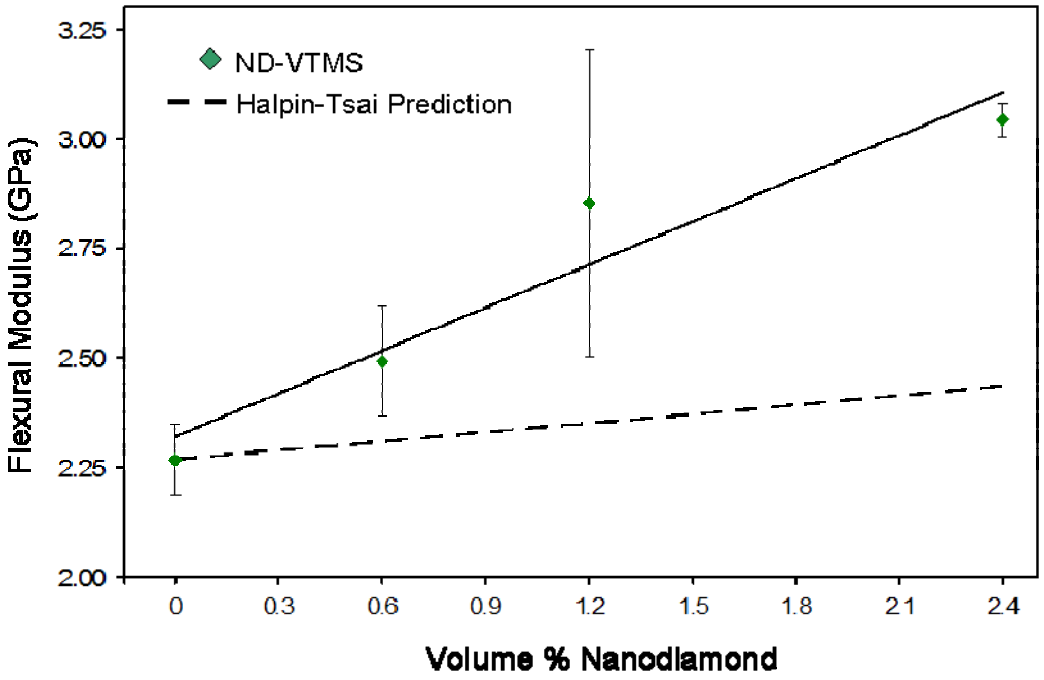

Figure 5.20 Flexural modulus data for ND-VTMS in vinyl ester resin composites. The dashed line represents the theoretical prediction using the Halpin-Tsai equations.

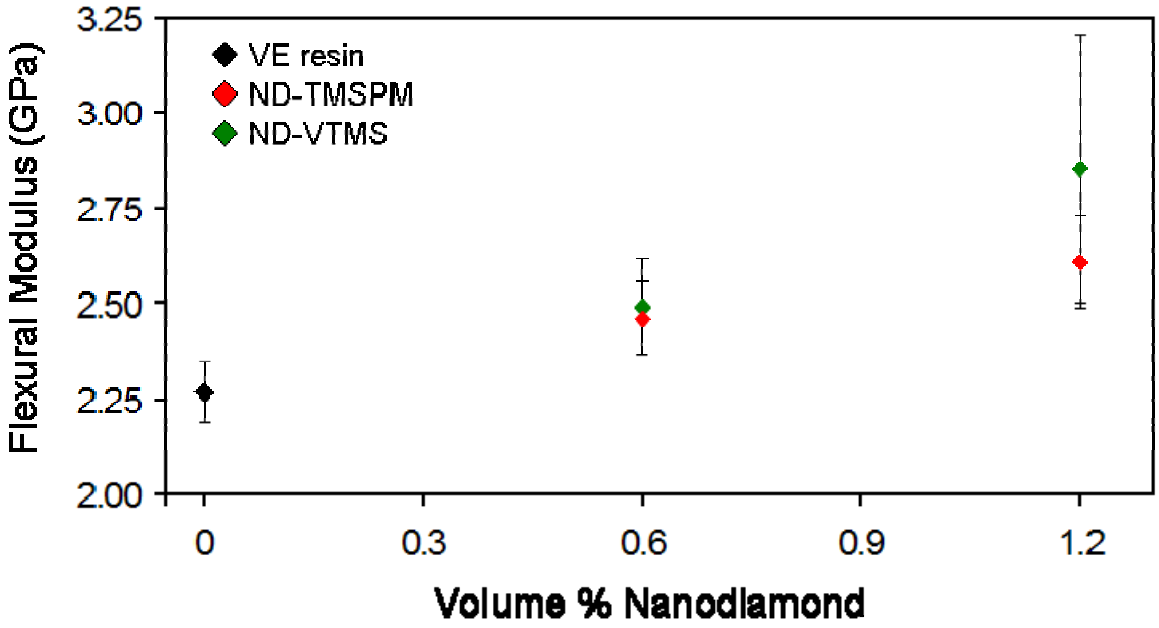

Figure 5.21 Comparison of flexural modulus for ND-VTMS and ND-TMSPM nanofillers.

The effect of the silane linker molecule's end group on the mechanical properties of the final composite is investigated by comparing composites with comparable nanodiamond loadings that have different silane linker molecules bound to the nanoparticle surface. In Figure 5.21, the nanocomposites with vinyltrimethoxysilane slightly outperform the nanocomposites with 3-(trimethoxysilyl)propyl methacrylate linkers in regards to enhancement of modulus of elasticity. Though the difference between the two sample sets is small, the better performance of the lower-molecular weight linker may suggest that stress transfer occurs most efficiently over a shorter series of covalent bonds than over a longer chain. The difference in performance of the VTMS and TMSPM linker molecules may also be due in part to the higher degree of surface functionalization achieved with VTMS linker than with TMSPM, discussed above.

Furthermore, using a smaller linker molecule may be attractive because the mass faction of linker molecule is reduced, and the presence of shorter surface functional groups may reduce any adverse increase in resin viscosity. Higher-molecular-weight sizing molecules would have a larger "shell" of organic material, which would decrease the inter-particle distances and could lead to particle-particle interactions at a lower nanoparticle concentration.[97]

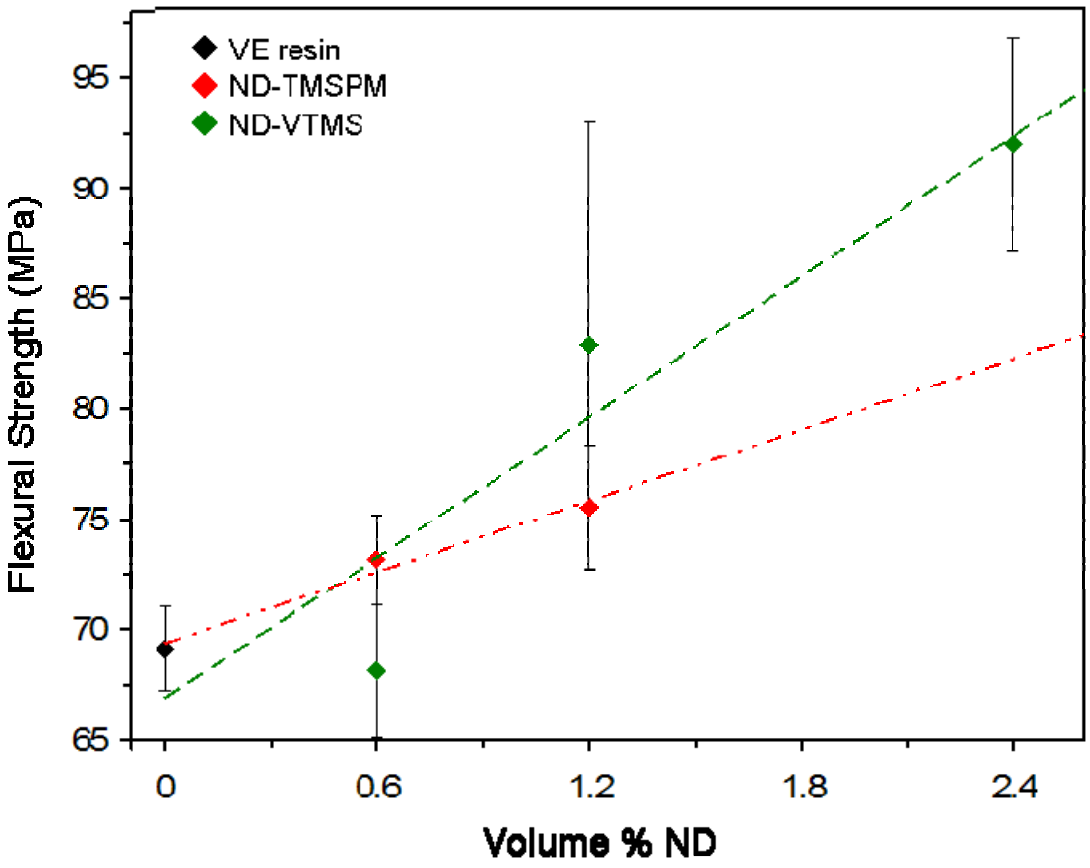

Figure 5.22 Flexural strength data for ND-VTMS and ND-TMSPM nanocomposites.

In addition to flexural modulus, flexural strength was characterized by three-point bending tests. Again, nanodiamond incorporation is effective at enhancing the

mechanical properties of the vinyl ester matrix. The nanocomposite displays a 20 percent improvement in yield strength at 1.2 volume percent and a 33 percent improvement at 2.4 volume percent. With the exception of the 0.6 volume percent ND-VTMS sample, the VTMS silane linker molecules outperform the TMSPM linker molecules in strength enhancement. The 0.6 volume percent ND-VTMS composite sample did not show an enhancement in flexural strength. This may be due to the higher residual solvent content that was detected during processing, as previously shown in Figure 5.17.

It is important to mention here that the inclusion of the nanodiamond filler did not adversely affect the vinyl ester's strain-to-failure properties. The unfilled resin consistently reached a flexural strain in excess of five percent, at which point testing standards require the test to be terminated. None of the nanodiamond composites displayed brittle fracture; all samples achieved a strain in excess of five percent without failure. This enhancement in stiffness and strength without a commensurate decrease in ductility is a highly desirable attribute for nanocomposite material systems.

5.4 Conclusions

The fabrication and characterization of nanodiamond-reinforced thermosetting composites has been successfully achieved using a processing method that employs simultaneous de-aggregation and surface functionalizationd. The processing challenges unique to thermosetting composites, specifically the need to drive off the solvent without thermally damaging the matrix polymer or inducing premature curing, were addressed and appropriate dispersing solvents have been identified.

Nanodiamond was surface functionalized with a number of bi-reactive silane linker molecules. For use in epoxy resin systems, (3-glycidyloxypropyl)trimethoxysilane was selected as the surface functionalization molecule and displayed good dispersion in DMF. For the vinyl ester resin composites, nanodiamond was functionalized with both trimethoxysilane and 3-(trimethoxysilyl)propyl methacrylate linker molecules. Chemical characterization of the ND-VTMS nanomaterial supports the hypothesis that silane linkers covalently bind to the nanodiamond surface sites.

Mechanical characterization suggests that nanodiamond is an attractive material for use in nanocomposite systems. Even low loadings of nanodiamond, under 2.5 volume percent, enhance the flexural strength and stiffness by 33 and 35 percent, respectively. The enhancement in flexural modulus significantly outperforms the prediction made using Halpin-Tsai equations.

CHAPTER VI

GENERAL CONCLUSIONS AND FUTURE RESEARCH DIRECTIONS

6.1 General Conclusions

Though this section is titled "Conclusions," I feel that this section may fit better as a prologue to the next phase of nanodiamond research. I would like to reiterate a few of the key tenets that I have garnered from studying nanodiamond and, more generally, nanomaterials for the last few years.

De-aggregation of nanodiamond is the crucial first step

The ability to work with the primary, 5-nm particles truly unlocks the "nano" potential of this material. The development of nanodiamond materials was relatively stagnant for the first four decades after its discovery. Once the ability to de-aggregate nanodiamond was demonstrated, however, the research community began to delve into the material with interest. The pace of development with nanomaterials has increased dramatically in the past four or five years.

I would draw an analogy to the development of carbon nanotube technologies. The potential of CNTs was inaccessible until effective methods to de-bundle the nanotubes became known. Once researchers had access to CNT dispersions, the technological development accelerated, and we now are beginning to see CNT technology make measurable impact on society.

The difference between composites made with UDD and ND is substantial. Though at low concentrations, the two material systems perform similarly in terms of modulus enhancement, the systems diverge as nanoparticle loading is increased. Furthermore, other key metrics are degraded with the inclusion of UDD but are enhanced when the same concentration of ND is added instead. An example of this is ductility of ND-polymer composites; when the nanoparticles are well dispersed, the enhancement in stiffness and strength does not come at a sacrifice to strain-to-failure. For an engineer looking to enhance the properties of her polymer composite system, this opens a new materials selection option that is very appealing.

Re-agglutination is a persistent and significant challenge

The challenge to incorporate dispersed nanodiamond does not end at the de-aggregation step. The entire synthesis process, in fact, must be sensitive to the nanodiamond's strong propensity to re-agglutinate. In my work, this at times presented additional challenges when I was working to form various samples. For example, a common practice to remove undesirable products is to perform a washing procedure where the desired product is spun down in a centrifuge, the supernatant discarded, and the sample is re-dispersed in fresh solvent. This process, however, is inappropriate for ND composites because conditions that allow the ND to re-aggregate must be avoided. (This process is further complicated by the fact that de-aggregated nanodiamond is extremely difficult to drive out of solution via centrifugal force.)

When designing the synthesis process, one selection criteria that is ever present is the need to keep the nanodiamond dispersed once the effort to de-aggregate the material

has been made. Consequently, minimizing the number of process steps reduces opportunities for agglutination. For this reason, the ability to simultaneously de-aggregate and functionalize nanodiamond is highly attractive. This minimizes the number of steps and ensures that the nanodiamond is still dispersed after surface functionalization.

Surface area can work for you or against you

The massive specific surface area of nanodiamond is one of the crucial factors that makes ND such a good potential additive for use in composite materials. However, this massive surface area, left unsatisfied, will drive the nanodiamond toward agglutination. The appropriate surface chemistry must be performed to keep the nanoparticles well solvated. Surface functionalization dominates the long-term stability of de-aggregated ND. For example, stable dispersions of hydrophilic nanoparticle can be made in non-polar solvents if oleic acid surfactant is used, but otherwise nanodiamond immediately falls out of solution regardless of de-aggregation steps.

Surface chemistry is not important only to form stable dispersions; the selection of surface functional groups influences the material properties of the nanocomposite. In the nanocomposite study using PAN, nanodiamond did a better job enhancing the mechanical properties if there was a higher concentration of carboxylic acid functional groups on the nanoparticles. The –COOH groups interacted favorably with the PAN polymer chains; maximizing the desirable surface functionality had a measurable effect on the nanocomposite's properties.

6.2 Future Research and Development Directions

Firstly, I believe there is a great deal of optimization that can be done on the current nanodiamond material systems. I would suspect that with a reasonable amount of effort, significant improvements are possible over the currently reported gains in crucial metrics such as thermal conductivity, modulus enhancement, and strength enhancement. Perhaps investigating combinations of surface agents or varying the concentrations will have beneficial effects. This will take additional experimental work, but the overall groundwork has been laid out and this effort is to extend the impact of the prior work.

I expect that many breakthroughs will emerge for nanodiamond applications in fluids systems. Prior investigations of nanodiamond in fluid systems, at Vanderbilt and within the broader research community, report encouraging enhancements in thermal conductivity. The implementation of ND additives for fluids, however, was hampered by the rapid settling of UDD particles. With dispersed ND, the stability issue is resolved. In fact, it is prohibitively difficult to drive the dispersed diamond particles out of solution using physical forces. For the first time, the implementation of nanodiamond additives to real-world scenarios that require long-term stability is possible.

Further developments in the nanofluids research will likely incorporate an investigation into lubricity effects. Initial reports have indicated that adding small quantities of nanoparticles to lubricants can dramatically reduce the coefficient of friction, reduce wear, and increase load before seizure. Nanodiamond is the most ideal nanomaterial currently known for lubricant applications because of nanodiamond's high

hardness, small and uniform size, and quasi-spherical shape. Again, UDD is inappropriate for this application because of the broad distribution of sizes and shapes, but dispersed ND is nearly monodisperse in particle size. Research and development funding will place an ever-increasing importance on finding new venues to achieve enhanced energy efficiency; this may be an interesting and rewarding field of nanodiamond research.

REFERENCES

1. Feynman, R. P., *The Pleasure of Finding Things Out*. Perseus Publishing: New York, 2000; p 270.

2. Shenderova, O. A.; Zhirnov, V. V.; Brenner, D. W., Carbon Nanostructures. *Critical Reviews in Solid State and Material Sciences* **2002,** 27, (3/4), 227-356.

3. Sperling, L. H., *Introduction to Physical Polymer Science*. 4th ed.; John Wiley & Sons: Hoboken, New Jersey, 2006; Vol. 1.

4. Smith, W. F.; Hashemi, J., *Foundations of Materials Science and Engineering*. 4th ed.; McGraw-Hill: New York, 2006.

5. Ratner, M.; Ratner, D., *Nanotechnology: A gentle introduction to the Next Big Idea*. 1 ed.; Prentice Hall PTR: Upper Saddle River, NJ, 2002.

6. Dai, L., Aligned carbon nanotubes for multifunctional nanocomposites and nanodevices: from plastic optoelectronics to bioceramics. *Advances in Applied Ceramics* **2008,** 107, (4), 177-189.

7. Muratore, C.; Clarke, D. R.; Jones, J. G.; Voevodin, A. A., Smart tribological coatings with wear sensing capability. *Wear* **2008,** 265, (5-6), 913-920.

8. Jou, W. S.; Cheng, H. Z.; Hsu, C. F., The electromagnetic shielding effectiveness of carbon nanotubes polymer composites. *Journal of Alloys and Compounds* **2007,** 434, 641-645.

9. Park, J. M.; Kim, D. S.; Kim, S. J.; Kim, P. G.; Yoon, D. J.; DeVries, K. L., Inherent sensing and interfacial evaluation of carbon nanofiber and nanotube/epoxy composites using electrical resistance measurement and micromechanical technique. *Composites Part B-Engineering* **2007,** 38, (7-8), 847-861.

10. Mazumdar, S. K., *Composites manufacturing: materials, product, and process eningeering*. CRC Press: Boca Raton, FL, 2001.

11. Jones, A. P., The mineralogy of cosmic dust: astromineralogy. *European Journal of Mineralogy* **2007,** 19, (6), 771-782.

12. Danilenko, V. V., On the History of the Discovery of Nanodiamond Synthesis. *Physics of the Solid State* **2004,** 46, (4), 595-599.

13. Kroto, H. W.; Heath, J. R.; O'Brien, S. C.; Curl, R. F.; Smalley, R. E., C60: Buckminsterfullerene. *Nature* **1985,** 318, 162-163.

14. Iijima, S., Helical microtubules of graphitic carbon. *Nature* **1991,** 354, 56-58.

15. Dolmatov, V. Y., Detonation synthesis ultradispersed diamonds: properties and applications. *Russian Chemical Reviews* **2001,** 70, (7), 607-626.

16. Krueger, A., The structure and reactivity of nanoscale diamond. *Journal of Materials Chemistry* **2008,** 18, 1485-1492.

17. Holt, K. B., Diamond at the nanoscale: applications of diamond nanoparticles from cellular biomarkers to quantum computing. *Philisophical Transactions of the Royal Society, A* **2007,** 365, (1861), 2845-2861.

18. Davidson, J. L.; Kang, W. P., Applying CVD Diamopnd and Particulate Nanodiamond. In *Synthesis, Properties and Applications of Ultrananocrystalline Diamond*, Gruen, D. M.; Shenderova, O. A.; Vul', A. Y., Eds. Springer: 2005; Vol. NATO Science Series II:Mathematics, Physics, and Chemistry, pp 357-373.

19. Li, L.; Davidson, J. L.; Lukehart, C. M., Surface functionalization of nanodiamond particles via atom transfer radical polymerization. *Carbon* **2006,** 44, (11), 2308-2315.

20. Baidakova, M.; Vul', A., New Prospects and frontiers of nanodiamond clusters. *Journal of Physics D: Applied Physics* **2007,** 40, 6300-6311.

21. Osawa, E., Monodisperse single nanodiamond particulates. *Pure and Applied Chemistry* **2008,** 80, (7), 1365-1379.

22. Krüger, A.; Kataoka, F.; Ozawa, M.; Fujino, T.; Suzuki, Y.; Aleksenskii, A. E.; Vul, A. Y.; Osawa, E., Unusually tight aggregation in detonation nanodiamond: Identification and disintegration. *Carbon* **2005,** 43, (8), 1722-1730.

23. Jiang, T.; Xu, K., FTIR study of ultradispersed diamond powder synthesized by explosive detonation. *Carbon* **1995,** 33, (12), 1663-1671.

24. Krueger, A.; Liang, Y.; Jarre, G.; Stegk, J., Surface functionalisation of detonation diamond suitable for biological applications. *Journal of Materials Chemistry* **2006,** 16, 2322-2328.

25. Banard, A. S.; Sternberg, M., Crystallinity and surface electrostatics of diamond nanocrystals. *Journal of Materials Chemistry* **2007,** 17, 4811-4819.

26. Banard, A. S., Self-assembly in nanodiamond agglutinates. *Journal of Materials Chemistry* **2008,** 18, 4038-4041.

27. Osawa, E.; Ho, D.; Huang, H.; Korobov, M. V.; Rozhkova, N. N., Consequences of strong and diverse electrostatic potential fields on the surface of detonation nanodiamond particles. *Diamond and Related Materials* **2009,** 18, (5-8), 904-909.

28. Osawa, E., Recent progress and perspectives in single-digit nanodiamond. *Diamond and Related Materials* **2007,** 16, (12), 2018-2022.

29. Eidelman, E. D.; Siklitsky, V. I.; Sharanova, L. V.; Yagovkina, M. A.; Vul', A. Y.; Takahashi, M.; Inakuma, M.; Ozawa, M.; Osawa, E., A stable suspension of single ultrananocrystalline diamond particles. *Diamond and Related Materials* **2005,** 14, 1765-1769.

30. Ozawa, M.; Inaguma, M.; Takahashi, M.; Kataoka, F.; Krüger, A.; E; Omacr; Osawa, Preparation and Behavior of Brownish, Clear Nanodiamond Colloids. *Advanced Materials* **2007,** 19, (9), 1201-1206.

31. Krueger, A.; Ozawa, M.; Jarre, G.; Liang, Y.; Stegk, J.; Lu, L., Deagglomeration and functionalisation of detonation nanodiamond. *physica status solida (a)* **2007,** 204, (9), 2881-2887.

32. Hounsome, L. S.; Jones, R.; Martineau, P. M.; Fisher, D.; Shaw, M. J.; Briddon, P. R.; Öberg, S., Origin of brown coloration in diamond. *Physical Review B* **2006,** 73, (12), 125203.

33. Williams, G.; Seger, B.; Kamat, P. V., TiO2-Graphene Nanocomposites. UV-Assisted Photocatalytic Reduction of Graphene Oxide. *ACS Nano* **2008,** 2, (7), 1487-1491.

34. Maxwell, J. C., *A Treatise on Electricity and Magnetism*. 2d ed.; Clarendon Press: Oxford, 1881.

35. Choi, S. U. S., Nanofluids: From Vision to Reality Through Research. In *Journal of Heat Transfer*, ASME: 2009; Vol. 131, p 033106.

36. Eastman, J. A.; Choi, S. U. S.; Li, S.; Yu, W.; Thompson, L. J., Anomalously increased effective thermal conductivities of ethylene glycol-based nanofluids containing copper nanoparticles. In AIP: 2001; Vol. 78, pp 718-720.

37. Shawn, A. P.; David, G. C.; Paul, V. B.; Zhenbin, G.; Robert, G. S., Thermal conductivity of nanoparticle suspensions. In *Journal of Applied Physics*, AIP: 2006; Vol. 99, p 084308.

38. Murshed, S. M. S.; Leong, K. C.; Yang, C., A combined model for the effective thermal conductivity of nanofluids. *Applied Thermal Engineering* **2009,** 29, 2477-2483.

39. Wen, D.; Lin, G.; Vafaei, S.; Zhang, K., Review of nanofluids for heat transfer applications. *Particuology* **2009,** 7, (2), 141-150.

40. Garg, J.; Poudel, B.; Chiesa, M.; Gordon, J. B.; Ma, J. J.; Wang, J. B.; Ren, Z. F.; Kang, Y. T.; Ohtani, H.; Nanda, J.; McKinley, G. H.; Chen, G., Enhanced thermal conductivity and viscosity of copper nanoparticles in ethylene glycol nanofluid. *Journal of Applied Physics* **2008,** 103, (7), 074301.

41. Lotfi, H.; Shafii, M. B., Boiling heat transfer on a high temperature silver sphere in nanofluid. *International Journal of Thermal Sciences* **2009,** 48, (12), 2215-2220.

42. Vajjha, R. S.; Das, D. K., Experimental determination of thermal conductivity of three nanofluids and development of new correlations. *International Journal of Heat and Mass Transfer* **2009,** 52, (21-22), 4675-4682.

43. Ju, Y. S.; Kim, J.; Hung, M. T., Experimental Study of Heat Conduction in Aqueous Suspensions of Aluminum Oxide Nanoparticles. *Journal of Heat Transfer* **2008,** 139, 092403.

44. Torii, S.; Yang, W.-J., Heat Transfer Augmentation of Aqueous Suspensions of Nanodiamonds in Turbulent Pipe Flow. *Journal of Heat Transfer* **2009,** 131, 043203.

45. Xie, H.; Yu, W.; Li, Y., Thermal performance enhancement in nanofluids containing diamond nanoparticles. *Journal of Physics D: Applied Physics* **2009,** 42, 095413.

46. Tyler, T.; Shenderova, O.; Cunningham, G.; Walsh, J.; Drobnik, J.; McGuire, G., Thermal transport properties of diamond-based nanofluids and nanocomposites. *Diamond and Related Materials* **2006,** 15, 2078-2081.

47. Osswald, S.; Yushin, G.; Mochalin, V.; Kucheyev, S. O.; Gogotsi, Y., Control of sp2/sp3 Carbon Ratio and Surface Chemistry of Nanodiamond Powders by Selective Oxidation in Air. *Journal of American Chemical Society* **2006,** 128, 11635-11642.

48. Li, L. NANOCARBON/POLYMER BRUSH MATERIALS: SYNTHESIS, CHARACTERIZATION AND APPLICATION. Vanderbilt University, Nashville, TN, 2007.

49. Mochalin, V. N.; Gogotsi, Y., Wet Chemistry Route to Hydrophobic Blue Fluorescent Nanodiamond. In 2009; Vol. 131, pp 4594-4595.

50. Rosen, M. J., *Surfactants and Interfacial Phenomena*. 3rd ed.; John Wiley & Sons: Hoboken, New Jersey, 2004; p 444.

51. Marshall, M. W.; Popa-Nita, S.; Shapter, J. G., Measurement of functionalised carbon nanotube carboxylic acid groups using a simple chemical process. *Carbon* **2006,** 44, (7), 1137-1141.

52. Liang, Y.; Ozawa, M.; Krueger, A., A General Procedure to Functionalize Agglomerating Nanoparticles Demonstrated on Nanodiamond. *ACS Nano* **2009,** 3, (8), 2288-2296.

53. Zhang, L.; He, R.; Gu, H.-C., Oleic acid coating on the monodisperse magnetite nanoparticles. *Applied Surface Science* **2006,** 253, (5), 2611-2617.

54. Kakac, S.; Pramuanjaroenkij, A., Review of convective heat transfer enhancement with nanofluids. *International Journal of Heat and Mass Transfer* **2009,** 52, 3187-3196.

55. Shenogin, S.; Xue, L. P.; Ozisik, R.; Keblinski, P.; Cahill, D. G., Role of thermal boundary resistance on the heat flow in carbon-nanotube composites. *Journal of Applied Physics* **2004,** 95, (12), 8136-8144.

56. Li, C. H.; Peterson, G. P., Mixing effect on the enhancement of the effective thermal conductivity of nanoparticle suspensions (nanofluids). *International Journal of Heat and Mass Transfer* **2007,** 50, (23-24), 4668-4677.

57. Park, J. S.; Choi, C. K.; Kihm, K. D., Temperature measurement for a nanoparticle suspension by detecting the Brownian motion using optical serial sectioning microscopy. *Measurement Science and Technology* **2005,** 16, 1418-1429.

58. Shenderova, O.; Tyler, T.; Cunningham, G.; Ray, M.; Walsh, J.; Casulli, M.; Hens, S.; McGuire, G.; Kuznetsov, V.; Lipa, S., Nanodiamond and onion-like carbon polymer nanocomposites. *Diamond and Related Materials* **2007,** 16, (4-7), 1213-1217.

59. Behler, K. D.; Stravato, A.; Mochalin, V.; Korneva, G.; Yushin, G.; Gogotsi, Y., Nanodiamond-Polymer Composite Fibers and Coatings. In *ACS Nano*, 2009; Vol. 3, pp 363-369.

60. Maitra, U.; Prasad, K. E.; Ramamurty, U.; Rao, C. N. R., Mechanical properties of nanodiamond-reinforced polymer-matrix composites. *Solid State Communications* **2009,** 149, (39-40), 1693-1697.

61. Wang, D. H.; Tan, L.-S.; Huang, H.; Dai, L.; Osawa, E., In-Situ Nanocomposite Synthesis: Arylcarbonylation and Grafting of Promary Diamond Nanoparticles with a Poly(ether-ketone) in Polyphosphoric Acid. *Macromolecules* **2009,** 42, 114-124.

62. Petrov, I.; Shenderova, O.; Grishko, V.; Tyler, T.; Cunningham, G.; McGuire, G., Detonation nanodiamonds simultaneously purified and modified by gas treatment. *Diamond and Related Materials* **2007,** 16, 2098-2103.

63. Zhao, S.; Schadler, L. S.; Duncan, R.; Hillborg, H.; Auletta, T., Mechanisms leading to improved mechanical performance in nanoscale alumina filled epoxy. *Composites Science and Technology* **2008,** 68, 2965-2975.

64. S. Hajir Bahrami, P. B. K. S., Thermal behavior of acrylonitrile carboxylic acid copolymers. *Journal of Applied Polymer Science* **2003,** 88, (3), 685-698.

65. Sreekumar, T. V.; Chandra, L.; Srivastava, A.; Kumar, S., Oxidative stabilization of polyacrylonitrile in the presence of carbon nanotubes. *Carbon* **2007,** 45, 1105-1107.

66. Hu, H.; Bhowmik, P.; Zhao, B.; Hamon, M. A.; Itkis, M. E.; Haddon, R. C., Determination of the acidic sites of purified single-walled carbon nanotubes by acid-base titration. *Chemical Physics Letters* **2001,** 345, (1-2), 25-28.

67. Eidelman, E. D.; Siklitsky, V. I.; Sharonova, L. V.; Yagovkina, M. A.; Vul, A. Y.; Takahashi, M.; Inakuma, M.; Ozawa, M.; Osawa, E., A stable suspension of single ultrananocrystalline diamond particles. *Diamond and Related Materials* **2005,** 14, (11-12), 1765-1769.

68. Chae, D. W.; Kim, B. C., Effects of zinc oxide nanoparticles on the physical properties of polyacrylonitrile. *Journal of Applied Polymer Science* **2006,** 99, (4), 1854-1858.

69. Goyal, R. K.; Tiwari, A. N.; Negi, Y. S., Microhardness of PEEK/ceramic micro- and nanocomposites: Correlation with Halpin-Tsai model. *Materials Science and Engineering: A* **2008,** 491, (1-2), 230-236.

70. Laine, R. M.; Choi, J.; Lee, I., Organic-Inorganic Nanocomposites with Completely Defined Interfacial Interactions. In 2001; Vol. 13, pp 800-803.

71. Njuguna, J.; Pielichowski, K., Polymer Nanocomposites for Aerospace Applications: Fabrication. In 2004; Vol. 6, pp 193-203.

72. Hu, Y.; Shenderova, O. A.; Hu, Z.; Padgett, C. W.; Brenner, D. W., Carbon nanostructures for advanced composites. *Reports on Progress in Physics* **2006**, (69), 1847-1895.

73. Hussain, F.; Hojjati, M.; Okamoto, M.; Gorga, R. E., Review article: Polymer-matrix Nanocomposites, Processing, Manufacturing, and Application: An Overview. In 2006; Vol. 40, pp 1511-1575.

74. Gupta, R. K.; Kennel, E.; Kim, K.-J., *Polymer Nanocomposites Handbook*. 1 ed.; CRC Press: Boca Raton, FL, 2008; p 549.

75. William D. Callister, J., *Materials Science and Engineering An Introduction*. 6 ed.; John Wiley & Sons: Hoboken, NJ, 2003; p 489.

76. Abadie, M. J. M., *Handbook of Polymer Blends and Composites*. 1 ed.; Papra Technology Limited: Shawbury, UK, 2002; Vol. 1.

77. Coleman, J. N.; Khan, U.; Gun'ko, Y. K., Mechanical reinforcement of polymers using carbon nanotubes. *Advanced Materials* **2006,** 18, (6), 689-706.

78. Moniruzzaman, M.; Winey, K. I., Polymer nanocomposites containing carbon nanotubes. *Macromolecules* **2006,** 39, (16), 5194-5205.

79. Tsai, J. L.; Hsiao, H.; Cheng, Y. L., Investigating Mechanical Behaviors of Silica Nanoparticle Reinforced Composites. *Journal of Composite Materials* **2010,** 44, (4), 505-524.

80. Manjunatha, C. M.; Taylor, A. C.; Kinloch, A. J.; Sprenger, S., The tensile fatigue behaviour of a silica nanoparticle-modified glass fibre reinforced epoxy composite. *Composites Science and Technology* **2010,** 70, (1), 193-199.

81. Zhao, Z. F.; Gou, J., Improved fire retardancy of thermoset composites modified with carbon nanofibers. *Science and Technology of Advanced Materials* **2009,** 10, (1), 6.

82. Seyhan, A. T.; Alejandra de la, V.; Tanoglu, M.; Schulte, K., Thermal curing behavior of MWCNT modified vinyl ester-polyester resin suspensions prepared with 3-roll milling technique. In 2009; Vol. 47, pp 1511-1522.

83. Singh, R. P.; Zhang, M.; Chan, D., J. Mater. Sci. In *Toughening of a brittle thermosetting polymer: Effects of reinforcement particle size and volume fraction*, 2002; Vol. 37, p 781.

84. Guo, Z.; Pereira, T.; Choi, O.; Wang, Y.; Hahn, H. T., Surface functionalized alumina nanoparticle filled polymeric nanocomposites with enhanced mechanical properties. *Journal of Materials Chemistry* **2006,** 16, 2800-2808.

85. Yong, V.; Hahn, H. T., Processing and properties of SiC/vinyl ester nanocomposites. *Nanotechnology* **2004,** 15, (9), 1338.

86. Yong, V.; Hahn, H. T., Monodisperse SiC/vinyl ester resin nanocomposites: Dispersant formulation, synthesis, and characterization. *Journal of Materials Research Society* **2009,** 24, (4), 1553-1558.

87. Guo, Z.; Liang, X.; Pereira, T.; Scaffaro, R.; Thomas Hahn, H., CuO nanoparticle filled vinyl-ester resin nanocomposites: Fabrication, characterization and property analysis. *Composites Science and Technology* **2007,** 67, (10), 2036-2044.

88. Gou, Z.; Wei, S.; Shedd, B.; Scaffaro, R.; Pereira, T.; Hahn, H. T., Particle surface engineering effect on the mechanical, optical and photoluminescent properties of ZnO/vinyl-ester resin nanocomposites. *Journal of Materials Chemistry* **2007,** 17, 806-813.

89. Spitalsky, Z.; Kromka, A.; Matejka, L.; Cernoch, P.; Kovarova, J.; Kotek, J.; Slouf, M., Effect of nanodiamond particles on properties of epoxy composites. *Advanced Composites Letters* **2008,** 17, (1), 29-34.

90. Yong, V.; Hahn, H. T., Dispersant optimization using design of experiments for SiC/vinyl ester nanocomposites. *Nanotechnology* **2005,** 16, (4), 354.

91. Virginia, Y.; Hahn, H. T., Rheology of silicon carbide/vinyl ester nanocomposites. In 2006; Vol. 102, pp 4365-4371.

92. Marksteiner, D.; Wasser, S.; Schartl, W., Photochemical Gluing of Colloidal Particles by a Simple Interparticle Polymerization Route. *Langmuir* **2009,** 25, (22), 12843-12846.

93. Xu, X.; Yu, Z.; Zhu, Y.; Wang, B., Influence of surface modification adopting thermal treatments on dispersion of detonation nanodiamond. *Journal of Solid State Chemistry* **2005,** 178, 688-693.

94. Korobov, M. V.; Avramenko, N. V.; Bogachev, A. G.; Rozhkova, N. N.; Osawa, E., Nanophase of Water in Nano-Diamond Gel. *Journal of Physical Chemistry C* **2007,** 111, 7330-7334.

95. Zhang, X. Z.; Huang, Y. D.; Wang, T. Y.; Hu, L. J., Effects of Coating Structures on Interfacial Properties of Carbon Fibre/Polyacrylacetylene Composites. *Polymers & Polymer Composites* **2007,** 15, (1), 35-43.

96. Sperling, L. H., *Polymeric multicomponent materials: an introduction*. 1 ed.; John Wiley & Sons: New York, NY, 1997; p 397.

97. Chen, Y.; Zhou, S.; Chen, G.; Wu, L., Preparation and characterization of polyester/silica nanocomposite resins. *Progress in Organic Coatings* **2005,** 54, (2), 120-126.